universität wien

MASTERARBEIT / MASTER'S THESIS

Titel der Masterarbeit / Title of the Master's Thesis

„FitzHugh-Nagumo Dynamics on Ring Networks“

verfasst von / submitted by

Karl Bernhard Riepl, BSc

angestrebter akademischer Grad / in partial fulfilment of the requirements for the degree of

Master of Science (MSc)

Wien, 2023 / Vienna, 2023

Studienkennzahl lt. Studienblatt / degree programme code as it appears on the student record sheet:	UA 066 821
Studienrichtung lt. Studienblatt / degree programme as it appears on the student record sheet:	Masterstudium Mathematik
Betreut von / Supervisor:	Univ.-Prof. Dr. rer. nat. Dipl.-Phys. Jörg Menche
Mitbetreut von / Co-Supervisor:	Dipl.-Phys. Dr. Felix Müller

Acknowledgements

At this point, I would like to thank my supervisor Jörg for letting me be part of his research group and allowing me to gain insights into what life in research is like. Also, I would like to thank the group, especially Felix, for the help you have provided me with.
I also want to thank my family and friends who have supported me along this lengthy journey. Without all of you this would not have been possible.

Abstract

Synchronization phenomena in systems of interacting elements have been observed in vastly different disciplines and thus have gotten an increasing amount of attention in research. A widely used approach for investigations are networks. In this thesis networks with a global ring structure (Watts-Strogatz networks) are equipped with FitzHugh-Nagumo dynamics where individual units exhibit a limit cycle behaviour to study the relation between network structure and emerging synchronization pattern. A numerical approach is used and the dynamics are visualized from different aspects to obtain insights regarding the topic. Additionally, a coherence measure is introduced which is utilized to classify synchronization patterns. The findings are that by manipulating the network size N, network density ρ, rewiring probability p and scaled coupling $\frac{\sigma}{N}$ the emergent synchronization patterns can be influenced reliably. Moreover, the parameter space of number of neighbors k and scaled coupling $\frac{\sigma}{N}$ is explored and distinct regions could be identified which correspond to emergent synchronization patterns.

Kurzfassung

Synchronisationsphänomene wurden in zahlreichen und verschiedensten Systemen von interagierender Einheiten beobachtet, wodurch Interesse in der Forschung bezüglich des Themas erweckt wurde. In der Analyse werden aufgrund ihrer vielseitigen Anwendbarkeit und Aussagekraft oftmals Netzwerkrepräsentationen verwendet. In dieser Masterarbeit werden Netzwerke mit globaler Ringstruktur (Watts-Strogatz Netzwerke) mit FitzHugh-Nagumo Dynamiken versehen, wobei sich jede Netzwerkeinheit in einem Grenzzyklus-Regime (Limit Cycle) befindet. In diesem Aufbau wird mithilfe von numerischen Simulationen eine Relation zwischen Netzwerkstruktur und Synchronisationsmuster hergestellt werden. Des Weiteren wird die Dynamik aus verschiedenen Aspekten visualisiert, um Erkenntnisse zu gewinnen und ein Kohärenzmaß eingeführt, welches in weiterer Folge zum Klassifizieren von Synchronisationsmuster verwendet wird. In den Analysen wurde ein Zusammenhang zwischen Netzwerkgröße N, Netzwerkdichte ρ, skalierte Kopplungsstärke $\frac{\sigma}{N}$ und Wahrscheinlichkeit p für Neuverlegung von bestehenden Verbindungen und auftretenden Synchronisationsmustern gefunden. Darüber hinaus wurde der Parameterraum von Anzahl der Nachbarn k und Kopplungsstärke $\frac{\sigma}{N}$ erforscht und Parameterbereiche identifiziert im Bezug auf entstehedes Synchronisationsmuster.

Contents

List of Figures

1. Introduction

Synchronization effects have been observed in a wide range of systems such as the Josephson effect [1], the swaying of the Millenium Bridge in London [2] or chemical oscillators [3]. Consequently, there is a significant interest in research to uncover the underlying driving forces. The general understanding is that there is a relation between structure and functionality of networks. A paradigmatic example in biology is the synchronization of the flashes of fireflies. Synchronization has also been noticed in pacemaker cells of the heart and brain neurons. The latter is thought to play a key role in memory and cognition tasks. However, at the same time unwanted synchronization of brain regions is associated with epileptic seizures [4]. The common factor in examples like these is that there is a population of independent units which interact. Resulting in the emergence of global phenomena which are not exhibited by individuals, e.g. birds/fish align and form flocks/swarms. A powerful and versatile approach is to use networks to describe interacting systems. This has gotten a significant amount of attention in recent years and is applied in ongoing research in various fields such as biology, chemistry, computer science, medicine, social sciences and physics. Recently, it was observed that there are biological networks with a global ring structure which led to the hypothesis that it might be a more common feature. However, networks do not have an ambient space and to represent them they are embedded into a space that depends on the chosen layout algorithm. Subsequently, a global feature like the ring structure usually gets lost in the process. Thus, an algorithm was developed to measure and score the "ringyness" of networks [5]. Then, the authors screened over 5.000 biological networks and found that around eight percent had a ring structure verifying the hypothesis. For example, the lipid co-regulation network, the gene expression network, the immune signalling network, the fibroblast proximity network and the soil moisture network have a global ring structure.

The objective of this thesis is to investigate the relation between network structures and emerging synchronization patterns with focus on ring networks. At first, the model dynamics, network assumptions and coherence measure are presented. Then, to study this high dimensional problem numerical simulations are utilized. For this purpose, various visualization of the dynamics are used to detect patterns and relate them to synchronization patterns. Then, the observed patterns in visualizations are related to synchronization patterns on ring networks and described in greater detail. Additionally, the

coherence measure is categorized corresponding to synchronization patterns. Lastly, this categorization is utilized to explore the parameter space of network density and coupling. This resulted in a partition of this space into regions with overlap corresponding to synchronization patterns.

The thesis is organized as follows: In chapter 2 networks and model dynamics are described and assumptions stated. In chapter 3 the different visualizations are established. Then, in chapter 4 the observed synchronization patterns are described with the use of the visualizations. In chapter 5 a more systematical exploration of the parameter space is are presented. Finally, in chapter 6 the findings are summarized and possible further steps to research this topic are discussed.

2. Model Description

Model graphs are used to investigate the relation between network structure and synchronization pattern. There exists a plethora of graph generating models to obtain different types of graphs where some of the most widespread ones are Erdös-Rényi graphs, Barabási-Albert model and Watts-Strogatz networks. These are used to represent different systems to model epidemics on networks [6], the World Wide Web [7] or the brain [8].
In this thesis, the focus lies on networks with a global ring structure representing a spatiotemporal perodicity. These are introduced in section 2.1. Then, non-linear dynamics are introduced in section 2.2. Lastly, an order parameter and an additional measure are introduced in section 2.3 and 2.4, respectively.

2.1. Watts-Strogatz Networks

In general, graphs or networks are versatile and powerful tools to describe, represent and analyze real world scenarios. These real world scenarios are usually complex and high dimensional when described with mathematical models. Therefore, a rigorous analysis might not be possible. Additionally, the interaction of individual units leads to phenomena on a global scale which are not exhibited by an individual. This is in the sense of "The system is more than the sum of its parts" [9].
In the following the mathematical definition is stated as well as the terminology that is used:

- A graph G is an ordered pair of sets (V, E) where V is the set of vertices and $E \subseteq \{(i,j) \mid i,j \in V \, and \, i \neq j\} \subseteq V \times V$ is the set of edges.
- Undirected graphs: if there exists an edge $(i,j) \in E \Rightarrow (j,i) \in E$.
- Node degree: the number of adjacent links for a given node i in an undirected graph.
- Unweighted graphs: all edges are the same in the sense that there are no associated weights.
- No self loops: a vertex cannot be connected to itself, i.e. $(i,i) \notin E \; \forall i$.
- The adjacency matrix A has dimensions $\#vertices \times \#vertices$ and is used to represent graphs. For an unweighted graph the entries $a_{ij} \in \{0,1\}$ where $a_{ij} = 1$ if there exists an edge between

vertices i and j and $a_{ij} = 0$ else. Note that for undirected networks A is symmetrical with respect to the diagonal and no self loops mean $a_{ii} = 0 \; \forall i$.

- Graph density $\rho \in [0, 1]$: fraction of edges in a graph to the maximal possible edges $\frac{|E|}{2*|V|*(|V|-1)}$ where $|\,.\,|$ denotes the cardinality of a set. Note that every edge is counted twice, thus the factor $\frac{1}{2}$ is in the formula.
- Connected Graph: there exists a path from vertices i to j for all $i, j \in V$ where a path is an ordered sequence of adjacent vertices to get from i to j. If there exists a vertices pairs without a path then, the graph is disconnected and consists of connected components.
- The mathematical object is called graph and the representation of an application/scenario is called network. Also, the terminology of vertices and edges changes to nodes and links.
- For the rest of the thesis the terminology networks, nodes and links is used.

Although there is a wide range of network generating models and different network types, only Watts-Strogatz networks are used since the focus lies on networks with a global ring structure, as observed in biological ones [5]. Watts-Strogatz networks have three model parameters N, k and p where N is the number of nodes, k is the number of neighbors and $p \in [0, 1]$ is a rewiring probability which introduces randomness into the network. Then, the network generating process is as follows: Firstly, a ring lattice with N nodes is generated. Secondly, every node i is connected to its k nearest neighbors, i.e. $i - \frac{k}{2} \, mod \, N$ and $i + \frac{k}{2} \, mod \, N$. Lastly, a link is rewired with probability p while avoiding self loops and link duplication.
Note that this procedure generates unweighted, undirected, connected graphs without self-loops. This is used in the for the rest of this thesis. In the context of networks regular means that node degrees are similar on the network. If the rewiring probability $p = 0$ then the generated Watts-Strogatz network is called k-regular. As $p > 0$ increases randomness is introduced into the networks thus becoming less regular. Note that $p = 1$ corresponds to a random network which is a network where nodes are linked according to a probability p.

Following these steps $WS(N, k, p)$ generates a network with N nodes where each node i is connected to its k nearest neighbors. Then, links in the network are rewired with probability p. Watts-Strogatz network with $N > 3$, $k = 2$ and $p = 0$ are referred to as perfect ring networks. These have the minimal possible density to form a ring. Therefore, no rewiring probability p is introduced to them since the ring property would be destroyed and they could become disconnected, as illustrated in Figure 2.1a. In higher density Watts-Strogatz networks rewiring is introduced and the number of rewired links linearly depends on p and number of links $= \frac{N*k}{2}$ as shown in Figure 2.1b.

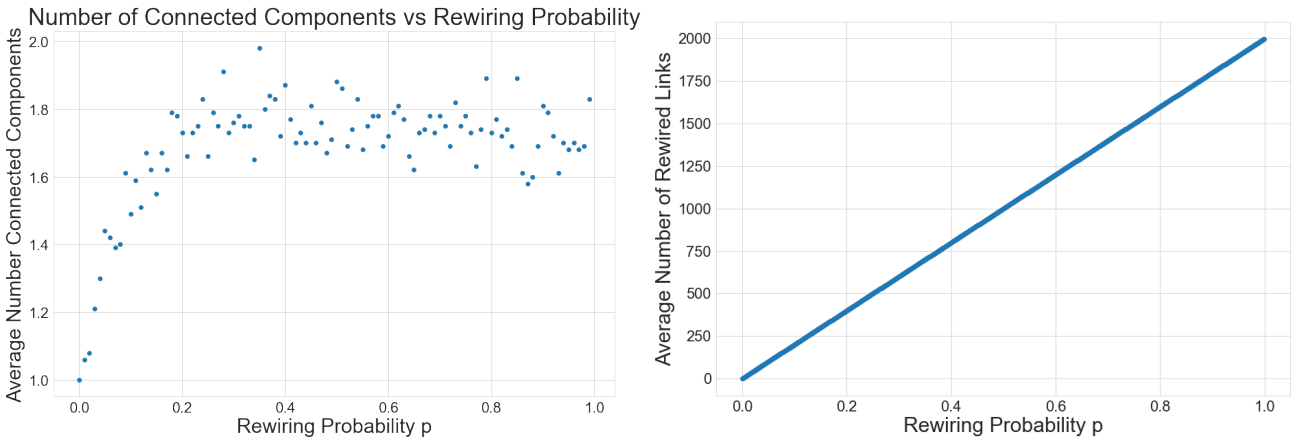

(a) WS(100, 2, p) for $p \in \{0, 0.01, 0.02, \ldots, 1\}$.

(b) WS(500, 4, p) for $p \in \{0, 0.001, 0.002, \ldots, 1\}$.

Figure 2.1.: (a) 100 simulation were run for every rewiring probability. Then, the average number of connected components vs rewiring probability $p \in \{0, 0.01, 0.02, \ldots, 1\}$ is shown for a perfect ring network with 100 nodes. (b) The rewiring probability $p \in \{0, 0.001, 0.002, \ldots, 1\}$ vs expected number of rewired links.

Firstly, p can be used to drive the network towards the small world property where the average shortest path length l decreases as the number of rewired links increases, as illustrated in Figure 2.2. This is used to classify ranges of the rewiring probability. These ranges are used in chapters 3 and 4. Firstly, values of $0 \leq p < 10^{-3}$ are considered "very small" where only small changes occur for l. Secondly, in the range $10^{-3} \leq p < 10^{-2}$ distinct changes happen and l reliably decreases which is referred to as "small". Thirdly, for $10^{-2} \leq p < 10^{-1}$ this trend continues but starts to flatten at the end which is called "intermediate". Fourthly, the decrease of l flattens further for "strong" rewiring $10^{-1} \leq p < 2 * 10^{-1}$. Lastly, l approaches its limiting case where almost no changes happen for "very strong" rewiring $2 * 10^{-1} = 0.2 \leq p \leq 1$.

Note that adding rewiring essentially equates adding randomness into a network or with other words, the regularity can be controlled. Using Watts-Strogatz networks has the advantages that both the randomness and the network density can be controlled on top of having a global ring structure. Therefore, they are the optimal choice to advance with and put non-linear dynamics on.

2.2. FitzHugh-Nagumo Model

The FitzHugh-Nagumo model comes from neuroscience and is a simplification of the Hodgkin-Huxley to isolate and describe the spiking behaviour of neurons [10]. Even though it is a paradigmatic model of brain neurons, it has a wider range of applications [11].

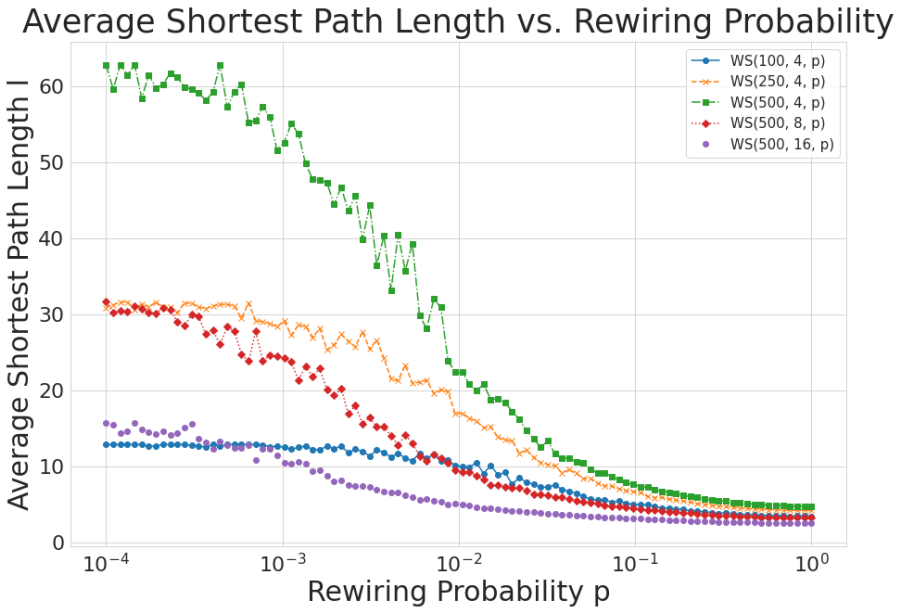

Figure 2.2.: The average shortest path length l over ten simulation runs is plotted against increasing rewiring probabilities p. Note that the most significant changes happen for rewiring probabilities $p \in [10^{-3}, 10^{-1}]$ across network configurations. In this thesis ranges of rewiring values are classified into value ranges which are used later: very small $p < 10^{-3}$, small $10^{-3} \leq p < 10^{-2}$, intermediate $10^{-2} \leq p < 10^{-1}$, strong $10^{-1} \leq p < 2 * 10^{-1}$ and very strong $2 * 10^{-1} = 0.2 \leq p \leq 1$.

2.2.1. Uncoupled Dynamics

The model is described by two coupled differential equations which represent fast and slow aspects of the dynamics where both are required to describe spiking behaviour. This is characterized by a (FitzHugh-Nagumo) neuron being in an equilibrium state. Then, a signal excites it causing the fast variable to spike, i.e. propagate a signal. With increasing time the slow variable is activated to dampen and return the dynamics to the equilibrium otherwise the neuron would fire constantly. The FitzHugh-Nagumo model equations are

$$\frac{dv(t)}{dt} = v(t) - \frac{v^3(t)}{3} - w(t) \tag{2.1}$$

$$\frac{dw(t)}{dt} = \frac{1}{\tau}(v(t) - bw(t) + a) \tag{2.2}$$

where $v(t)$ is the fast variable, $w(t)$ is the slow variable and a, b and τ are constant parameters. The parameter a is a threshold, where the neuron fires if a signal/perturbation is greater than it, otherwise remains in the equilibrium state. The parameter b represents the slope of the nullcline of the slow variable and $\frac{1}{\tau}$ represents an amount of $v(t)$ and $w(t)$ per time unit resulting in slow and fast dynamics. Thus, when $\tau > 1$ the phase velocity is slower in $w(t)$ direction than in $v(t)$ direction.

There are no explicit solutions to the FitzHugh-Nagumo model and it can only be solved graphically

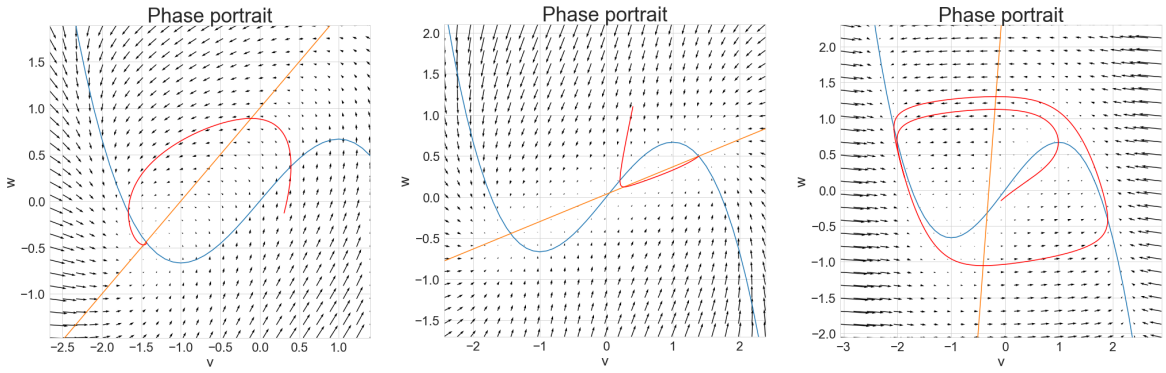

(a) $a = 1$, $b = 1$ and $\tau = 1$ (b) $a = 0.1$, $b = 3$ and $\tau = 1$ (c) $a = 0.3$, $b = 0.1$ and $\tau = 5$

Figure 2.3.: The choice of the model parameters in equations 2.1, 2.2 leads to qualitative changes in the dynamical behaviour shown in red where in (a) a stable fixed point exists, (b) the system is in a bistable regime with two stable and one unstable fixed point and in (c) the neuron is in a limit cycle regime. The nullclines are drawn in blue (Equation 2.3) and orange (Equation 2.4).

which relies on the nullclines of the variables:

$$\frac{dv(t)}{dt} = 0 \Rightarrow w(t) = v(t) - \frac{v^3(t)}{3} \tag{2.3}$$

$$\frac{dw(t)}{dt} = 0 \Rightarrow w(t) = \frac{1}{b}(v(t) + a). \tag{2.4}$$

Note that $\frac{1}{\tau}$ cancels but contributes to the velocities in the phase plane. The intersection of the nullclines is a euqilibrium point where the threshold parameter a shifts equation 2.4 up and down and b controls its the slope. The dynamical behaviour changes depending on the parameter choices. For example, the FitzHugh-Nagumo neuron can have a stable fixed point, be in a bistable regime or exhibit a limit cycle behaviour, as illustrated in Figure 2.3. In fact, eight bifurcations have been observed to occur in [12]. In this thesis, the parameters are chosen such that neurons exhibit a limit cycle behaviour and are referred to as FitzHugh-Nagumo oscillators or oscillators. Oscillations can be represented on the unit circle by mapping the positions on the curve into an angle on the unit circle. This angle is called phase and is used in following chapters. The choice of oscillatory units on the network is motivation by the periodicity observed in many biological systems and network. For example, on a microscopic scale, the cell cycle and circadian rhythm or on a macroscopic scale annual plants or solar cycle. Furthermore, in networks like those, the individual units do not exist in isolation but interact with their environment and/or each other.

2.2.2. Coupled Dynamics

The next step is to connect individual units. Hence, take $N \in \mathbb{N}$ identical FitzHugh-Nagumo oscillators where each one represents a node in a Watts-Strogatz network and couple them according to their neighbor relations. Consequently, a coupling term has to be introduced into the equations

$$\frac{v_i(t)}{dt} = v_i(t) - \frac{v_i^3(t)}{3} - w_i(t) + I_{n_i} \tag{2.5}$$

$$\frac{w_i(t)}{dt} = \frac{1}{\tau}(v_i(t) - b * w_i(t) + a) \tag{2.6}$$

where

$$I_{n_i} = \frac{\sigma}{N}\sum_{j=1}^{N} a_{ij}(v_i - v_j) = \frac{\sigma}{N}\sum_{j\, neighbor\, of\, i} (v_i - v_j). \tag{2.7}$$

The parameter $\sigma \geq 0$ is the coupling strength, then $\frac{\sigma}{N}$ is the scaled coupling and a_{ij} are the entries of the adjacency matrix.

Firstly, other coupling schemes exist, e.g. in the slow variable which is also a legitimate choice. However, the fast variable is of greater interest in this thesis. Secondly, the evolution of the system is impacted by the scaled coupling which is investigated in detail in section 5. Thirdly, compared to uncoupled dynamics the diameter of the limit cycle increases with an increasing scaled coupling, as illustrated in Figure 2.4. The interest is in the overall synchronizability thus the exact diameter of the limit cycle is negligible. Fourthly, the stronger the coupling the higher the influence FitzHugh-Nagumo oscillators have on each other which can result in speeding up the synchronization of a network. However, there are more nuances (described in section 5.1) and there is a critical scaled coupling when oscillators are locked and do not exhibit a limit cycle behaviour anymore. In this case, oscillators in the phase plane travel from the initial states to the limit cycle and then to the intersections of the nullcline in Equation 2.4 and the limit cycle where they become stationary, as shown in Figure 2.4d. The critical value strongly depends on network configuration. For example, in a small perfect ring network $WS(4, 2, 0)$ the critical scaled coupling $= \frac{\sigma}{N} = 5$, as illustrated in Figure 2.4d. A quantitative value range for scaled coupling and network density to lock the dynamics is shown in section 5.4d. In addition, shortly before the critical coupling is reached, there is a small value range where oscillators exhibit activity but do not synchronize, as illustrated in Figure 3.10e. Note that the focus of this thesis lies on emerging synchronization patterns thus, the locking of the system is not of interest and not pursued further. Lastly, the oscillators converge (more or less) individually to the limit cycle before the coupling takes effect, see Figure 2.4. Afterwards, they influence and perturb each other leading to not overlapping trajectories compared to the uncoupled scenario. The coupling between nodes causes them to "pull and

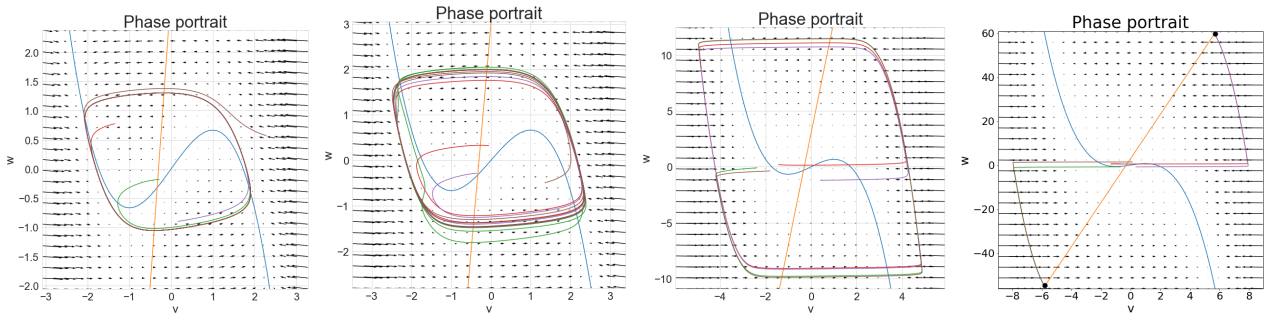

(a) $\sigma = 0$ (b) $\sigma = \frac{1}{2}$ (c) $\sigma = 5$ (d) $\sigma = 20$

Figure 2.4.: A small perfect ring network $WS(4, 2, 0)$ with FithHugh-Nagumo model parameters $a = 0.3$, $b = 0.1$, $\tau = 5$ and different coupling strengths. The nullclines are drawn in blue (Equation 2.3) and orange (Equation 2.4). The other colors correspond to single neurons starting in random initial states. (a)-(c) Note that the diameter of the limit cycle increases as the coupling is increased. (d) There is network dependent critical coupling which locks the oscillators in the sense that the limit cycle behaviour is suppressed. Starting from the initial states they move the the limit cycle where they converge to the nullcline in Equation 2.4 where they become stationary. In this network structure, the critical coupling strength $\sigma = 20$ which translates to a scaled coupling $= \frac{\sigma}{N} = 5$.

push" each other so that they merge in the phase plane, i.e. their phases are the same. This is called phase synchronization.

In the following the coupled dynamics 2.5, 2.6 are used to investigate the relation between emerging synchronization patterns on ring networks. The formation of patterns or behaviours on networks of interacting units is called emergent phenomenon. These are characterized as global (and often complex) behaviour that arises from simpler interacting units. For example, the magnetism of ferromagnets is a global property depending on the alignment of individual spins or birds/fish align with their nearest neighbors and form flocks/swarms. In the context of synchronization of oscillators extensive research has been done for Kuramoto oscillators as reviewed in [13] and [14]. The investigations cover various network types such as small-world networks [15] and scale-free networks [8] as well as different network generating models. Basically, in the Kuramoto model every unit is described by its natural frequency, a coupling constant and a sinusoidal coupling scheme which is the simplest model to investigate phase dynamics. In comparison, the FitzHugh-Nagumo model is more complex due to its non-linearity, excitability and recovery dynamics. Hence, potentially there are additional and more complex emerging synchronization patterns.

Note that a population of N oscillators has a $2 * N$-dimensional parameter space which makes it quite challenging to analyze. Thus, numerical simulations are used instead of trying to control it where the Euler method is used to approximate the differential equations. The underlying idea of this scheme is that the first derivative can be approximated with the tangent line which can only be used for first

order differential equations. Basically, this means that a curve can be approximated with the tangent on a known point. However, this is only true for a small enough neighborhood around that point. Additionally, the Euler method is ill suited for discontinuous initial value problems. Nevertheless, the FitzHugh-Nagumo model consists of first order differential equations which exhibit a continuous oscillation (for the parameter choice in this thesis). Then, the Euler method schemes is a step by step procedure for a first order initial value problem $\dot{x} = f(x)$ where the solution is unknown. The initial state x_0 is known and acts as the starting point for the approximation. Then, for fixed step size δt and number of steps $N \in \mathbb{N}$ the scheme is as follows:
Start: x_0
Iteration: $x_n = x_{n-1} + \delta t * f(x_{n-1})$, $n = 1, \ldots, N$.

Note that the approximation curve is a linear interpolation between the point $x_0, x_1, \ldots, x_N$ and the approximation error to the exact solution depends on the step size and number of steps. Nevertheless, the Euler method a widely used approximation scheme for numerical computations where an approximation to a solution suffices. [16]. In the setting of this thesis, the coupling between oscillators leads to their synchronization for small enough approximation error which was reliably observed for $\delta t = 10^{-2}$ so that it is not needed to carefully deal with the error in the further analysis. Additionally, the use of the Euler method in numerical simulations lead to the use of time steps t_s and corresponding values of the fast variable $v(t_s)$ where the number of time steps is given by $= \frac{simulation\,run\,time}{step\,size} = \frac{T}{\delta t}$.
Sidenote: The larger a network the higher the computational complexity. Therefore, to guarantee the feasibility of numerical simulations and that oscillators can synchronize the number of time steps is set to be $\frac{T}{\delta t} = 2,000 * 10^2$ for network sizes $N < 100$, $\frac{T}{\delta t} = 1,500 * 10^2$ up to network sizes $n = 500$ and $\frac{T}{\delta t} = 1,000 * 10^2$ for network sizes $N = 1,000$.

2.3. Order Parameter for the Global Coherence

Coherence is collective property in a network of oscillators and a order parameter is introduced to quantify it and make it comparable. Additionally, by scaling this measure to be in the interval $[0, 1]$, it becomes a parameter describing the ratio of synchronously firing units on the network [17]. Additionally, the evolution of a system is encoded in the order parameter, thus emergent synchronization patterns. This is used to distinguish between qualitatively different synchronization patterns in sections 3.6 and 5.2. With that in mind, the following coherence measure is used which is inspired by [17] and calculated

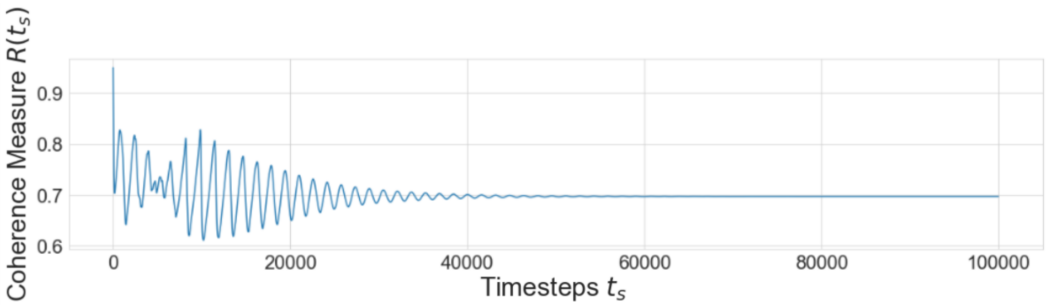

Figure 2.5.: The coherence measure converges to a coherence state in this simulation run using a Watts-Strogatz network with $N = 1,000$ nodes, $k = 200$ neighbors, $p = 0$ rewiring probability and $\frac{run\,time}{step\,size} = \frac{T}{\delta t} = 1,000 * 10^2$ time steps. The parameters for the FitzHugh-Nagumo dynamics are $a = 0.3, b = 0.1, \tau = 5$ and scaled coupling $= \frac{1}{100}$.

according to

$$R(t) = 1 - \hat{R}(t) = 1 - \frac{1}{N^2} \sum_{i,j=1}^{N} \frac{(v_i(t) - v_j(t))^2}{c^2} \tag{2.8}$$

where $c = max(limitcycle) - min(limitcycle)$ of the fast variable on the limit cycle. Note that $R(t) = 1$ corresponds to total synchronicity and $R(t) = 0$ corresponds to total asynchronicity. To measure the fast variable v suffices since in a coupled system like this since the slow variable w follows. Note that the exact value of the coherence measure differs when v or w is measured. This is caused by different phase velocities along the limit cycle where oscillators move slower in w direction and thus remaining longer there compared to v direction. Resulting in a higher coherence value when the measure is used for w. Further, the main role of w in the original dynamics is to return the system into its equilibrium state, whereas v causes the spiking behaviour. Therefore, v is of more interest. Nevertheless, the measure exhibits the same qualitative behaviors for both variables.

Note that (i) the normalization of the coherence measure leads to a restricted choice for initial states. They have to be taken from within the limit cycle, otherwise the normalization factor c could result in $R(t) < 1$. (ii) For the parameter choice $a = 0.3$, $b = 0.1$ and $\tau = 5$ the interval $[-2, 2]$ is contained in the limit cycle for the fast variable. Therefore, initial states $v_i(0), w_i(0)$ are drawn from $[-2, 2]$ according to a uniform distribution for all i throughout the thesis.

Now, the evolution of the coherence measure for a network of FitzHugh-Nagumo oscillators with random initial states is illustrated in Figure 2.5. At first, oscillators approach the limit cycle before the coupling takes effect. Then, as it takes effect, they try to align in terms of phases which results in oscillations of the coherence measure. Afterwards, as the network synchronizes, the amplitude of the oscillation of the measure decreases and it converges to a coherence state. There are other behaviours of the coherence measure which are covered in section 3.6.

2.4. Fast Fourier Transform

The Fourier Transform is the foundation of the most commonly used algorithms for signal processing. Its application are broad from seismology [18] to magnetic resonance imaging [19]. One of these algorithms is the Fast Fourier Transform (FFT) which is an efficient computational tool which transforms a signal from the time domain into its frequency representation. More precisely, it decomposes a given function into a weighted sum of basic functions which encode the frequency spectrum. Then, amplitudes, frequencies and periods can be determined for further use. Moreover, the input for the FFT is a discrete set which is given by the Euler method in this thesis. This is used to analyze and compare the frequency spectra of the coupled oscillators. Then, for a discrete set of $n \in \mathbb{N}$ samples the FFT uses the discrete Fourier Transform:

$$A_k = \sum_{s=0}^{n-1} a_s e^{-2\pi i s \frac{k}{n}} \tag{2.9}$$

where $e^{-2\pi i \frac{k}{n}}$ are the n^{th} roots of unity. The roots divide the complex unit circle into $\frac{2\pi}{n}$ radians representing frequency components and by the Nyquist theorem the largest frequency that can be detected depends on the sampling rate. Those lead to technical restrictions which are not further elaborated. A more in-depth description on the FFT can be found in [20] or [21].

On the one hand, the FFT is used to analyze the activity of nodes on the network where differences in the frequency spectra are caused by the coupling. However, there might only be minor discrepancies since all oscillators are identical. For example, in the uncoupled case the frequency spectra are nearly identical while nodes are in distinct phases. It is called frequency synchronization when frequencies of the individual units of a network become more and more similar. On the other hand, the coherence measure can be analysed with the FFT to obtain insights. For example, low magnitude indicates convergence to a coherence state, as it can be observed in Figure 2.5. This is further described in sections 3.2 and 3.6.

2.5. Summary Model Description

In this thesis, numerical simulations are used to investigate the connection between networks with global ring structure and emerging synchronization patterns of coupled FitzHugh-Nagumo oscillators. For that purpose, Watts-Strogatz networks are used since the regularity, density and randomness can be controlled well. For further analysis an order parameter is introduced in the form of a coherence measure. Additionally, the FFT is utilized to investigate oscillations of individual units and the coherence measure.

The assumptions are that:

- only unweighted, undirected and connected networks without self-loops are used
- networks consist of identical FitzHugh-Nagumo oscillators and
- the coupling is the same along all links.

In the following chapter, visualizations of FitzHugh-Nagumo dynamics on ring networks are introduced. Moreover, the appearing patterns are described and interpreted so that they can be used to identify synchronization patterns.

3. Methods to Visualize FitzHugh-Nagumo Dynamics on Networks

With the FitzHugh-Nagumo model and Watts-Strogatz network introduced and the underlying assumptions stated the next steps can be taken. In the following, the dynamics are visualized from different aspects to study emerging patterns in them. The aim is to identify occurring phenomena and interpret them such that they can be used to identify synchronization patterns. In order to achieve that, a class was implemented in Python to simulate FitzHugh-Nagumo dynamics on a network of interest as well as a variety of visualizations to explore different aspects of synchronization. Those can be found in the GitHub repository "FitzHugh-Nagumo-on-Networks" [22]. The computational complexity increases in a non-linear fashion for stepsize in the Euler method, network size and simulation run time. Therefore, the stepsize $\delta t = 10^2$ is fixed throughout the thesis. Note that choosing a programming language is accompanied by peculiarities, e.g. nodes in a Watts-Strogatz network are enumerated counterclockwise. In the following, the appearing patterns in different visualizations are introduced and what they represent so that synchronization patterns can be discussed in the next chapter. This chapter is organized as follows: In section 3.1 behaviours in the phase plane are discussed, in section 3.2 node activities and corresponding frequency spectra are studied, in section 3.3 the spatiotemporal propagation of the node dynamics are explored, in 3.4 chimera patterns are delved into, in section 3.5 the heatmap of the activity matrix is analyzed. and in section 3.6 the evolution of the coherence measure is described.

3.1. Evolution in the Phase Plane

Since every oscillator is described by differential equations it is reasonable to investigate trajectories in the phase plane. However, if the entire trajectories of every node on the network are plotted, they overlap and not much insight can be gained. Therefore, individual oscillators are represented as red dots following their trajectories which depends on initial states and the parameter choice in the FHN model. Then, the positions can be observed for any given time step and a pattern identified corresponding to the evolution of the network.

In this regard, the fast variable v is on the x-axis and the slow variable w is on the y-axis of the phase plane. Additionally, the nullclines are drawn in blue and orange. Then, the limit cycle behaviour of the dynamics is visualized in the phase plane by generating sequences of images (and/or generating a video/GIF). Initial states $(v_i(0), w_i(0))$ are drawn uniformly at random from $[-2, 2] \times [-2, 2]$ $\forall i$. Initially, it appears that oscillators travel to the limit cycle individually before the coupling takes effect. Then, as the coupling takes effect oscillators perturb each other such that the trajectories are contained in a tube around the limit cycle. Then, as the network gets more coherent oscillators form clumps in the phase plane indicating that phases synchronize. Additionally, closeness of trajectories to the limit cycle indicate that frequency spectra of individual nodes are similar which is independent of network size. However, this does not imply similarity of phases which can be observed in Figure 3.1.

There seem to be two long-term behaviours for oscillators in the phase plane:

(i) Oscillators synchronize and distribute evenly on the limit cycle such that there exist phases $\theta_1, \ldots, \theta_m$ where $2 < m \leq N$ corresponding to the number of clumps on the limit cycle, as illustrated in Figure 3.1. This is the most common synchronization pattern which indicates that there are waves travelling on the network. However, this is the case for all except one synchronization pattern so that further visualizations are required.

(ii) Oscillators synchronize where only two clumps exist which corresponds to two phases θ_1, θ_2: as illustrated in Figure 3.2. This corresponds to the blinking pattern synchronization which is described in 4.2.

In summary, by illustrating oscillators as dots on their trajectories for a fixed time step makes it possible to observe their positions in the phase plane. Enabling to visualize phase synchronization when clumps are formed. Moreover, the blinking synchronization pattern can be identified. Additionally, the closer trajectories are to the limit cycle the higher the similarity of frequency spectra. A natural next step is to investigate the activity of individual nodes.

3.2. Individual Node Analysis

The phase plane illustrates the dynamical behaviour and synchronization is shown in terms of closeness to the limit cycle and clumps of oscillators. Since the synchronization of oscillators is strongly reflected in their time series it is sensible to look at the time domain. Similarities in the exhibited oscillation can be inspected by eye to a certain degree and investigated in greater detail with a frequency analysis using the FFT. For that purpose the final $10,000$ time steps of a simulation run are used.

Firstly, the activities of all oscillators i in the fast variable $v_i(t_s)$ are plotted. Even though the network size might be large the plot appears more or less regular depending on the coherence. If nodes have

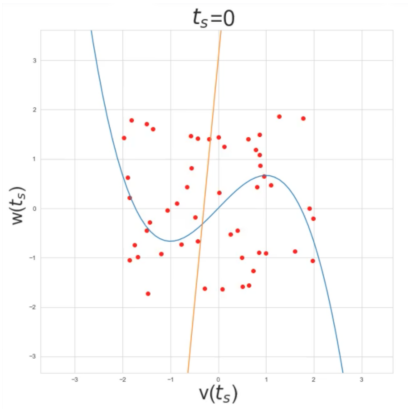

(a) Dynamics at initial states.

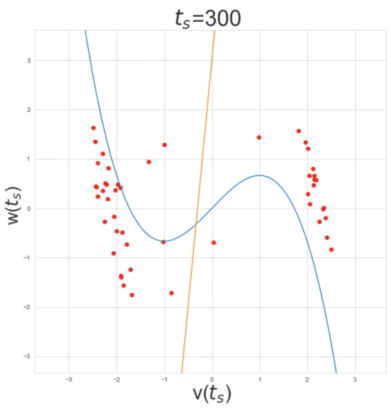

(b) Oscillators get close to the limit cycle.

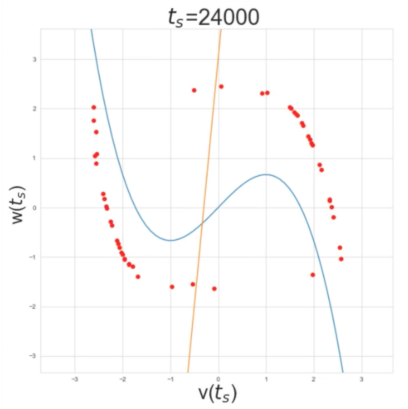

(c) Oscillators run along limit cycle.

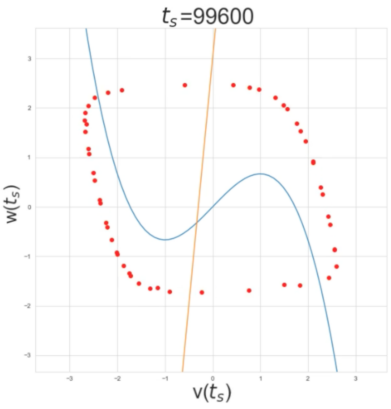

(d) Oscillators distribute along limit cycle.

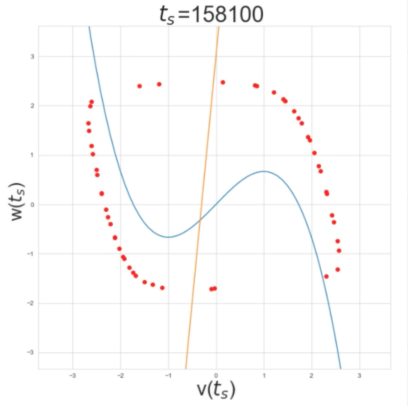

(e) Oscillators spread more evenly along limit cycle.

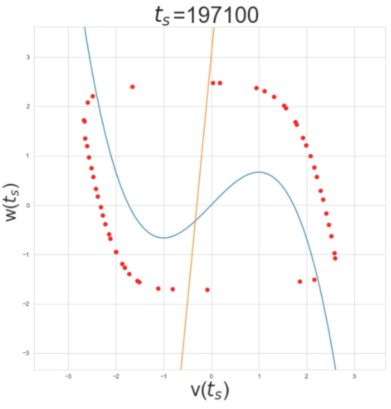

(f) The oscillators find a steady state.

Figure 3.1.: A small perfect ring network $WS(50, 2, 0)$, FithHugh-Nagumo model parameters $a = 0.3$, $b = 0.1$, $\tau = 5$, a scaled coupling $\frac{1}{5}$ and $\frac{T}{\delta t} = 2,000 * 10^2$ time steps are used. The initial states are drawn uniformly at random from $[-2, 2]$ which impacts the emerging pattern. Note that the same parameter values are used in Figure 3.2 where the only difference is the initial states. To map out the space of initial states is not feasible due to its high dimensionality. Nevertheless, tendencies can be observed by controlling the coupling strength which is described in sections 4.2 and 4.3. The sequence of plots shows the oscillators in the phase plane at different time steps t_s (in the title). (a) All oscillators are at their initial states. (b) Within relatively few time steps the oscillators go to the limit cycle but are perturbed by the coupling such that they move within a tube around the limit cycle. (c) The oscillators run along the limit cycle within a reasonable amount of time steps. (d), (e) and (f) the oscillators try to distribute themselves evenly along the limit cycle suggesting they find a steady state.

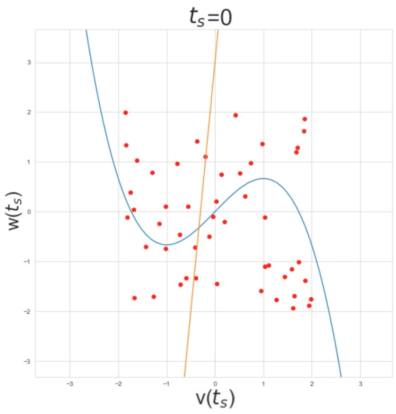

(a) Dynamics at initial states.

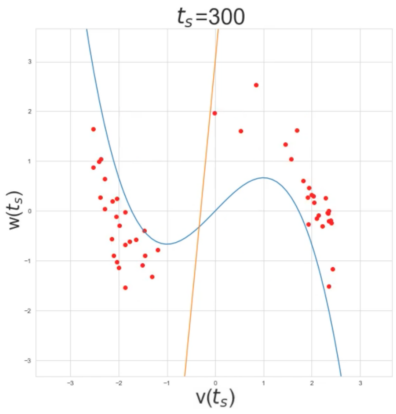

(b) Oscillators get close to limit cycle.

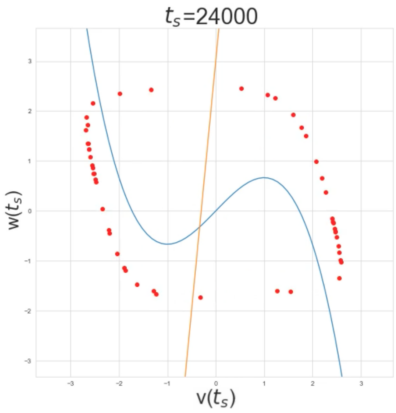

(c) Oscillators run along limit cycle.

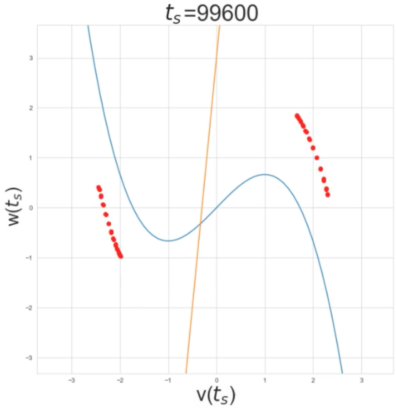

(d) Oscillators clump together.

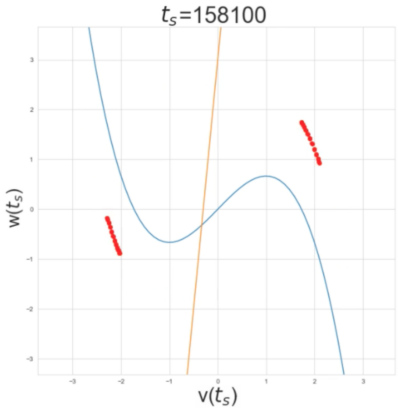

(e) The clumps get smaller.

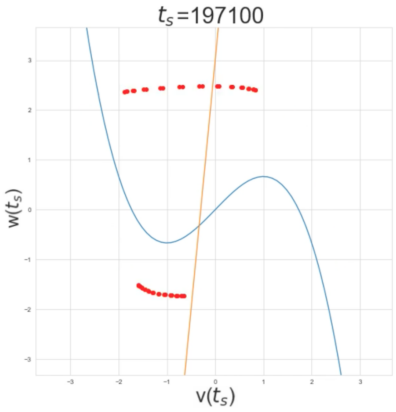

(f) The oscillators find steady state.

Figure 3.2.: A small perfect ring network $WS(50, 2, 0)$, FithHugh-Nagumo model parameters $a = 0.3$, $b = 0.1$, $\tau = 5$, a scaled coupling $\frac{1}{5}$ and $\frac{T}{\delta t} = 2,000 * 10^2$ time steps are used. The initial states are drawn uniformly at random from $[-2, 2]$ which impacts the emerging pattern. As described in Figure 3.1, the emergent synchronization pattern is influenced by the initial states where tendencies are observed by manipulating the scaled coupling in sections 4.2 and 4.3. The sequence of plots shows the oscillators in the phase plane at different time steps t_s (in the title). (a) All oscillators are at their initial states. (b) Within relatively few time steps the oscillators go to the limit cycle but are perturbed by the coupling such that they move within a tube around the limit cycle. (c) The oscillators run along the limit cycle within a reasonable amount of time steps. (d) As time steps increase further the oscillators clump together on the limit cycle. (e) The clumps of oscillators get smaller, i.e. the phases get more similar. (f) The oscillators appear to find a steady state.

the same phase the corresponding oscillations overlap. For the blinking network synchronization this means that there are only two oscillations visible in the node activity which is illustrated in appendix section A.1. Therefore, if oscillations do not overlap then multiple phases exist and there are waves travelling on the network. Recognizing the regularity of the node activity is the extend of visual inspections. Nevertheless, it suggests similarity of the oscillators. To verify that, the FFT is used to transform the activity of $\lceil\sqrt{N}\rceil + 1$ randomly sampled nodes into the frequency domain where $\lceil . \rceil$ is the ceiling function and N the network size. For example, in a network of 200 nodes the frequency spectra for $\lceil\sqrt{200}\rceil + 1 = 16$ nodes are taken. In Figures of the frequency analysis, labels on the x-axis are $\frac{1}{frequency}$ = period and the magnitude on the y-axis. Furthermore, the frequencies are represented using a hat function where the peaks indicate the frequencies. Otherwise, when frequencies are nearly identical they overlap and reveal little by using classical vertical bars. Note that the similarity of frequencies does not imply phase coherence.

Based on the previous section, if the trajectories are close to the limit cycle for all oscillators then the exhibited activity is nearly identical resulting in a regular pattern in the plot. If they are in a tube around the limit cycle the pattern becomes less regular. However, the node activity pattern shows small differences since all oscillators are identical and relatively close to the limit cycle, as illustrated in Figure 3.3. Secondly, if oscillators on the network exhibit nearly identical oscillations thus nearly identical frequency spectra then the activity of an arbitrary node can be used as representative. In the implementation node 1 is always taken as representative. Then, frequency analysis of this single oscillation is performed where the plot uses again $\frac{1}{frequency}$ = period on the x-axis and the magnitude on the y-axis, see Figure 3.4. Illustrating a representative oscillation enables to extract the length of the period from the plot. In the following, this is used to compare different network structures and scaled couplings. However, the length of period of oscillator increases with the scaled coupling. When periods become too large it leads to a faulty frequency analysis of the FFT due to its technical limitations, as illustrated in Figure 3.5. This is investigated in more detail in section 5.1.

In summary, similarities in the exhibited oscillations and frequency spectra are visually captured by the individual node analysis indicating synchronization of frequencies but not phases. Additionally, when the node activity indicates similarity of oscillators as well as the frequency spectra of randomly sampled nodes then a representative oscillation can be taken. Then, the length of period can be extracted and compared for network structures and scaled coupling. In the following, the node activity is visualized directly on a network to illustrate the synchronization on it.

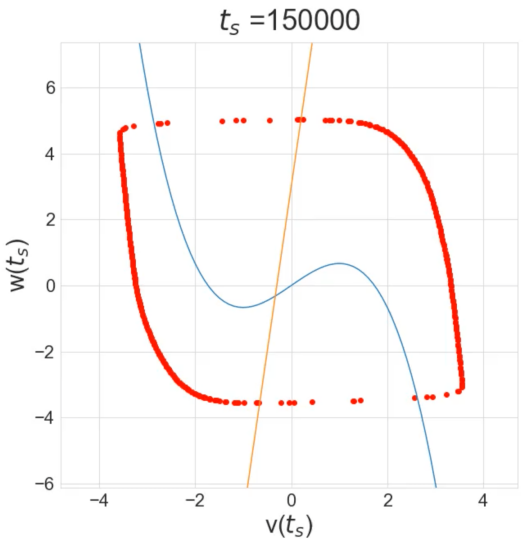

(a) Oscillators are at the limit cycle.

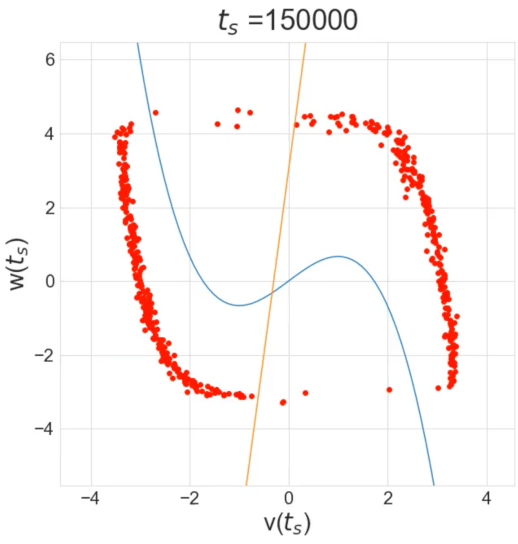

(b) Oscillators are scattered around the limit cycle.

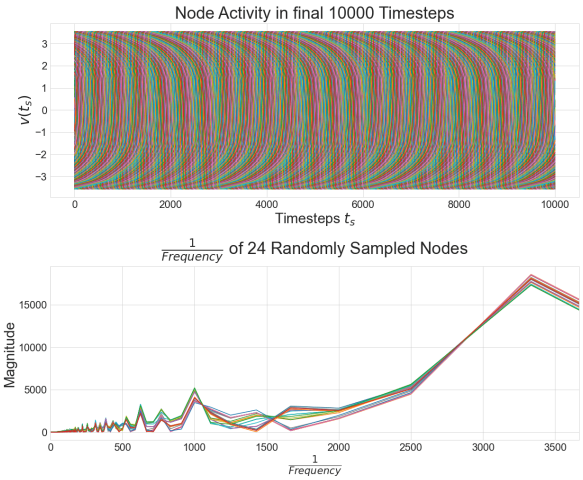

(c) The node activity is very regular and frequency spectra are nearly identical.

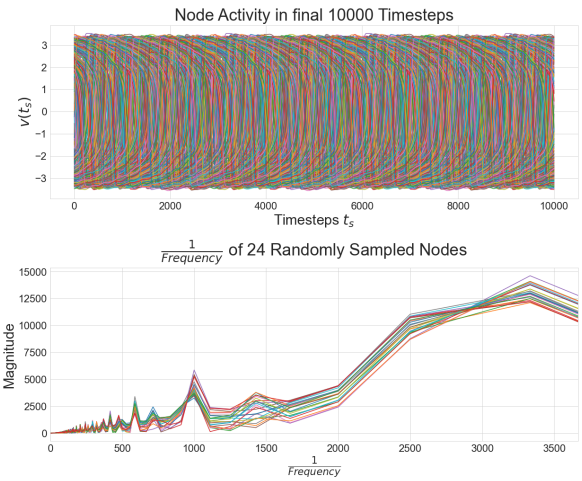

(d) The node activity is less regular and frequency spectra have more discrepancies.

Figure 3.3.: The closeness of oscillators to the limit cycle in the phase plane indicate similarity of the frequency spectra. (a)+(c) The oscillators are travelling on the limit cycle indicating similarity of frequencies which is confirmed by the node activity and the frequency spectra of randomly sampled nodes. In this plot a $WS(500, 100, 0)$, FithHugh-Nagumo model parameters $a = 0.3$, $b = 0.1$, $\tau = 5$ with scaled coupling $\frac{1}{50}$ are used and a total simulation run time of $\frac{T}{\delta t} = 1,500 * 10^2$ time steps. (b)+(d) The oscillators are scattered around the limit cycle. Nevertheless, the activity of nodes still exhibit a regular pattern with small discrepancies. The corresponding frequency analysis of randomly sampled nodes also is nearly identical with small differences. In this plot a $WS(500, 16, 0.01)$, FithHugh-Nagumo model parameters $a = 0.3$, $b = 0.1$, $\tau = 5$ with scaled coupling $\frac{1}{10}$ are used and a total simulation run time of $\frac{T}{\delta t} = 1,500 * 10^2$ time steps.

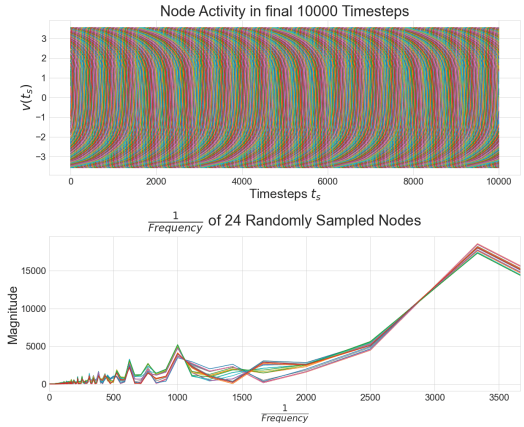

(a) Node activity of all nodes in the network and frequency spectra for randomly sampled nodes.

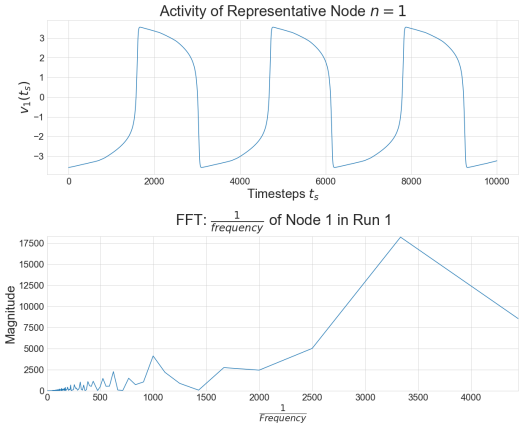

(b) A representative oscillator and its frequency spectrum.

Figure 3.4.: (a) The node analysis visualizes the node activity for the last 10,000 time steps. The pattern indicates high similarity of individual units on the network. This is confirmed by the frequency spectra obtained with the FFT for randomly sampled nodes. (b) A representative oscillation is illustrated and its frequency spectrum taken where $\frac{1}{frequency} =$ period is used on the x-axis. In this plot a $WS(500, 100, 0)$, FithHugh-Nagumo model parameters $a = 0.3$, $b = 0.1$, $\tau = 5$ with scaled coupling $\frac{1}{50}$ are used and a total simulation run time of $\frac{T}{\delta t} = 1,500 * 10^2$ time steps.

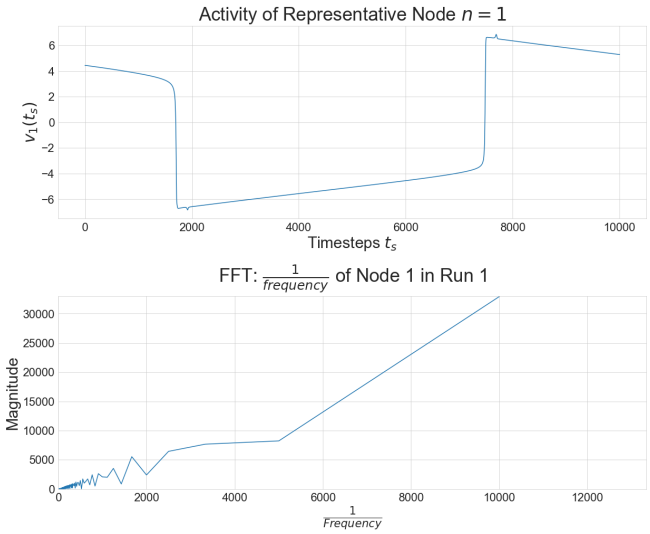

Figure 3.5.: A $WS(100, 4, 0)$, FithHugh-Nagumo model parameters $a = 0.3$, $b = 0.1$, $\tau = 5$, a scaled coupling $\frac{\sigma}{N} = 1.7$ and $\frac{T}{\delta t} = 1,000 * 10^2$ time steps are used. Then, the period of individual oscillators cannot be detected by the FFT due to its technical limitations. The length of periods increases with an increasing scaled coupling which is studied in section 5.1.

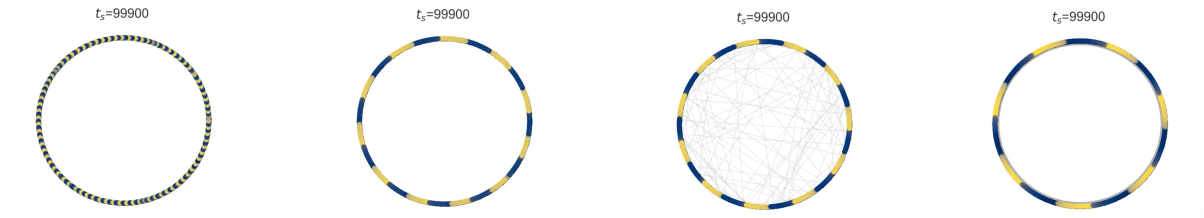

(a) WS(500, 8, 0) (b) WS(500, 64, 0) (c) WS(500, 64, 0.005) (d) WS(500, 100, 0)

Figure 3.6.: The scaled coupling $= \frac{1}{10}$ is the same for all network configurations and the wave lengths change due to the network density. FithHugh-Nagumo model parameters are set to $a = 0.3$, $b = 0.1$ and $\tau = 5$ and $\frac{T}{\delta t} = 1,000 * 10^2$ time steps are used.

3.3. Spatiotemporal Propagation of Individual Node Dynamics

So far, the dynamics are visualized in the phase space and as time series which is transformed into the frequency domain. Visualizing the activity directly on networks and therefore its evolution uncovers more about the spatiotemporal propagation of the FitzHugh-Nagumo dynamics. Furthermore, closeness of nodes in the plot of a Watts-Strogatz networks indicates neighbor relations. On the one hand, this highlights synchronization on a small scale of nearest neighbors. On the other hand, it visualizes emergent synchronization patterns on the global scale. To display the dynamics on networks the minimum and maximum value of the fast variable v on the limit cycle are taken to continuously assign colors to the interval $[minimum, maximum]$ from blue to yellow. Subsequently, for a fixed timestep t_s each node $i = 1, \ldots, N$ is colored according to $v_i(t_s) \in [minimum, maximum] = [blue, yellow]$. Then, emergent synchronization patterns can be observed as well as spatiotemporal propagation of the dynamics on the network by generating a sequence of images (and/or generating a video/GIF). The propagation of the dynamics on ring networks leads to the emergence of waves or travelling waves which travel either clockwise or counterclockwise. These waves are a generic phenomenon except for Watts-Strogatz networks with high randomness as evaluated in section 4.6. Note that one wave corresponds to one oscillation of the emergent pattern on the global network scale. The length of a single wave and therefore the maximal number of waves depends on the scaled coupling and the network structure especially on the network density, as illustrated in Figure 3.6. Note that for rewiring probabilities up to the intermediate range the wave length is unaffected.

Following that, in a Watts-Strogatz network of a fixed network size N and rewiring probability $p = 0$. Then, the lower the number of neighbors the shorter global waves become. Enabling a higher number of coexisting global waves. The intuition behind this phenomenon is that a higher number of neighbors leads to a higher degree of influence on each node. Therefore, the phase of individual nodes has to be better aligned with its neighbors allowing for fewer global waves. At $t_s = 0$ the colors on the network are distributed according to the uniformly random initial states $v_i(0)$ for all $i = 1, \ldots, N$.

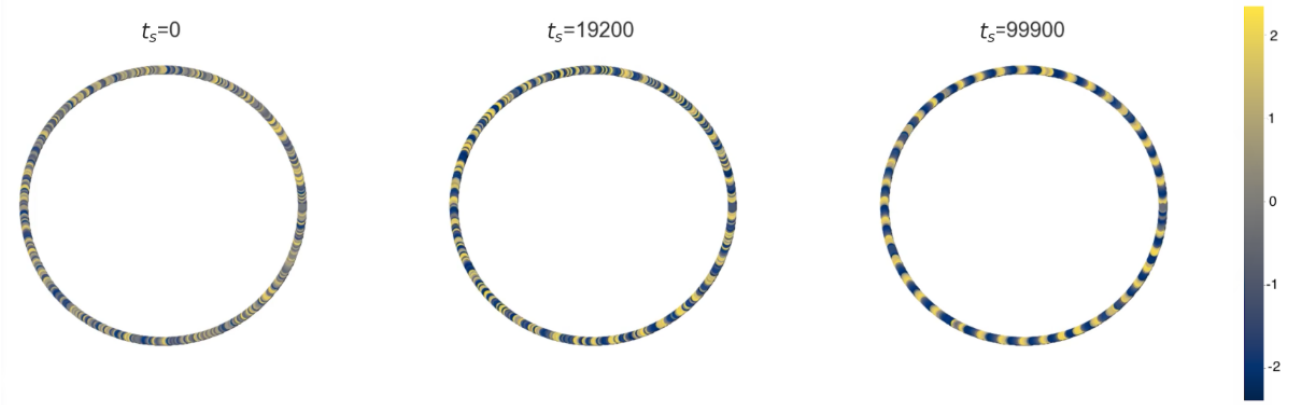

Figure 3.7.: The pattern formation can be observed directly the network of interest. At first the color pattern is random corresponding to the initial states. Then, after $\approx 20,000$ time steps patterns can be observed to emerge. Then, with increasing time steps the network synchronized leading to a pattern formation. Also, the spatiotemporal propagation of the FitzHugh-Nagumo dynamics can be revealed using sequences of images (or videos). In this plot a $WS(500, 16, 0)$, FithHugh-Nagumo model parameters $a = 0.3$, $b = 0.1$, $\tau = 5$, a scaled coupling $\frac{1}{100}$ and $\frac{T}{\delta t} = 2,000 * 10^2$ timesteps are used. The colorbar continuously assigns colors from blue to yellow to the fast variable v on the limit cycle.

Then, within relatively few time steps patterns start to emerge on the network as it can be seen in Figure 3.7. Oscillators adapt to each other within $20,000$ time steps leading to travelling waves. Note that this happens when the scaled coupling is above a minimal value so that oscillators influence each other and below a critical value, as discussed in section 2.2.2. The direction waves travel (clockwise or counterclockwise) depends on the initial states which was not investigated further. If waves travel in only one direction then it is referred to as global wave synchronization, as described in section 4.3. If there are waves travelling in opposite directions this implicates that there are regions where they are emitted which are referred to as generating regions. Alongside, there are regions where they clash and annihilate each other which are referred to as annihilating regions. The number of generating and annihilating regions on the network depends on the network structure and scaled coupling. Where exactly these regions manifest seems to depend on the initial states which was not investigated further. Besides that, there is always an even number of generating and annihilating regions. Assume there exist a generating region on the network. Then, waves are emitted in both directions on the ring network and ultimately clash and annihilate each other in a different region. Therefore, generating and annihilating regions always appear in pairs and are referred to as region pair. This synchronization pattern is referred to as region pairs, as described in section 4.4. Note that it is ambiguous how to collect regions into pairs from this terminology and thus depends on the context. In the visualization of the spatiotemporal propagation it is suggested that there is a standing wave phenomenon at region pairs which is further scrutinized with other visualizations.

In summary, synchronization patterns on the network are revealed by using sequences of images.

Moreover, the propagation direction of waves can be extracted which enables to identify global wave and region pair synchronization. Additionally, it is suggested that at region pairs there is a standing wave phenomenon. Hence, to investigate this observation and to visualize the coherence of a network are the next steps.

3.4. Chimera Pattern Plot

So far, synchronization of oscillators is shown in the phase plane, as time series with corresponding frequency spectrum and as global pattern. However, phase synchronization is challenging to extract from these. Therefore, the fast variable v (which corresponds to phases) is utilized to illustrate coherence of a network. First of all, chimera states were discovered by Abrams and Strogatz and refer to spatial regions of coherence and incoherence on the same network of identical Kuramoto oscillators [23]. In networks of identical oscillators the terminology chimera pattern is used most commonly.
In the plot the node labels $n = 1, \ldots, N$ are used on the x-axis and the fast variable $v_n(t_{snapshot})$ on the y-axis for a fixed time step $t_{snapshot} \in \{t_s : 0 \leq t_s \leq \frac{T}{\delta t}\}$. Oscillators are shown as blue dots to clearly distinguish them from the phase plane plot. To meaningfully visualize chimera patterns $t_{snapshot}$ is chosen after the onset of synchronization where the coupling took effect. Chimera states are often long lived transients and the lifetime increases with the network size [24]. A visual analysis of the evolution of chimera patterns can be made by generating a sequence of images (and/or generating a video/GIF). This plot is especially useful for ring networks since node labels indicate spatial closeness and neighbor relations. Also, due to the ring topology nodes 1 and N are neighbors making the borders of the plot periodic. In the sense that shifting node labels $i \mapsto i \pm l \, mod \, N$ for $l \in \mathbb{N}$ would shift the pattern to the left or right. Despite that, the chimera plot is not restricted to ring networks [24].

In Figure 3.8 different scenarios are showcased to interpret the appearing patterns. Firstly, patterns are inspected which do not represent chimeras, i.e. the entire network is either in a coherent or incoherent state. In a completely coherent network the individual oscillators are phase locked resulting in a horizontal line as illustrated in Figure 3.8a. This synchronization pattern is called global coherence which is discussed in section 4.1. In a network of global wave synchronization the chimera pattern is composed of arc shapes which represent waves on the network, see Figure 3.8b. Since these waves propagate on the network the arcs have to travel to either the left or right hand side and the direction is indicated by the opened side of arcs. Note that the number of global waves on the network can be counted in the chimera plot which can be used to approximate the number of nodes in one wave. In other words, the curvature of arcs indicates the wave length. For example, in Figure 3.8b there are $\frac{network\,size}{number\,of\,waves} \rightarrow \frac{1{,}000}{7} = 142.8 \approx 142$ nodes per wave. This suggests that wave lengths can vary slightly

or that nodes exist which are between two waves (phase wise). Furthermore, the opened side of arcs indicates that waves propagate to node of decreasing label numbers which corresponds to clockwise propagation on the network. Additionally, generating a video of the evolution of the chimera pattern shows that waves travel across the plot (in the opened direction of the arc). Note that one wave crosses over the boundary at node $1,000$ to node 1 showcasing the periodicity of the plot.
Besides that, dots congregate at the top and bottom parts of the plot whilst the middle is sparse. Inspecting the phase velocities on the limit cycle (Figure 2.4) note that in areas where v is close to its minimum/maximum oscillators move mostly in the direction of the slow variable w. Consequently, spending more time there in comparison to when v takes values around zero where the oscillators move mostly in the direction of the fast variable v. As a result, spending little time in the middle range of values of v. In contrast, Figure 3.8c illustrates a completely incoherent network corresponding to chaotic pattern which is covered in section 4.6. Here, oscillators do not agglomerate in the top and bottom parts of the plot as before.

Secondly, utilizing these insights to interpret the pattern in Figure 3.8d yields that there is a larger region of coherence which correspond to a generating region from which travelling waves are emitted. Therefore, this pattern corresponds to region pair synchronization which is analyzed in section 4.4. The annihilating region can be identified by following the waves until two arcs face each other. In this plot this is the case around node 180. Additionally, there seems to be a region of incoherence. However, this is an artefact of the time step the snapshot is taken. Since there are generating and annihilating region with waves travelling between them there cannot be a region of incoherence on the network. Besides that, region pairs correspond to clumps of nodes which are locked together in the chimera plot, as illustrated in Figure 3.8e. This also represents a region pair synchronization for a different network structure, as explored in section 4.4. Note that waves are emitted from generating region in both directions and approach annihilating regions from both directions. Therefore, nodes in these regions have to exhibit a standing wave phenomenon.
In spite of that, detecting region pairs can be challenging if they are spatially close on the network and/or one region is close to node 1/node N. Both of these cases are present in Figure 3.8e. Additionally, the arc shape representing waves is less pronounced. In contrast to travelling waves the number of global waves cannot be counted. On the one hand, generating and annihilating region are not travelling waves and therefore should not be counted. On the other hand, the number of waves depending on the time of the snapshot. If it is taken at a timepoint where two waves are generated such that they are still part of the generating region then it would have to be counted as two waves. The same holds for annihilating regions when waves clash. Nevertheless, region pairs can be identified by closely inspecting

the pattern. For example, in Figure 3.8e on the sides of node 260 vertically ordered oscillators are tilted such that the opened arc side is facing away. Therefore, this is a generating region and the regions next to it must be annihilating regions. However, identifying regions in this step by step fashion is not sensible.

Note that oscillators that are around the top of the plot ($v_k \approx 3$) are at the peak of the oscillation. Then, the horizontal line below are oscillators that are the direct neighbors of nodes at the peak and so on. Since they are located on these tilted lines that signifies that there are slight differences in the phases of oscillator which are part of different travelling waves (=tilted vertical lines). These small discrepancies between phases corresponds to the observation in the phase plane where oscillators align evenly along the limit cycle.

Lastly, if region of coherence and incoherence exist simultaneously on the network then the pattern becomes challenging to extract information from, as illustrated in Figure 3.8f. This pattern corresponds to chimera patterns which are discussed in section 4.5. Neither regions with travelling waves nor region of incoherence are distinct such that the pattern is reminiscent of the chaotic pattern. The main difference is that nodes tend to accumulate at top and bottom regions. However, another visualization is utilized to reliably distinguish them.

Nevertheless, if wave directions can be identified then combine the chimera pattern plot and the spatiotemporal propagation on the network. Then, wave directions can be extracted and linked to the synchronization pattern directly on the network, as illustrated in Figure 3.9.

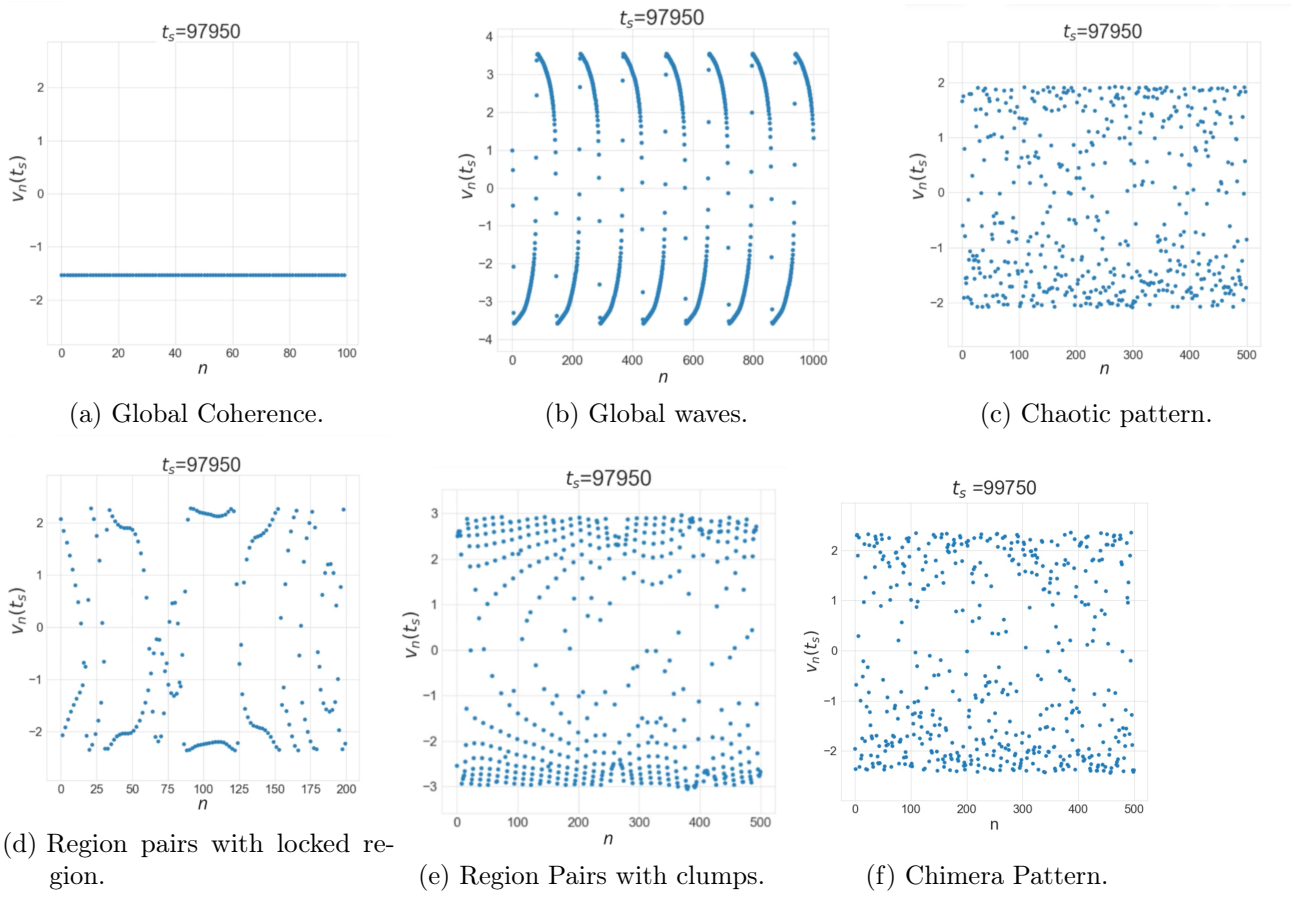

(a) Global Coherence.

(b) Global waves.

(c) Chaotic pattern.

(d) Region pairs with locked region.

(e) Region Pairs with clumps.

(f) Chimera Pattern.

Figure 3.8.: Showcase of different chimera pattern plots corresponding to emergent dynamics for FithHugh-Nagumo model parameters $a = 0.3$, $b = 0.1$ and $\tau = 5$. (a) All oscillators are phase locked in a totally coherent network resulting in a line in a $WS(100, 20, 0)$ where all initial states are equal to obtain global coherence, as described in section 4.1. (b) There are only waves traveling in one direction on the network represented as arcs in a $WS(1,000, 200, 0)$ with scaled coupling $= \frac{1}{100}$. (c) The network of oscillators is totally incoherent in a $WS(500, 8, 0.4)$ with scaled coupling $= \frac{1}{50}$. (d) There are two region pairs on the network making the pattern more challenging to read in a $WS(200, 2, 0)$ with scaled coupling $= \frac{1}{10}$. Oscillators are phase locked in a generating regions (between node 80 and node 120 and around node 50). From there waves are emitted which clash around node 180. The other annihilating region is between nodes 50 and 80 making it challenging to identify. Potentially misclassifying the area as region of incoherence. (e) Network with region pairs which are challenging to identify in a $WS(500, 16, 0)$ with scaled coupling $= \frac{1}{10}$. One annihilating region is close to nodes $1/N$, one generating region is around node 260 and the other region pair is around nodes 380 and node 420. The two region pair plots indicate discrepancies in synchronization patterns in dependence of the network structure. (f) Network with chimera pattern where regions of coherence and incoherence exist. However, it is challenging to identify those regions and another visualization is required. For example, around node 430 vertical lines vaguely resemble arcs. The major difference to the chaotic pattern is that oscillators tend to agglomerate at top and bottom regions of the plot. This pattern emerged in a $WS(500, 16, 0.1)$ with scaled coupling $= \frac{1}{50}$.

In summary, global coherence, global waves, region pairs are revealed in the chimera pattern plot. Additionally, the propagation direction of waves can be read. However, when chimera patterns manifest it becomes challenging to extract information from the plot. Therefore, another visualization is required to reliably detect and identify regions of coherence and incoherence.

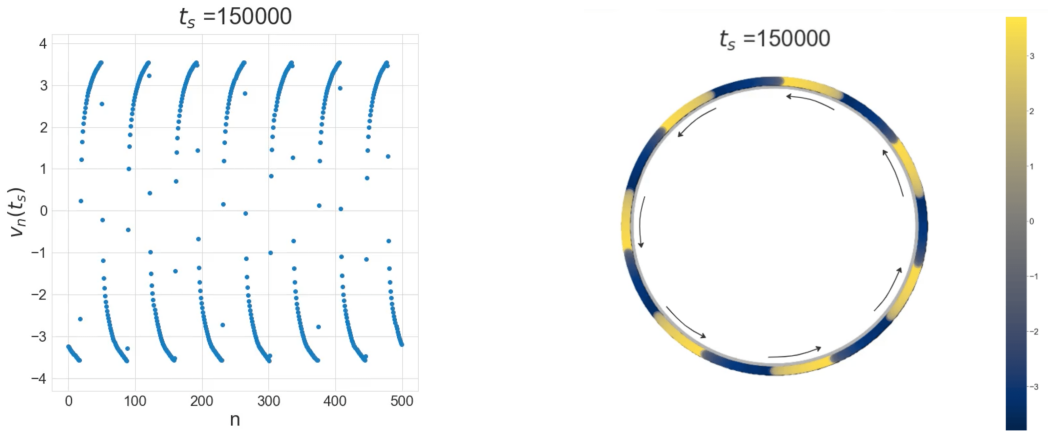

(a) Propagation direction is revealed. (b) Synchronization pattern on the network.

Figure 3.9.: Comparing different visualizations enables to connect observations. (a) The wave direction can be extracted from the chimera pattern which is indicated by the opened side of the arc. Additionally, showing that there are global waves which travel in only one direction on the network. (b) The synchronization pattern on the network can be unambiguously interpreted with the observations from the chimera pattern. All waves are travelling in one direction and no region pairs exist. A $WS(500, 100, 0)$ with scaled coupling $= \frac{1}{50}$ is used and FithHugh-Nagumo model parameters are set to $a = 0.3$, $b = 0.1$ and $\tau = 5$. The colorbar continuously assigns colors from blue to yellow to the fast variable v on the limit cycle.

3.5. Heatmap

To recapitulate, the introduced visualizations enable to identify different synchronization patterns in the absence of regions of incoherence. To address this, the evolution of the entire network is visualized which additionally connects previous visualization. This holds the distinct advantage of representing synchronization patterns, their emergence and other quantities discussed below since it does not depend on a fixed timestep.

For this purpose, a heatmap is generated using the activity matrix of the fast variable $M_v \in \mathbb{R}^{timesteps \times nodes} = \mathbb{R}^{\frac{T}{\delta t} \times N}$ of the entire network which is colorcoded with the same coloring scheme as the spatiotemporal propagation of the dynamics on the network. Recall from section 3.3 that the interval [minimum, maximum] of v on the limit cycle is colored from blue to yellow. The plot uses the node labels on the x-axis and time steps on the y-axis. Note that the boundaries at node 1 and N are periodic in the same way as the chimera plot.

At $t_s = 0$ random color pattern can be found due to the uniformly random initial states. Then, at early times colors start to reorganize such that patterns emerge in relatively few time steps. From simulations that number appears to be $20,000$ time steps for varying network densities, stepsize $\delta t = 10^{-2}$ in the Euler method and for a scaled coupling $\frac{coupling}{network\ size} \approx \frac{1}{10}$. Afterwards, patterns continue to evolve. Nevertheless, the heatmap of a network reveals synchronization patterns as well the following quantities:

(i) The propagation direction of the dynamics on the network which is indicated by the slope of lines. A positive slope corresponds to counterclockwise propagation and a negative slope corresponds to clockwise propagation. Therefore, global wave synchronization can be identified, as illustrated in Figure 3.10a which is further described in section 4.3.

(ii) Identifying region pairs thus region pair synchronization, as shown in Figure 3.10b. By knowing the wave directions it follows that "downward hats" are generating regions and "upward hats" are annihilating regions.

(iii) Region pairs can be overthrown and integrated into a larger region. For example, in Figure 3.10b there is a region pair around node 200 which is completely overthrown by time step $50,000$.

(iv) As mentioned above the individual lines correspond to global waves. Thus, the propagation velocity of waves is visualized by the slope of the yellow/blue lines in terms of $\frac{nodes}{time\,steps}$. This can be used to compare it between different network structures and scaled couplings.

(v) The standing wave phenomenon at generating and annihilating regions is illustrated.

(vi) Waves travel with nearly constant velocity in coherent regions. With the exception that the propagation speed becomes unstable/changes close to region pairs.

(vii) Regions of coherence and incoherence are revealed thus chimera patterns can be identified, as illustrated in Figure 3.11. Chimera pattern synchronization is further described in section 4.5.

In addition, identifying region pairs as described in (ii) can be used for synchronization patterns including Figure 3.10c. Although, the "upward" and "downward" hats are less pronounced. Note that around time step 90.000 at node 90 and node 380 there are annihilating regions. Between them are generating regions which resemble flat curves indicating high propagation velocity. Also, note that annihilating regions can move on the network but not necessarily do so. Potentially suggesting that for $t \to \infty$ the regions clash and are overthrown.

Concerning (iii): Before region pairs are overthrown the wave velocity becomes unstable as it can be observed in Figure 3.10b around time step 30.000. However, as noted in (vi) the change in propagation speed is not necessarily a precursor for an overthrowing event. The underlying dynamics are not known and topic of future research. Starting at a generating region the phase velocity has a jumping behaviour where nodes remain close to minimum (or maximum) for a certain number of time steps before jumping/rushing over intermediate values to maximum (or minimum). In other words the phase velocity is close to zero before rapidly increasing to propagate to neighboring nodes where the velocity

plummets again. Afterwards, it stabilizes and waves travel at a (nearly) constant speed until they get close to an annihilating region where they have a jumping behaviour again. Generally, travelling waves have a nearly constant velocity on the whole network (except around region pairs). Besides that, region pairs seems to be favored to be overthrown if a generating and an annihilating region are spatially close on the network. This closeness can be identified in the heatmap. However, even if a region pair is close it does not follow that it will be overthrown (at least during the simulation run times). For example, in Figure 3.10b there is a spatial close region pair around node 400. Why was it not overthrown and persisted in time? Studying the underlying dynamics is topic of future research.
Despite this, a region pair can also be overthrown if it is not spatially close. It seems that the global wave is strong enough to destabilize the pair and absorb the entire region. This intuition follows [13] where the authors describe that the coupling is strengthened with an increasing number of synchronous oscillators which then are able to recruit more oscillators to the region. As a sidenote, an overthrowing event can only be observed in the heatmap plot or by generating videos/GIFs of the spatiotemporal propagation of the dynamics.

Concerning (vi) and using (i) it becomes apparent that the propagation speed need not be constant. Note that waves propagate away from the generating regions with high velocity in Figure 3.10c. Then, as the waves travel away the propagation speed decreases (indicated by the slope) as annihilating regions are approached. In Figure 3.10d, note that there are even larger differences in propagation speed. Also, it can be observed that the number of region pairs increases and that they become challenging to identify. The intuition is that the effectiveness of the coupling is weakened for increasingly large networks with low density. Resulting in oscillators requiring longer to synchronize thus synchronization patterns emerge slower. Additionally, there are greater differences in propagation speed and wave lengths.

Besides that, in Figure 3.10e the heatmap pattern for nearly locked dynamics are illustrated. This shows that no synchronization of the network occurs even though oscillators exhibit activity. Then, in Figure 3.10f the heatmap for locked dynamics are shown. At first, there is minor node activity before the dynamics are locked. No synchronization can be observed in these two cases. Therefore, they are not pursued in this thesis.

In summary, the heatmap visualizes the evolution of the entire network. Thereby emergent synchronization patterns including chimera patterns can be identified. Additionally, it reveals overthrowing events and wave propagation speed. Finally, the remaining quantity of interest is the order parameter to permit inspection and comparability of the coherence of a network.

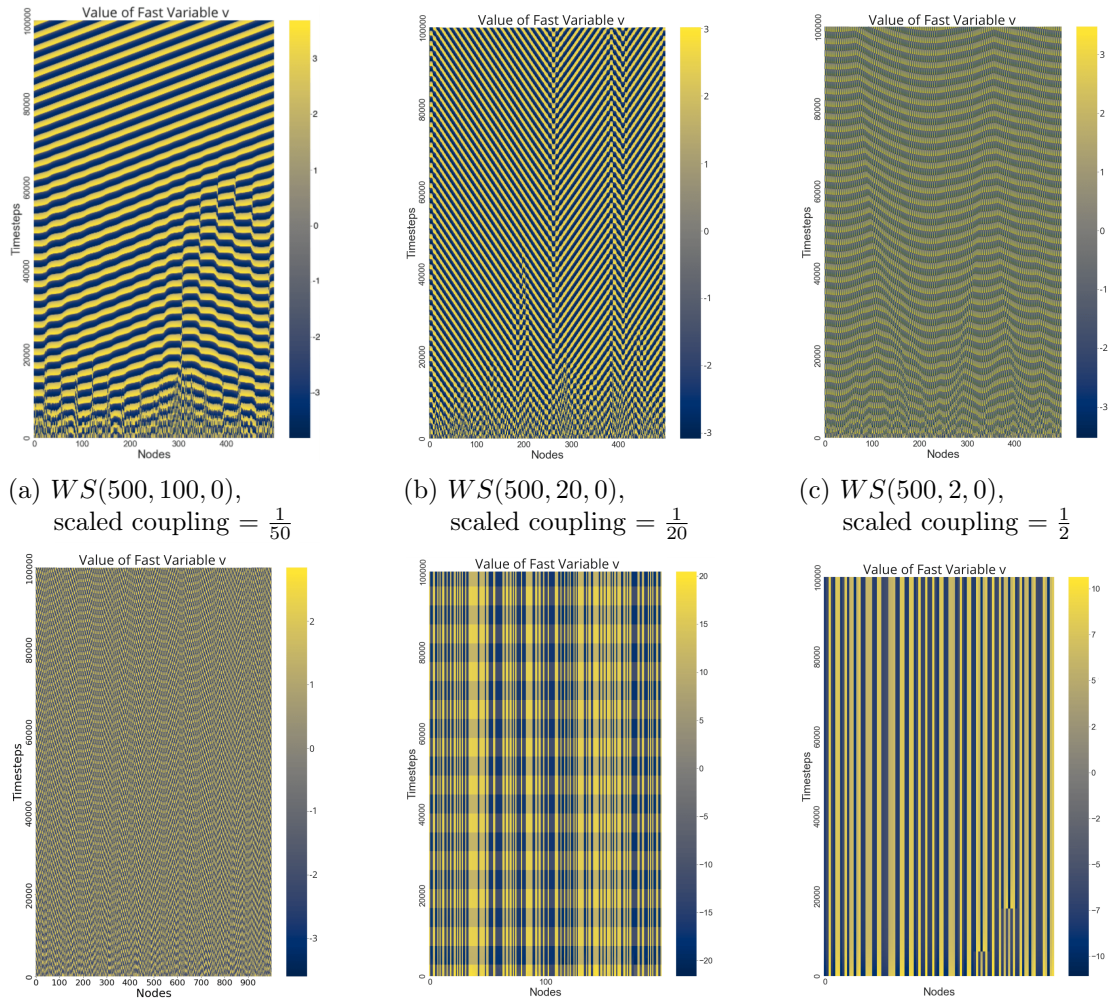

(a) $WS(500, 100, 0)$, scaled coupling $= \frac{1}{50}$

(b) $WS(500, 20, 0)$, scaled coupling $= \frac{1}{20}$

(c) $WS(500, 2, 0)$, scaled coupling $= \frac{1}{2}$

(d) $WS(1,000, 2, 0)$, scaled coupling $= \frac{1}{10}$

(e) $WS(200, 102, 0)$, scaled coupling $= 0.8$

(f) $WS(100, 4, 0)$, scaled coupling $= 5$

Figure 3.10.: The heatmap colorcodes the time series of the fast variable v of the entire network which makes it possible to visualize emerging synchronization patterns on a global scale of the coupled dynamics. Synchronization patterns depend on the network structure and scaled coupling. Various quantities can be read from this illustration as described above. (a) The heatmaps has only lines corresponding to a global wave synchronization. (b) Region pairs are straightforward to identify where "upward hats" are generating regions and "downward hats" are annihilating regions. Note that there is a generating region close to node 1. (c), (d) In comparison, region pairs are less pronounced and more challenging to identify due to an increased network size and low network densities (perfect ring networks). Nevertheless, "upward hats" can be identified in (c) and generating regions are flat curves. The same applies to (d) but there are greater differences in propagation speed and less pronounced region pairs. (e) The dynamics in a high density network $\rho \approx 0.5$ with strong scaled coupling $= 0.8$ is nearly locked. Individual units still have some minor activity leading to irregular oscillations in the coherence measure which leads to misclassifications which is covered in section 5.2. (f) The dynamics can be locked even in low density networks. Initially, oscillators travel to the limit cycle where the follow it until they reach the intersections with the nullcline in Equation 2.4. There they become stationary which is reflected in the unchanging colors of the vertical bars. Note that different network structures are used to illustrate these synchronization patterns indicating that there is a relation between network configuration, scaled coupling and emergent synchronization pattern. The FitzHugh-Nagumo model parameters are $a = 0.3$, $b = 0.1$, $\tau = 5$, $\frac{T}{\delta t} = 1,000 * 10^2$ time steps and uniformly random generated initial states are used.

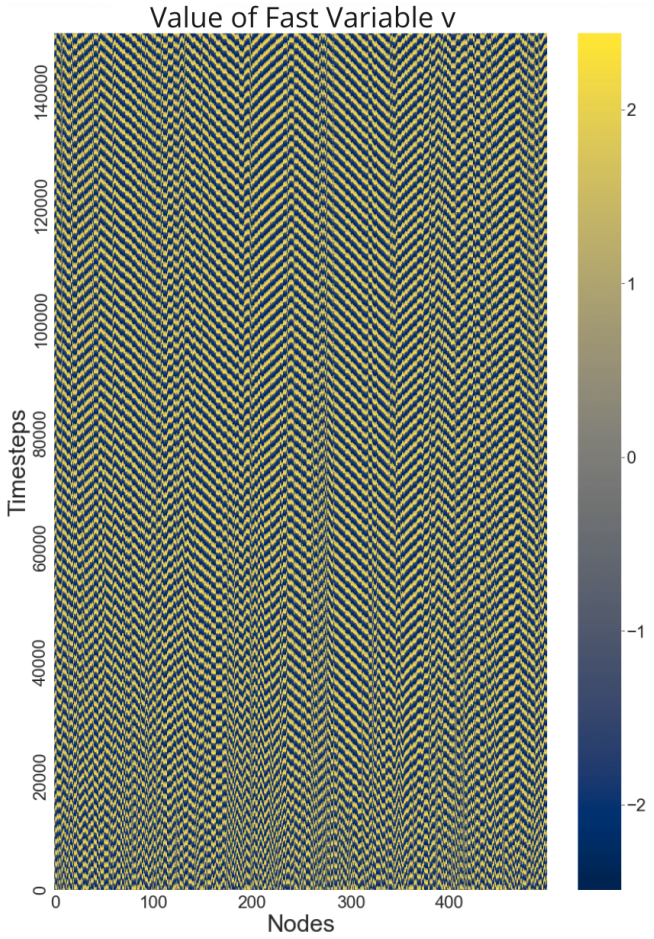

Figure 3.11.: The heatmap reveals regions of coherence and incoherence thus enabling to identify chimera patterns. Chimeras are often long lived transients [24]. Note that regions of incoherence are not a continuation of initial randomness. For example, around node 280 the initial randomness subsides and a region of incoherence manifests. This pattern emerged on a $WS(500, 16, 0.1)$ with scaled coupling $= \frac{1}{50}$, FitzHugh-Nagumo model parameters are $a = 0.3$, $b = 0.1$, $\tau = 5$, $\frac{T}{\delta t} = 1,500 * 10^2$ time steps and uniformly random generated initial states are used.

3.6. Coherence Measure

Up to this point, synchronization patterns can be identified with the use of the presented visualizations. However, those are not able to quantify the coherence of a network. Therefore, the last remaining quantity is the coherence measure which encodes the evolution of a network thus the emergent synchronization pattern. Consequently, Equation 2.8 is utilized to visualize $R(t_s)$ on the y-axis as a function of timesteps t_s on the x-axis.

Initially, at $t_s = 0$ the coherence measure starts close to 1 which is most likely caused by initial states being drawn from a uniform distribution, as illustrated in Figure 2.5. Then, as time steps increase it plummets and starts to oscillate. On top of that, in a significant amount of simulation runs it was observed that the amplitude of the oscillation decreases within relatively few time steps ($t_s \approx 5,000 - 10,000$ for $\delta t = 10^{-2}$) before increasing again. This phenomenon is independent of network configuration. The intuition is that at early times the coupling starts to take effect at the scale of nearest neighbors which leads to a temporary synchronization of oscillators. Then, with increasing time steps the coupling takes effect in an increasing vicinity on the network. At these larger scales oscillators are not synchronized thus perturbing each other in the sense that the coherence measure oscillates with increasing amplitude. However, this phenomenon might also be induced by the initial states being drawn from an uniform distribution. To draw the initial states from another probability distribution was not investigated further and is a topic of future research.

Nevertheless, after the onset of synchronization $t_s > t_{cpl}$ the network of oscillators is synchronized to a certain level of coherence, i.e. the oscillation of the coherence measure is contained within a specific range. However, t_{cpl} might be larger than feasible in simulation runs. For example, in Figure 3.14 the simulation run corresponding to the green evolution of the coherence measure satisfies $R(t_s) \in [0.69, 0.75]$ for $t_s > t_{cpl} = 140,000$. In addition, this plot indicates that a precision level might not make sense and that there are different regimes of the coherence measure. Consider the following idealized scenario:

There are two identical oscillators travelling around a limit cycle and are exactly on opposite sides of the cycle, as illustrated in Figure 3.12. For simplicity take the unit circle as limit cycle. Assume that the phase velocity is the same in v and w direction. Further assume that oscillator 1 is at the maximum value and oscillator 2 is at the minimum value of the fast variable v and denote the timepoint t_{async}. Now calculating the coherence of this two-oscillator-network according to Equation 2.8 results in $R(t_{async}) = 0$, i.e. totally asynchronous. However, as both oscillators move along the limit cycle the (relative) distance between them changes for time steps $t_s > t_{async}$. This causes the measure to increase until a time step t_{sync} where the first variable of both oscillators is the same $v_1(t_{sync}) = v_2(t_{sync})$. At this timepoint t_{sync} the coherence measure $R(t_{sync}) = 1$. Afterwards, the measure decreases until both

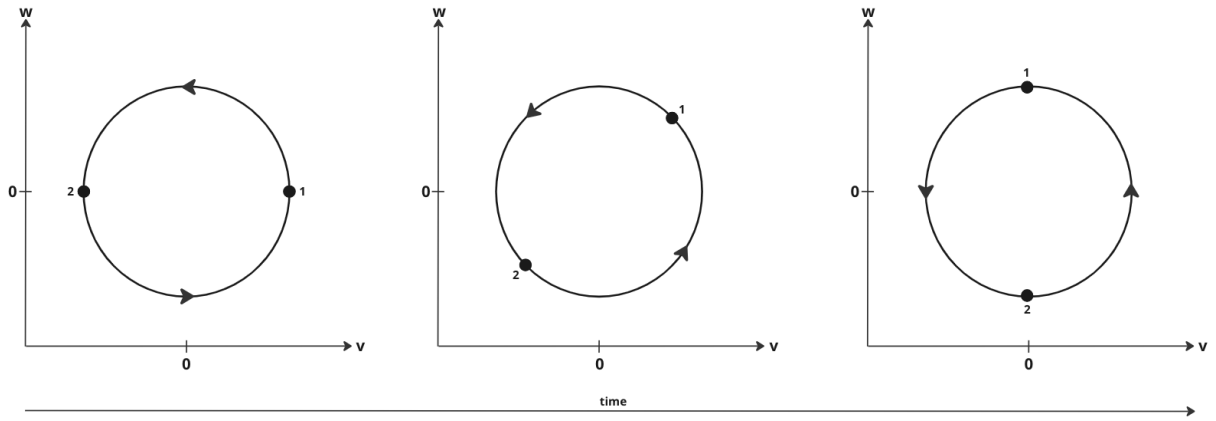

Figure 3.12.: Schematic illustration of a two oscillator network which phases' are shifted by π as they run around the limit cycle. For simplicity the limit cycle is assumed to be the unit circle and phase velocities are the same.

oscillators are at their respective maximum and minimum. Therefore, the coherence measure is not converging to a level of coherence but oscillating over the entire interval $[0, 1]$.

It follows that:

1) the length of the period of the coherence measure depends on the length of period of oscillators on the network and

2) in this idealized scenario the period of the coherence measure must have half the period of the individual oscillators. In contrast, the limit cycle of the actual dynamics is reminiscent of a parallelogram with different phase velocities along the two axes. Thus, the oscillation of the coherence measure is more nuanced and may not follow the $1 : 2$ ratio of the idealized scenario. The FFT is used to obtain the frequency spectrum of the coherence measure with the corresponding node activity to investigate this phenomenon .

The evolution of the coherence measure is influenced by the initial states, as illustrated in Figure 3.13. The coherence measure correspond to five simulation runs for where only the initial states are different. Note that in the first few thousand time steps they are nearly identical. However, small differences in the initial states lead to observable differences at later time steps. Despite these differences the coherence measures in this plot exhibit the same qualitative behaviour in the sense that they oscillate with similar periods, have similar amplitudes and oscillate regularly. This indicates that the same synchronization pattern emerged for all five simulations.

In contrast, the influence of the initial states can lead to different synchronization patterns. Then, the behaviour of the coherence measures varies between simulations where the network parameter are the same and only initial states change, as shown in Figure 3.14. Therefore, the measure is categorized according to the behaviour which reflects different synchronization patterns. The last $10,000$ time steps (for $\delta t = 10^{-2}$) are used and the period of the coherence measure is obtained with the FFT to label it

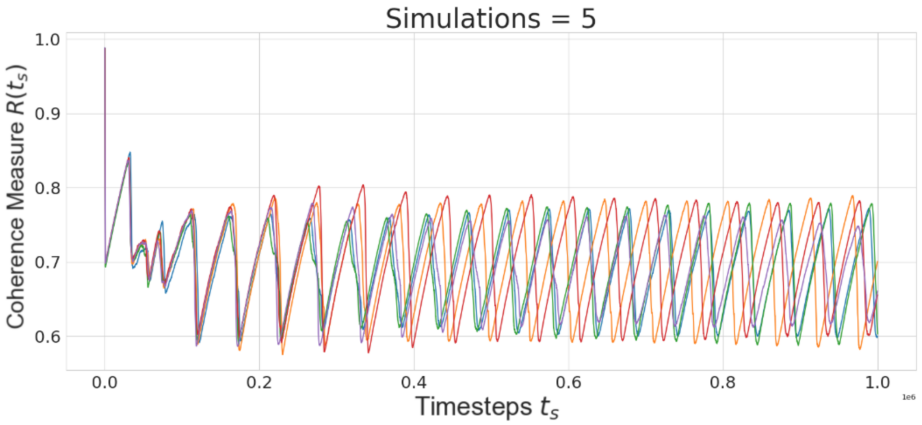

Figure 3.13.: The coherence measure for five different simulation runs is plotted. At the beginning of the simulation the measures are nearly identical before starting to differ from one another. Indicating that the coherence measure sensitively depends on the initial states. The network and FitzHugh-Nagumo model parameters are the same for the five simulations: $WS(1,000, 100, 0.01)$, scaled coupling $= \frac{1}{10}$, $a = 0.3, b = 0.1, \tau = 5$, $\frac{T}{\delta t} = 1,000 * 10^2$ timesteps and uniformly random generated initial states.

according to the following criteria:

- Coherent state: The coherence measure converges to a coherence state $s_l \in [0, 1]$, as illustrated in Figure 2.5. If $2 * Amplitude = maximum(oscillation) - minimum(oscillation) \leq \eta$ for a fixed threshold $\eta \in \mathbb{R}_+$. Then, the measure is called coherent and corresponds to global wave synchronization (in section 4.3). In this thesis, $\eta = 10^{-3}$ is used. Note: If the measure oscillates with small enough amplitude then it is considered to be in a synchronous state.

- Regular oscillating: The coherence measure exhibits regular oscillations which are larger than the threshold η and there is one peak (= local maximum) between two consecutive minima. This behaviour of the measure corresponds to the blinking pattern (in section 4.2). In Figure 3.14 the simulation corresponding to the blue coherence measure is in the regular regime.

- Irregular oscillation: The coherence measure exhibits irregular oscillations which are larger than the threshold η and there exist at least two peaks between consecutive minima of the oscillations. In the absence of rewiring this corresponds to region pairs (in section 4.4) and if rewiring is introduced then additionally to chimera and chaotic patterns (in sections 4.5, 4.6, respectively). In Figure 3.14 the simulation corresponding to the green coherence measure is in the irregular regime indicating region pairs.

Remark: (i) Based on the different regimes of the coherence measure it becomes evident that the behaviour encodes the evolution of the network and the emergent synchronization pattern. Therefore,

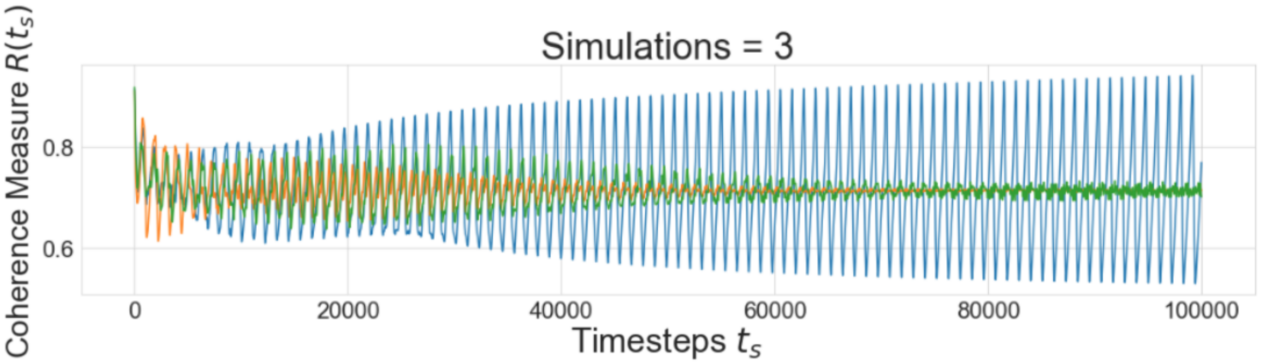

(a) The evolution of the coherence measure for the entire duration of the simulation run time.

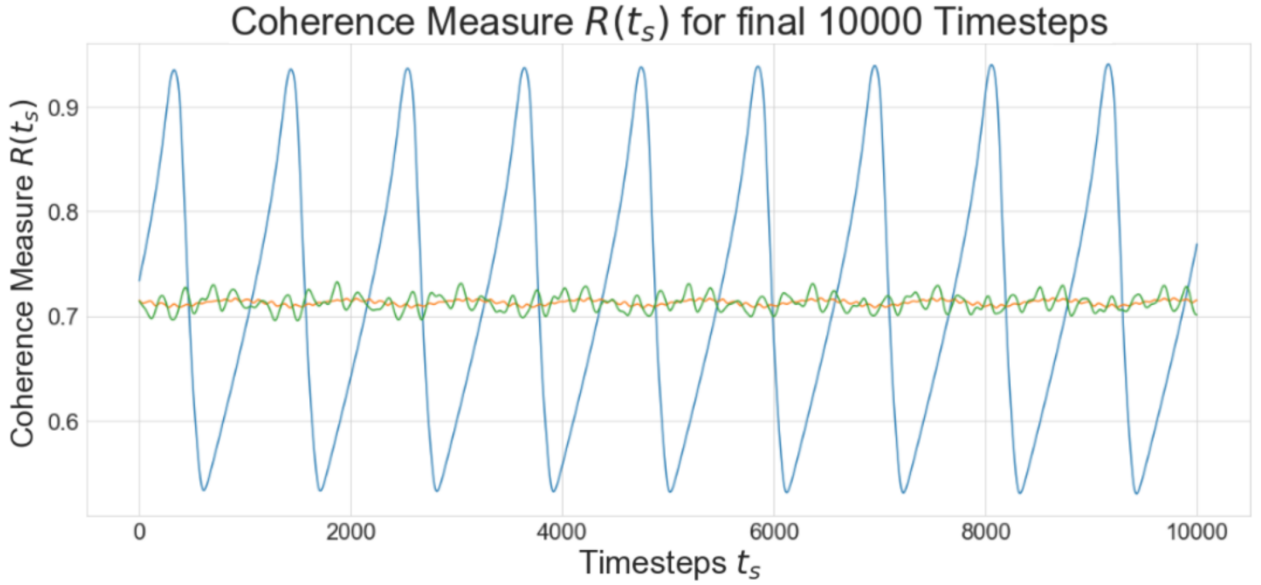

(b) The last 10,000 time steps of the coherence measure to categorize and visually discern the different regimes.

Figure 3.14.: The coherence measure of three different simulation runs is plotted. The network parameters for every run are fixed to be $WS(50, 2, 0)$, scaled coupling $= \frac{1}{10}$, FitzHugh-Nagumo model parameters $a = 0.3, b = 0.1, \tau = 5$ and $\frac{T}{\delta t} = 1,000 * 10^2$ time steps. The initial states are newly generated for every simulation where they are drawn from the interval $[-2, 2]$ uniform at random. Observe that the coherence measure evolves differently which reflects different emerging synchronization patterns between the simulations. This is due to the influence of different initial states. By varying the scaled coupling it is possible to observe tendencies of the synchronization which is described in sections 4.2 and 4.3.
The blue simulation run is in the regularly oscillating regime, the green and orange ones are in the irregularly oscillating regime.

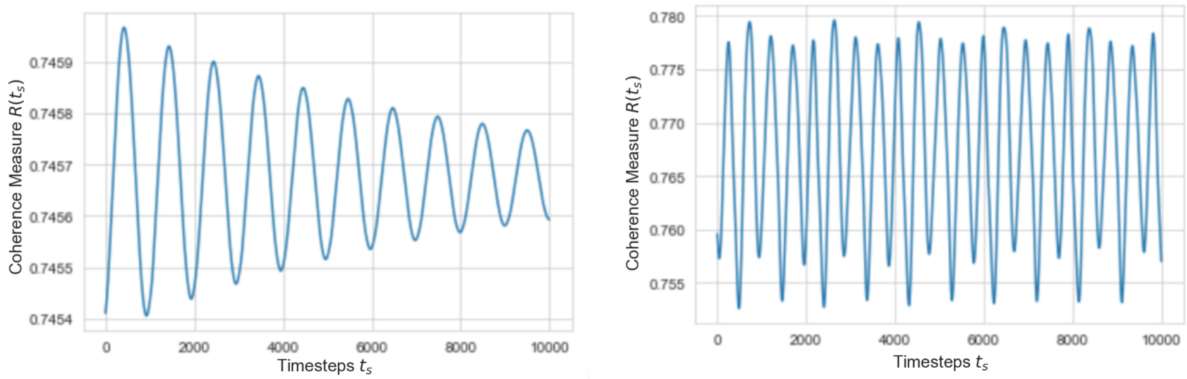

(a) Coherent regime

(b) Regularly regime

Figure 3.15.: By the characterization of the regimes of the phase coherence measure in (a) is coherent since the oscillations are $< \eta$ and (b) in the regular oscillating regime since the oscillations $> \eta$ and there is one peak between two minima.

this classification is used in chapter 5.

(ii) This categorization of regimes has limitations. Note that this characterization allows for oscillation that are increasing or decreasing in amplitude as well as oscillations with different amplitude, as can be seen in Figure 3.15.

(iii) Note that depending on the characterization regimes can be defined differently. Depending on the threshold the orange run in Figure 3.14b could be considered to be in the coherent regime. Or one might be interested in the overall shape of the measure and disregard small noise levels and irregularities. Then, the orange run could be considered to be in the regular regime. Characterizations like these were not followed further and are topics for future research.

As noted above, the coherence measure encodes synchronization patterns as well as their evolution. In Figure 3.16 an overthrowing event is depicted from three different aspects to illustrate observations. Note that the coherence measure in Figure 3.16a exhibits a high level of irregularities in the oscillations on top of being the irregular regime. This seems to be caused by an overthrowing event of a region pair. Recall from section 3.5, the region between generating and annihilating is destabilized such that it becomes incoherent (see Figure 3.16b) which causes additional irregularities in the coherence measure until the region is integrated into a larger coherent one. Note that the existence of region pairs on the network is encoded in the irregular oscillations. The downstream implication is that the main source of irregularities are oscillators which are not synchronized well within their neighborhood in the sense that there is variation in phase velocities.

In summary, the evolution of the coherence measure encodes the emerging synchronization patterns. This is used to categorize it in three different regimes which correspond to blinking pattern, global waves and region pairs in the absence of rewiring. If $p > 0$ then the irregular regime additionally

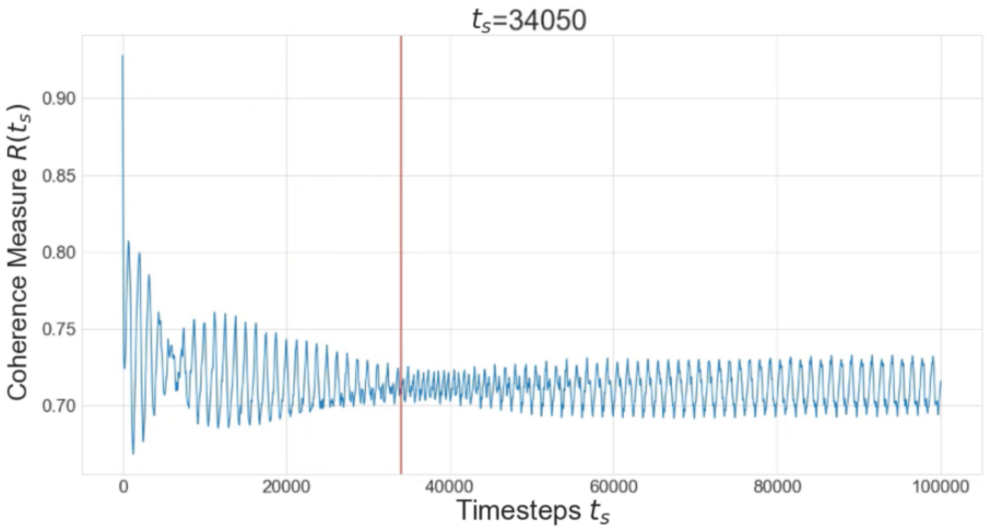

(a) The overthrowing leads to irregular oscillations in the measure. The red vertical line corresponds to the time of the snapshot $t = 34,050$.

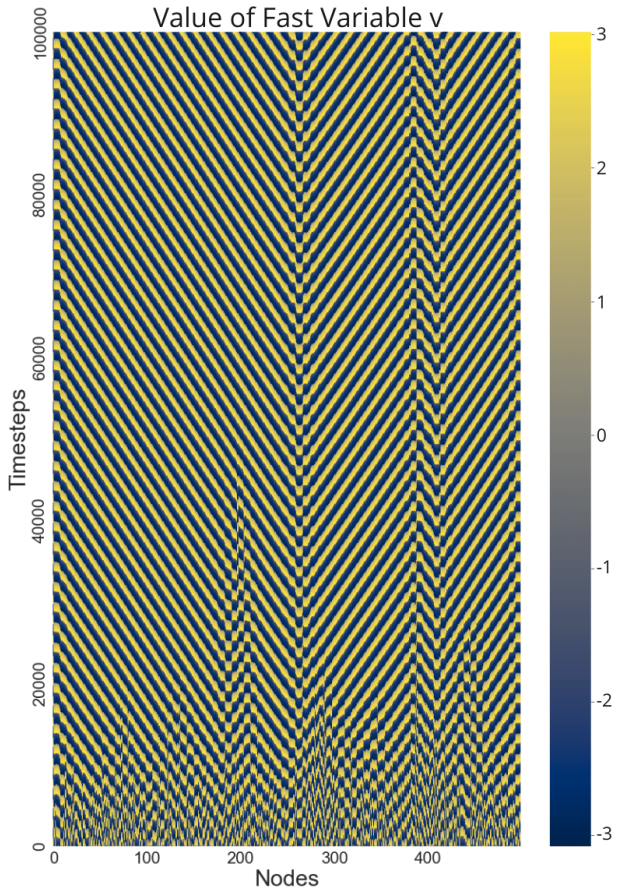

(b) The overthrown region pair is around node 200. Observe that the phase velocity of the global wave is not constant around the region pair.

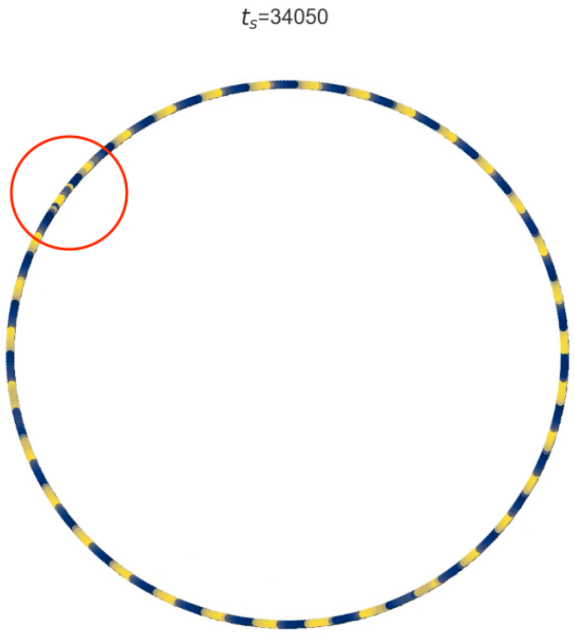

(c) A region pair is overthrown which causes incoherent blinking in the area marked by the red circle.

Figure 3.16.: An overthrowing event is shown from three different aspects. (a) The irregularly oscillating coherence measure is shown where the red line indicates the timestep of the snapshot. Note the especially irregular behaviour of the measure around the red line. (b) The overthrowing event and the change in the phase velocity can be observed in the heatmap. (c) The area on the network is highlighted where the region pair is overthrown where individual nodes are incoherent with respect to their neighbors and global wave. A $WS(500, 20, 0)$, FitzHugh-Nagumo model parameters $a = 0.3$, $b = 0.1$, $\tau = 5$, a scaled coupling $\frac{1}{10}$ and $\frac{T}{\delta t} = 1,000 * 10^2$ timesteps are used. The colorbar continuously assigns colors from blue to yellow to the fast variable v on the limit cycle.

corresponds to chimera and chaotic pattern.

3.7. Summary

The evolution of the dynamics on networks is visualized from different perspectives which enables to identify appearing patterns. These are interpreted and it is described what is represented by them. This makes it possible to further connect pattern to emergent synchronization patterns on the network. In the following the visualizations are used to detect and describe the synchronization patterns that were observed.

4. Synchronization Patterns

At this point, the visualizations are introduced and it is described what appearing patterns in them represent. Therefore, they can be utilized to describe and distinguish the emergence of emerging synchronization patterns in dependence on the network structure. This chapter covers the observed synchronization patterns and is organized as follows: In section 4.1 global synchronization is discussed, in section 4.2 blinking patterns are described with corresponding Figures in appendix section A.1, in section 4.3 travelling waves are delved into with corresponding Figures in appendix sections A.2 and A.3, in section 4.4 region pairs are analyzed with corresponding Figures in appendix sections A.4 - A.7, in section 4.5 chimera patterns are investigated with corresponding Figures in appendix section A.8 and lastly in section 4.6 chaotic patterns are presented with corresponding Figures in appendix section A.9.

4.1. Global Coherence

There are numerous papers investigating conditions leading to global coherence in networks of oscillators such as [25] and [26]. Global coherence corresponds to all nodes of the network being phase locked. This synchronization pattern could not be reproduced from the literature and was only achievable by setting all initial states to be equal, i.e. $v_i(0) = v_j(0)\ \forall i, j$ and $w_i(0) = w_j(0)\ \forall i, j$. Therefore, they are synchronous from the start thus independent of network structure and no emergent phenomenon exists. The authors of [25] hypothesise that rings might yield synchronization pattern other than global synchrony. In [13] the authors write that Watts-Strogatz networks have a poor synchronizability.
One potential reason is that in the literature, the FitzHugh-Nagumo model parameters are chosen to be in an excitable regime or that phase oscillators are used, e.g. Kuramoto model. In [13], synchronization was achieved in ring networks with a number of neighbors $\frac{k}{N} \geq \frac{1}{3}$. A commonly used approach is the introduction of a control parameter to achieve synchrony, for example in [27], [11]. Another approach is the fine tuning of parameters [28]. However, the focus of this works lies in the relation between synchronization pattern and network structure. Therefore, neither controller units nor parameter tuning were used.
Besides that, in this scenario the coupling term $I = 0$ where the phase of all identical oscillators is the

same. Note that the dynamics are interchangeable with the uncoupled case. For completeness, the patterns in visualizations would appear in the case of global coherence as follows:

- Phase plane: all oscillators are in one clump.
- Node analysis: all oscillations and fequency spectra are the same and overlap.
- Spatiotemporal propagation: all nodes are either blue or yellow depending on the time of a snapshot.
- Chimera pattern: there is one horizontal line containing all oscillators.
- Heatmap: There are horizontal blue and yellow lines alternating.
- Coherence Measure: $R(t_s) = 1$ for all t_s.

In summary, global coherence was only achieved by starting in a network of synchronous oscillators thus completely independent of network structure. In the present work it appears that global coherence cannot be obtained as emerging synchronization pattern which might be causes by the oscillatory regime of FitzHugh-Nagumo oscillators. However, further investigation is needed to confirm or deny that with certainty.

4.2. Blinking Pattern

Foremost, this synchronization pattern was observed to manifest in small perfect ring networks with $N < 100$ and rewiring probability $p = 0$. Additionally, the emerging pattern is influenced by the initial states. Note that the phase space is high dimensional and to control it is beyond the reach of this thesis. Nevertheless, a tendency of the emerging synchronization pattern can be observed by manipulating the scaled coupling. The higher the scaled coupling the more simulation runs arrive in a blinking scenario. Note that the coupling has an upper limit before the dynamics are locked which is discussed in 5.1. More precisely, 500 simulation runs with a fixed network structure $WS(50, 2, 0)$, scaled coupling $\frac{\sigma}{N} = \frac{50}{50} = 1$, FitzHugh-Nagumo model parameters $a = 0.3, b = 0.1, \tau = 5$ and $\frac{T}{\delta t} = 1.500 * 10^2$ time steps were run and in approximately 50% of the simulation the blinking pattern emerged. New initial states were generated for every simulation run. Then, another 500 simulations were run for a scaled coupling $= \frac{1}{2}$ where approximately 35% arrived in the blinking pattern. Once more, the emphasis is on the high dimensionality of this problem so that only sparsely sampling of the phase space is feasible. In spite of that, it was achieved to detect tendencies by varying the scaled coupling.
In the blinking pattern, oscillators are alternatingly in one of two coexisting phases θ_1, θ_2 which implies

that one global oscillation is represented by two nodes. The unique feature is that there is no observable propagation direction of the dynamics. The corresponding patterns are unambiguously identifiable in the visualizations which are shown in appendix section A.1.

The two phases θ_1, θ_2 correspond to two clumps in the phase plane which are on opposite sides of the limit cycle and there are $\frac{network\,size}{2}$ oscillators in either clump. The corresponding node analysis confirms that θ_1, θ_2 are shifted by π and that the frequency spectra are nearly identical. The intuition is that these small discrepancies disappear for increasing time steps. Then, one node is taken as representative node and its frequency spectrum plotted. It can be observed that the length of periods is increased compared to the plots in section 3.2. This is caused by the increased scaled coupling which is examined in more detail in chapter 5. Secondly, the blinking property is visualized by the spatiotemporal propagation of the dynamics on the network. In the corresponding plot, nodes are alternatingly at the maximum and minimum of the fast variable v before exchanging positions (and color). Prior to reaching this synchronization pattern a generating region manifests on the network which emits waves as described in section 4.4. As time progresses the generating region grows until the entire ring network is enveloped such that no waves are emitted and the network blinks.

In the corresponding chimera pattern plot, oscillators agglomerate on two horizontal lines representing the two phases θ_1, θ_2. On these lines nodes are phase locked. After the initial randomness in the heatmap the pattern is stabilized within few time steps and it resembles a checkered board. Note that oscillations are in horizontal lines. Therefore, the slope is zero indicating that there is no propagation direction. Further, the time evolution of nodes is represented vertically which reveals that all individual nodes exhibit a standing wave phenomenon. Hence, there is a standing wave phenomenon over the entire network.

Recall the idealized scenario with two oscillators in section 3.6. In accordance with this, the coherence measure oscillates regularly. In contrast, the oscillation is contained in the interval $[0.5, 1]$. The rationale is that clumps contain equally many oscillators thus half of the summands in the coupling term $I = \sum(v_i - v_j) \approx 0$ causing the possible range for $R(t)$ to shrink or with other words the amplitude of the oscillation decreases. This occurs regardless of differences in limit cycle shape and phase velocities. Subsequently, if there are multiple evenly distributed clumps on the limit cycle then the coherence measure oscillates. Then, comparing the frequency analysis of coherence measure and representative node yields that the idealized $1:2$ ratio does not apply. Lastly, the coherence measure and its frequency spectrum are illustrated for three simulation runs with identical network structure but different initial states. Note that two of the three coherence measures are nearly identical as validated by their respective frequency spectra. This suggests that for fixed network structure arriving at a synchronization pattern

yields similar coherence measure behaviours and frequency spectra which is further examined in the following sections. Additionally, it can be observed that other synchronization patterns can manifest indicated by the orange measure.

In summary, the blinking pattern synchronization was only attained in small perfect rings. However, larger perfect ring networks can potentially also wind up in this pattern for increasing simulation run times. Additionally, the coherence measure oscillates regularly with high magnitude.

4.3. Global Waves

As previously noted, the initial states impact the emergent synchronization pattern on networks. For a strong scaled coupling $\frac{\sigma}{N} = \frac{50}{50} = 1$ on small perfect ring networks $WS(50, 2, 0)$ the other synchronization pattern are waves which travel in only one direction. Recall, this network structure and scaled coupling are fixed and 500 simulations run where the other parameter are the same as before, i.e. FitzHugh-Nagumo model parameters $a = 0.3, b = 0.1, \tau = 5$ and $\frac{T}{\delta t} = 1.500 * 10^2$ time steps. Then, global waves emerge in approximately 50% of the simulations. However, by decreasing the scaled coupling more simulations arrive in the global wave pattern. To be more specific, 500 simulations were run with the same network structure, FitzHugh-Nagumo model parameters, a decreased scaled coupling $\frac{\sigma}{N} = \frac{1}{2}$ and new initial states for every run. Then, approximately 65% of simulations have global waves (and 35% blinking patterns). Reiterate that the phase space is high dimensional and could only be sparsely sampled. Nevertheless, a tendency is observed by controlling the scaled coupling.

If the scaled coupling is decreased further then region pairs start to manifest. However, the propagation speed of waves emitted from generating regions is high in perfect ring networks as observed in section 3.5 and results in oscillations of the coherence measure. This suggests that more runs would arrive at the blinking pattern for longer run times which is also encountered in section 5.2. The improvement of the detection of these cases is topic of future research.

In addition, global waves emerge in larger networks with higher density. To investigate the phase space is beyond this thesis so that the scaled coupling is used again. The scaled coupling has to be reduced to avoid locking the dynamics for increased network density. Then, 100 simulations with a $WS(500, 100, 0)$ with scaled coupling $\frac{\sigma}{N} = \frac{1}{50}$, FitzHugh-Nagumo model parameters $a = 0.3, b = 0.1, \tau = 5$, $\frac{T}{\delta t} = 1.500 * 10^2$ are run where new initial states are generated for every run. Then, global waves emerge in approximately 90% of the runs and in the other 10 region pairs manifest. The connection between global waves, scaled coupling and network density is further studied in section 5.2. For longer simulation run times the percentage of global waves would likely increase. The rationale is as follows: An increasing number of neighbors leads to an increased influence on individual nodes. Therefore, the coupling is strengthened

leading to an improved synchronization of the network.
Additionally, global waves travel with constant velocities and require a fixed number of nodes to be represented in either configuration. These two quantities depend on the network structure and scaled coupling. The synchronization patterns of those two network structures are mostly the same, as expected. Despite that, there exist subtle differences which are described below. In addition, global wave patterns are illustrated for small perfect ring networks in appendix section A.2 and for larger networks with higher density in appendix section A.3.

Firstly, the phase plane presents the same scenario for both network configurations. Oscillators distribute on the limit cycle implying that there are coexisting phases $\theta_1, \ldots, \theta_m$ where $2 < m \leq N$. Note that if $m < N$ implies that there are clumps of oscillators and if $m = N$ oscillators evenly distribute on the limit cycle. Heuristically, the length of a wave =: n_{wave} = 'number of nodes' represents a global oscillation. These nodes have to have different phases $\theta_1, \ldots, \theta_{n_{wave}}$ which holds for every global wave. Therefore, suggesting that n_{wave} many clumps travel on the limit cycle. However, between waves there might be minor shifts in the phases resulting in more clumps. Further investigations of this are topic of future research. In any case, indicating that if waves travel on the network then coexisting phases exist. This can visually be confirmed with the nodes' activities where a regular pattern is revealed indicating similarity of individual oscillators. This is confirmed by illustrating the frequency spectra of randomly sampled nodes. Therefore, one representative oscillation and its frequency spectrum is taken in both network configurations. Note that the length of period is increased for the higher density network. This relation is examined in greater detail in section 5.1.
Secondly, the spatiotemporal propagation reveals discrepancies between the two network structures. Beginning with small perfect ring networks it is illustrated that waves are interlaced on the network. This is represented as follows: If a node is close to e.g. the maximum of the oscillation then its neighbors are close to the minimum and vice versa indicating that the phase of neighbors is shifted by $\approx \pi$. Then, the phase of neighbors of neighbors is close to the first node and so on. It follows that the coupling omits direct neighbors and neighbors of neighbors represent waves. For example, observe this in Figure A.3d for a part between two nodes closest to the maximum on the network, i.e. bright yellow. Recall (from section 3.3) that yellow represents positive and blue negative values of the fast variable v. Then, note that within said region the phase of every second node corresponds to positive/negative values. By following every second node for decreasingly bright yellow then the last node in the region is dark blue. Therefore, this region contains only half of a global wave and travelling waves on a perfect ring network are interlaced where nodes alternatingly belong to different global waves.
In comparison, global waves on networks of increased size and density are not interlaced. Visually this

is captured by neighboring nodes being continuously colored from yellow to blue and back to yellow as illustrated in Figure A.5d. Additionally, it can be observed that the wave length also increases with increasing network density, as described in section 3.3. Thus, fewer global waves can coexist on the network. For both network configurations it is expected that global waves are stable and perfectly distribute on the network for $t \to \infty$.

Thirdly, the chimera pattern captures the interlacing phenomenon which is indicated by positive and negative values of the v being present in the same spatial regions. In contrast, the pattern for higher density networks shows that waves exist consecutively on the network. In either case, global waves are captured in the plot and the propagation direction can be read as described in section 3.4.

Recall from section 3.5 that the sign of the slope of lines in the heatmap indicate propagation direction. For global waves this results in sloped lines covering the entire plot after initial randomness has subsided. In small perfect ring networks the heatmap pattern appears as a checkered board reminiscent of the blinking pattern. In contrast, lines representing waves are comprised of blocks which corresponds to the interlacing phenomenon. However, it is challenging to extract the sign of the slope as well as the number of waves. In comparison, there are clear lines representing waves in higher density networks. In this case, it is straightforward to read the sign of the slope as well as the number of global waves. Note that the propagation velocity is higher in small networks even though the node activity is slower. This observation is topic of future research.

Clumps on the limit cycle result in oscillations of the coherence measure. As time progresses, the magnitude decreases such that the coherence measure converges to a coherence state. Note that the evolution of the coherence measure has small discrepancies for the two network structures. In small networks it appears that the coherence measure decreases faster compared to higher density ones. However, after the emergence of global waves the higher density network appears to converge faster to a coherent state. This might indicate that for smaller networks a higher threshold η is advisable.

Besides that, the frequency spectra of the coherence measures reveal that surprisingly the periods of oscillations follow the $1:2$ ratio of the idealized scenario in the higher density network, whereas the small perfect ring network does not. Additionally, for both network configurations the coherence measure and its frequency spectrum is illustrated for three simulation runs with different initial states, respectively. Note that all simulations arrive in the global wave synchronization illustrating that there is a high chance of obtaining this pattern. Then, the frequency spectra reveal the high similarity between the coherence measures for all three runs for both network structures. The major distinctions are the magnitudes corresponding the different runs. Indicating again that a given synchronization pattern for a fixed network structure can be classified with the regime of the measure. Moreover, the same

behaviour is exhibited if runs wind up in a synchronization pattern with little influence of the initial states. This seems to impact the magnitude of the oscillations, i.e. how fast the coherence measure converges to a coherence state.

Remark: If global waves manifest then coherence on a global scale implies coherence on a local scale. Heuristically, assume that the node dynamics are coherent on a global scale but incoherent on a local scale. Then, there are global waves travelling with nearly constant phase velocity around the network. Now take one such wave which requires a certain number of nodes to fit in on the network. These nodes are nearest neighbors (or neighbors of neighbors), however, the local dynamics are incoherent thus a smooth propagation of global waves is impeded.

In summary, global waves are likely to manifest in perfect ring networks when the scaled coupling is high. Additionally, they are the most common phenomenon in higher density networks (studied in section 5.2) which also corresponds to bolstered coupling. The corresponding coherence measure converges to a coherence state where it oscillates around with decreasing magnitude.

4.4. Region Pairs

There are two ways to manipulate network structures from the previous section to transition from global waves to region pairs. On the one hand, increasing the size in perfect ring networks to $N > 100$ nodes. On the other hand, decreasing the number of neighbors (i.e. density) in larger networks with higher density. Note that both modifications weaken the coupling. The chances of arriving in the region pairs pattern in dependence of the network structure is analysed in section 5.2. The emerging patterns are similar, but small discrepancies exist. These corresponding plots are illustrated in appendix section A.4 for a perfect ring with increased size, and in appendix section A.5 for larger network size with higher density, respectively.

First of all, multiple phases $\theta_1, \ldots, \theta_m$ coexistence since there are travelling waves on the network between region pairs indicating that oscillators distribute on the limit cycle in the phase plane. In contrast to global waves, travelling waves are emitted from generating regions but not simultaneously in both directions resulting in differences in the phase thus less clumps of oscillator appear. Note that clumps indicate phase locking.

Nevertheless, the revealed patterns resembles the one of global waves with the most significant distinction that oscillators are more scattered around the limit cycle. Therefore, suggesting higher discrepancies in the node activity which appears slightly less regular compared to waves for both network structures. This is also reflected in increasing differences in frequency spectra of randomly sampled nodes even though a high level of similarity is present. Hence, it may be indicated that they neither depend on

propagation direction nor on being part of a region pair or travelling wave. Therefore, a representative node can be taken and its frequency analyzed. Note that the increased density leads to an increase in the length of the period compared to the perfect ring network.
The spatiotemporal propagation of the dynamics illustrates discrepancies between both network structures. In particular, travelling waves are interlaced in perfect ring networks as before. Additionally, generating and annihilating regions show this interlacing phenomenon. In contrast to the blinking pattern synchronization, generating regions do not seem to expand. As noted before, that might change with increasing simulation run times. A major distinction to before is that the lengths and propagation velocities of waves can change as they travel on the network. The subtleties affecting where and how these phenomena manifest appear to depend on the initial states which was not further investigated. In comparison, in higher density networks nodes in regions pairs are phase locked and it seems that they have half the length of travelling waves. Moreover, neighboring nodes represent the same wave which suggests that the interlacing phenomenon can only manifest on perfect ring networks.

It is not possible to determine the the stability of region pairs from simulations. To investigate the underlying dynamics is topic of future research. For example, what exactly causes an overthrowing event?

Recall in chimera patterns, region pairs appear as clumps and waves are represented as arcs indicating propagation directions. Besides that, the increased network sizes in both cases make it more challenging to detect patterns in the chimera pattern. Additionally, in perfect ring networks lengths and propagation speed of waves can change which is reflected in different curvatures of corresponding arcs. Thus, the chimera pattern plot has to be closely examined to correctly classify it.

Also the heatmap illustrates differences between the two network structures. Higher density networks have prominent "hats" whereas in perfect rings those are flattened as described in section 3.5. This might suggest that perfect ring networks arrive in the blinking pattern for $t \to \infty$. However, longer run times and/or a theoretical analysis are required. Additionally, initial randomness seems to persist longer in both network configurations compared to previous synchronization patterns. Lower network densities result in an increase in the time required to synchronize which is in line with [24].
Sidenote: If the network size of perfect ring networks is increased further the heatmap pattern becomes more complex, as described in section 3.5.

Subsequently, the impact of region pairs on the coherence measure is addressed. On the one hand, the magnitude of the oscillation is larger compared to global wave pattern and does not appear to converge

to a coherence state. On the other hand, it exhibits irregular oscillation. Therefore, the coherence measure is in a different regime compared to the previous cases. Then, the frequency spectrum is taken which surprisingly reveals that the $1:2$ period ratio of the idealized example is followed in the perfect ring network. However, in the higher density network it does not. To establish an accurate relation is topic of future research.

Reiterating that three coherence measures and frequency spectra are generated for the same network structures and different initial states for both configurations. All runs exhibit irregular oscillations indicating region pair synchronization, thus can be achieved with certain network structure as shown in section 5.2. Additionally, the frequency spectra are similar again indicating that the initial states mainly influence the magnitudes.

Lastly, introducing rewiring in higher density networks which is illustrated in appendix section A.6 for very small and in appendix section A.7 for intermediate rewiring probability.
If very small rewiring is introduced there is no observable change in the the synchronization patterns across visualizations. Then, for small rewiring probability there are only few rewired links which appear to increase the number of region pairs even though the shortcuts decrease the average shortest path length. The oscillators are more scattered around the limit cycle. However, the patterns across all visualization are very similar to $p = 0$. It appears that the propagation speed is slightly disturbed close to rewired links. Nevertheless, the waves' length is unchanged indicating that the network density and coupling strength are the determining parameters, as illustrated in Figure 3.6. For intermediate values of p the average shortest path length decreases further, however, the synchronizability and corresponding region pair patterns remains roughly the same [13]. A natural next step is to increase it further.

In summary, region pairs manifest in networks with lower density and weaker scaled coupling compared to global waves. Additionally, they induce irregularities in the coherence measure.

4.5. Chimera Patterns

Following this, the network structure is manipulated to have more randomness by increasing the rewiring into the strong range. Additionally, decreasing the scaled coupling reliably causes regions of incoherence to manifest on the network. Note that both of those changes effectively weaken the coupling. The corresponding patterns are illustrated in appendix section A.8.

Multiple phases exist again since there are travelling waves in regions of coherence. The main distinction is that the diameter of the limit cycle shrinks due to the decreased scaled coupling. Also, oscillators are scattering around the limit cycle. However, the phase plane does not reliably indicate

chimera pattern which is reflected in the node analysis. The node activity pattern is regular and the frequency spectra of randomly sampled nodes are nearly identical, as in for region pairs. Heuristically, the decreased coupling and density result in less influence nodes have on each other, therefore, improving the converge of individual oscillators to the limit cycle which is the same for identical oscillators. Then, a representative oscillation and its frequency are illustrated showing the decrease of the period of individual oscillators due to the network modifications.

The spatiotemporal propagation of the dynamics reveals regions of incoherence which are visually represented by inconsistent wave lengths as well as disturbed color patterns. With other words neighboring nodes have different phases. This pattern makes chimeras clearly distinguishable from previous synchonization patterns. The chimera pattern plot becomes more challenging to extract information from with the incoherence present on the network. Note that it resembles the totally incoherent case in the chapter 3.4 (Figure 3.8c). The essential discrepancy is that oscillators aggregate at top and bottom and there are arcs that can be identified in narrow parts of the plot.

In heatmaps the added randomness is reflected in fluctuations of propagation velocities, i.e. slopes of lines vary along the network. Additionally, the propagation direction becomes ambiguous in regions of incoherence. Note that chimeras are not a caused by the initial randomness. There are region pairs present on the network but are challenging to identify due to the incoherence.

The presence of chimeras induces irregularities into the oscillation of the coherence measure. It seems that the magnitude of oscillations is higher compared to the presence of only region pairs. However, this is not reliable to determine the exact synchronization pattern but can be used to exclude blinking patterns and global wave synchronization. To further investigate the frequency spectra to correctly predict the synchronization pattern is topic of future research.

Nevertheless, (as previously) the coherence measures for three simulation runs and respective frequency spectra are taken. Note that for this network structure all runs arrive in the chimera pattern synchronization. Additionally, the frequency spectra are again similar solidifying the previous argument.

In summary, decreasing network density and increasing randomness is a reliable network manipulation to transition from region pairs to chimera synchronization where the associated coherence measure oscillates irregularly. Both modifications have the effect of weakening coupling and pursuing this line of thought yields the last pattern.

4.6. Chaotic Regime

Lastly, scaled coupling and network density are decreased while the rewiring is increased to the very strong range to enable incoherence of the network to exist, i.e. chaotic patterns. Increasing the

randomness in a network can be thought of adding noise with increasing intensity. The corresponding patterns are illustrated in appendix section A.9.

To begin with, multiple phases coexist and the diameter of the limit cycle shrinks compared to chimera patterns due to the decreased coupling and network modifications. Further, individual oscillators are scattered around but close to the limit cycle which due to the weak coupling between oscillators. The node activity is also reminiscent of before. Thus, the frequency spectra of randomly sampled nodes are similar. Moreover, the representative node and its frequency spectrum are close to the chimera pattern. Differences are revealed by the spatiotemporal propagation where the incoherence leads to a irregular pattern. Then, no wave length can be observed. The influence of nodes on each other does not suffice to synchronize them. Furthermore, this is reflected in the chimera pattern where neither region pairs nor arcs are identifiable. In addition, there is only a subtle trend of oscillators agglomerating at top and bottom areas.
The heatmap recapitulates that the coupling is not strong enough to synchronize oscillators such that regions of incoherence persist. Notably, in the plot distinct regions appear which seems to be a continuation of the initial randomness. In spite of that, there is an evolution in the plot due to the coupling and longer run times would be required to further investigate the pattern.
Besides that, the corresponding coherence measure is in the irregular regime and the magnitude does not deviate recognizably from chimera patterns. Therefore, advanced tools from signal analysis are required to detect discrepancies which is topic of future research.
Once more, coherence measures and corresponding frequency spectra of three simulations are shown. The same observation can be made as before, i.e. reaching a particular synchronization pattern results in similarity of frequency spectra of the coherence measures.

In summary, global incoherence is enabled by network structures with high rewiring, low density and a small scaled coupling. Then, the coherence measure exhibits irregular oscillations. The structure manipulation essentially weakens the coupling and links nodes so that they have a perturbing effect on each other.

4.7. Summary

By manipulating the network structure enables to influence the emerging synchronization pattern reliably. There exist five possible synchronization patterns that can manifest on ring networks with FitzHugh-Nagumo oscillators. Additionally, there is global coherence, which is only achieved if initial states are the same for every oscillator.

The following network structures (strongly) favor particular synchronization patterns:

- **Blinking pattern:** small perfect ring networks $N < 100$ with strong scaled coupling.
- **Global Waves:** (i) small perfect ring networks $N < 100$ decreasing scaled coupling or
  (ii) increased network size $N > 100$ and density.
- **Region Pairs:** (i) perfect ring networks $N > 100$ with lowered scaled coupling.
  (ii) increased network size $N > 100$ with decreased network density and decreased scaled coupling where additionally up to intermediate rewiring values can be present.
- **Chimeras:** increased network size $N > 100$, strong rewiring and decreased scaled coupling compared to region pairs.
- **Chaotic:** increased network size $N > 100$, very strong rewiring and further decreased scaled coupling.

Additionally, the regime of the coherence measure can be used to classify synchronization patterns. However, the exhibited behaviours are similar for region pair synchronization, chimera and chaotic patterns. Therefore, studying discrepancies of the frequency spectrum to distinguish those is a topic of future research. Nevertheless, in the absence of rewiring, the coherence measure is used to quantify the observations from above. The next step is to analyse the impact a single network parameter (varied over a range) has on the regime of the coherence measure.

5. Exploring Synchronization Patterns

At this point, the different synchronization patterns are presented and the corresponding manipulations of the network structure to obtain them. Furthermore, a substantial amount of information about the synchronization pattern is encoded in the regime of the coherence measure thus in the corresponding frequency spectrum. In the following this is utilized to quantify parameter ranges in terms of resulting emergent patterns. With that objective, the regimes of the coherence measure are used to reveal connections between network structure and synchronization pattern in the absence of rewiring.
In this regard, in section 5.1 one network parameter is manipulated while the others are held constant and in section 5.2 scaled coupling and network density are altered.

5.1. Manipulate Single Network Parameters

In the following, scaled couplings, number of neighbors (network densities) and network sizes are varied for rewiring probability $p = 0$, as illustrated in Figure 5.1 and Figure 5.2. The absence of randomness signifies that neither chimera nor chaotic synchronization occur. Firstly, in Figures 5.1a the coupling strength is increased in a Watts-Strogatz network with $N = 100$ nodes and $k = 4$ neighbors. At low coupling only region pairs can manifest and the coherence measure oscillates irregularly. Then, as σ increases the magnitude of the coherence measure strongly decreases indicating that the network becomes more coherent. More precisely, less region pairs can manifest and even if one appears, it is more prone to be overruled, i.e. cannot persist in time. This leads to global waves resulting in higher coherence where the coherence measure oscillates around a coherence state and has a small magnitude. Global waves are the predominant synchronization pattern within the range $\approx \frac{1}{4} - 2$ of the scaled coupling. However, as previously observed, coupled dynamics slow down with increasingly strong coupling causing periods to become too large for the FFT to detect. When the scaled coupling exceeds that range waves travel with non constant velocities leading to an increase in magnitude. Afterwards, there is a critical scaled coupling ≈ 3.5 where oscillators are locked together leading to a constant coherence measure and the frequency analysis fails.
The change in corresponding periods is shown in Figure 5.1b. As observed before increasing the scaled

coupling increases the period of oscillations of the coherence measure (and individual nodes) which are detectable by the FFT until ≈ 2. Then, the length of periods becomes too large for the FFT to identify resulting in a abrupt drop. Afterwards, in the range $\approx 2-3$ the only observation to make is that oscillators try to synchronize leading to changes in the coherence measure. Following that, oscillators are locked together resulting in a constant coherence measure which is indicated by periods ≈ 0. Note that the magnitude rises at the end due to the breakdown of the FFT analysis.
Consequently, in Watts-Strogatz network with fixed parameters N, k and $p = 0$ the emergence of global waves can be forced by controlling the coupling. The caveat is that the dynamics slow down and beyond a critical coupling oscillators are locked. Note that a higher number of neighbors would shift the curve of dots in the plot to the left since additional links strengthen the coupling.

Secondly, the network density ρ is increased while the network size N and scaled coupling $\frac{\sigma}{N}$ are fixed in Figures 5.1c - 5.1d. At low density levels only region pairs can manifest (since $p = 0$). Then, the number of possible region pairs decreases as the number of neighbors increases until only global waves emerge ($k \approx 20 \Rightarrow \rho \approx 0.2$) indicating a higher coherence in the network of oscillators. As observed before, the coupling is strengthened with increasing network density leading to higher coherence which is reflected in the decrease of the magnitude. However, when the network reaches a certain density (≈ 0.8) periods of oscillators become too large for the FFT to detect until there is a all to all connection. Note that lowering the scaled coupling in this plot would shift the curve to the right (and enlarging shifts it to the left) since oscillators would be locked later (or sooner).
The corresponding periods in Figure 5.1d reflect that region pairs manifest below a certain network density resulting in a wider range of periods. Then, the periods drop and become more uniform as global waves start to emerge around a network density $\rho \approx 0.2$. After that, the lengths of periods increase as the coupling gets strengthened by additional links (higher density).
Hence, the emergent synchronization pattern can be manipulated with the network density in a Watts-Strogatz network of fixed size N, $p = 0$ and fixed scaled coupling $\frac{\sigma}{N}$.

Thirdly, the network density ρ, the scaled coupling $\frac{\sigma}{N}$ and rewiring probability $p = 0$ are fixed for increasing network sizes in Figures 5.2a - 5.2b. Note that the fixed density indicates that the number of neighbors increases with the network size. Accordingly, the coherence improves as every node is connected to increasingly many neighbors resulting in a smaller magnitude of the coherence measure. As observed before, corresponding periods become longer as the dynamics are slowed down with the strengthened coupling. However, there are additional underlying dynamics resulting in a drop of the length of periods as illustrated in Figure 5.2b. Further investigation is topic of future research.
Subsequently, an increase in number of neighbors N leads to better synchronization of a network when

density ρ and scaled coupling $\frac{\sigma}{N}$ are kept constant. This is believed to be caused by the increase in number of neighbors.

Lastly, the number of neighbors k, the coupling strength σ and rewiring probability $p = 0$ are fixed in Figures 5.2c - 5.2d while the network size N is increased. Thus, the network density and scaled coupling decrease. As described in section 3.5, this causes more region pairs and substantial differences in the propagation velocities to manifest on the network. These phenomena lead to more irregularities in the oscillations of the measure and an increase of the magnitude.
The corresponding periods in Figure 5.2d decrease indicating a faster node activity and therefore faster oscillations of the coherence measure. It is to be expected that the opposite effect occurs compared to an increased coupling (where the dynamics are slowed down). Consequently, if the network size is increased while the number of neighbors and the coupling strength are fixed results in a diminished synchronizability of a network.
Remarks:

1. Reiterate that the rewiring probability $p = 0$ in Figure 5.1 and Figure 5.2. Therefore, chimera and chaotic synchronization patterns cannot emerge as described in section 4.5 - 4.6.

2. In these figures every point represents an average over ten simulation runs. The standard deviation across runs is on the order of 10^{-10} and less thus suggesting that the emerging synchronization pattern are (relatively) stable with respect to network structure even though the initial states are random. These appear to impact wave directions and the exact location where region pairs manifest. Solidifying that network structure and coupling strength are the key contributors to emergent synchronization pattern.

3. Global waves are favored in higher density networks and thereof dependent scaled coupling. More precisely, for a fixed network size N and rewiring $p = 0$ there exists a range of scaled coupling and network densities such that the emergence of global waves is almost guaranteed.

Recall from chapter 2.1 that the rewiring probability is not introduced into perfect ring networks. Therefore, to add rewiring $p > 0$ the number of neighbors $k = 4$ is increased and fixed alongside network size N and scaled coupling $\frac{\sigma}{N}$ in Figure 5.3a - 5.3b. As observed in the previous chapter, introducing rewiring is necessary so that regions of incoherence can emerge. Then, there is a distinct trend of increasing magnitudes as the rewiring probability increases. This is expected since the added randomness is comparable to noise with increasing intensity. The increased randomness in the network results in large differences of periods where no trend is present in Figure 5.3b. Nevertheless, it can be noted that at first there are mainly region pairs before chimeras start to manifest. Then, region pairs

disappear and chaotic synchronization emerges as the rewiring is increased.
Therefore, the synchronizability of networks declines with increasing rewiring probability. Thus resulting in larger variability of periods. This is particularly relevant for low network densities where as a result regions of incoherence emerge.

5.2. Manipulate Coupling Term and Network Density

At this stage, the impact of scaled coupling and network density on the emergent synchronization pattern is established. Additionally, the change in magnitudes and periods in the coherence measure indicates that there are distinct parameter regions where region pairs and global waves emerge. In the following, network density and scaled coupling are varied in a network of fixed size N and rewiring $p = 0$ to explore the parameter space more systematically. With that objective in mind the regimes of the coherence measure are used (coherent, regular, irregular) to classify the emergent synchronization pattern. Additionally, the case of the oscillators being locked together is registered.

Reminder:

- The coherent regime of the coherence measure corresponds to global wave synchronizations (from section 4.3).
- The regular regime of the coherence measure corresponds to blinking patterns (from section 4.2).
- The irregular regime of the coherence measure corresponds to region pairs in the absence of rewiring (from section 4.4).
- There is a critical coupling such that oscillators are locked. Additionally, oscillators are nearly locked shortly before the critical coupling is reached. This leads to irregular oscillations in the coherence measure which then is misclassified (from section 2.2.2).
- The phase space is high dimensional and can only be sparsely sampled.

Combining the manipulation of network structures to obtain different synchronization patterns from chapter 4 and the impacts of varying one network parameters from above to explore the parameter space of network density and scaled coupling. Then, this parameter space partitions into regions representing blinking pattern, region pairs, global waves and locked dynamics. For each of those a heatmap is plotted to reveal the area.

Firstly, the parameter region corresponding to global waves is revealed in Figure 5.4a. This indicates that for strong coupling and high network density the emergence of global waves is guaranteed (for long enough simulation run times). Additionally, this synchronization pattern can also emerge other

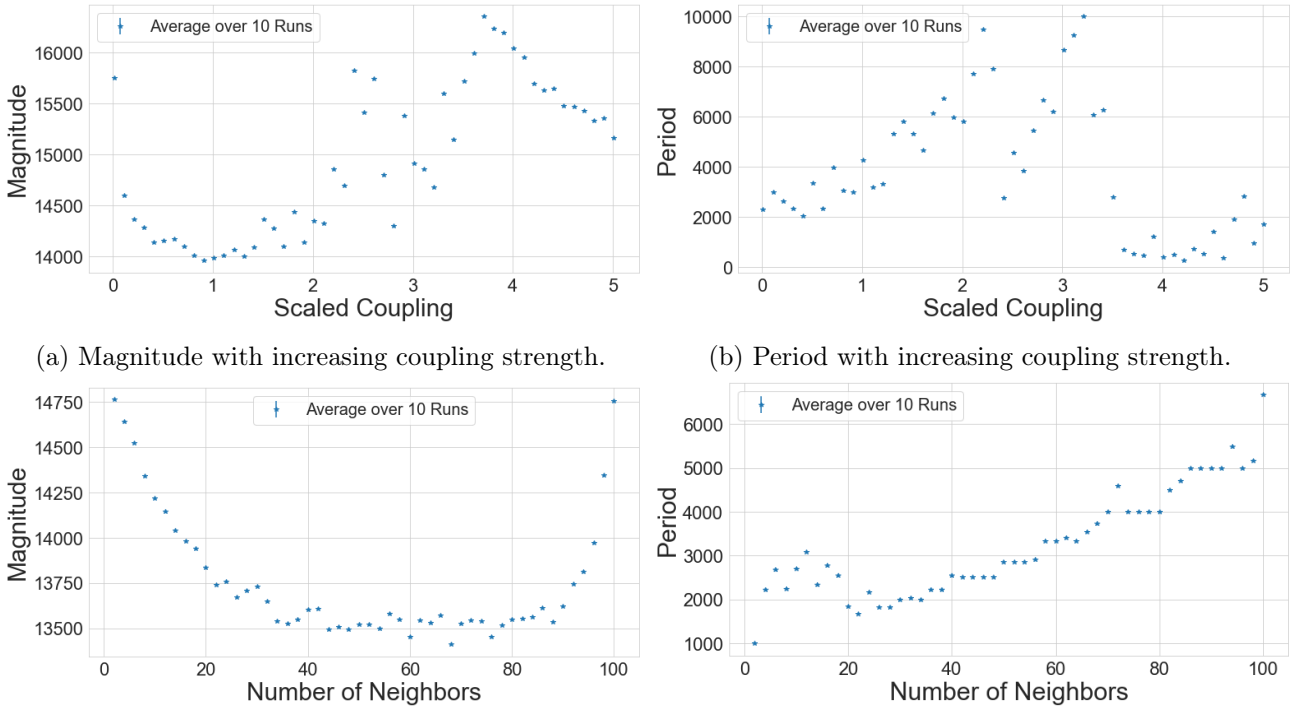

(a) Magnitude with increasing coupling strength.

(b) Period with increasing coupling strength.

(c) Magnitude with increasing number of neighbors.

(d) Period with increasing number of neighbors.

Figure 5.1.: Every data point represents ten simulations for fixed parameters except one which is varied. For every simulation run the coherence measure is computed and its frequency analysis made which is used to obtain magnitude and period. The last $20,000$ time steps of runs are used to improve accuracy of the frequency analysis. Then, the average of magnitude and period over these ten runs are shown in the plots. In (a)-(b) The coupling strength is varied where the first data point corresponds to a scaled coupling $= \frac{\sigma}{N} = \frac{1}{100}$. As observed in the previous chapter, region pairs manifest for low scaled couplings. Then, as the coupling increases the coherence of the network is improved resulting in a lower magnitude of the oscillation of the coherence measure. Global waves are most common in the area with low magnitude ($\approx \frac{1}{4} - 2$). At the same time periods increase for the increased coupling. Therefore, the FFT is unable to correctly identify periods and frequencies when the scaled coupling ≈ 2. Afterwards, a critical scaled coupling ≈ 3.5 is reached where oscillators are locked. The parameters are $N = 100$, $k = 4$, $p = 0$, $\frac{T}{\delta t} = 1,000 * 10^2$ time steps and scaled couplings $= \{\frac{20l+1}{200} : 0 \leq l \leq 25, l \in \mathbb{N}\}$. (c)-(d) The number of neighbors is varied from a perfect ring network to a completely connected network. At first region pairs manifest which is reflected in the higher magnitude. Then, the coherence of the network improves leading to global waves as the number of neighbors increases. The coupling is strengthened with the rising number of neighbors leading to longer periods of the coherence measure. Therefore, magnitudes and periods are not identified correctly by the FFT when $k \approx 80$. The parameters are $N = 100$, $p = 0$, scaled coupling $\frac{\sigma}{N} = \frac{1}{10}$, $\frac{T}{\delta t} = 1,000 * 10^2$ time steps and the numbers of neighbors $= \{2 \leq k \leq 100 : k\, even\}$. For implementation purposes a period ≈ 0 indicates that there is no oscillation, i.e. constant.

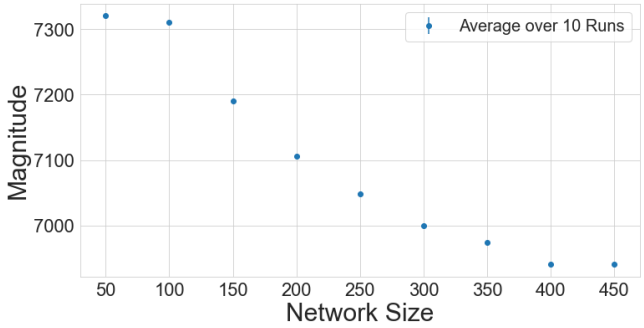

(a) Magnitude with increasing network size.

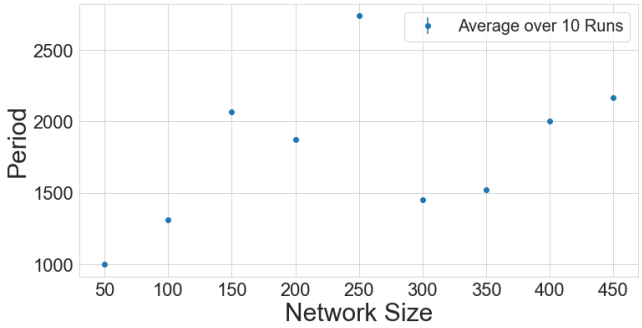

(b) Period with increasing network size.

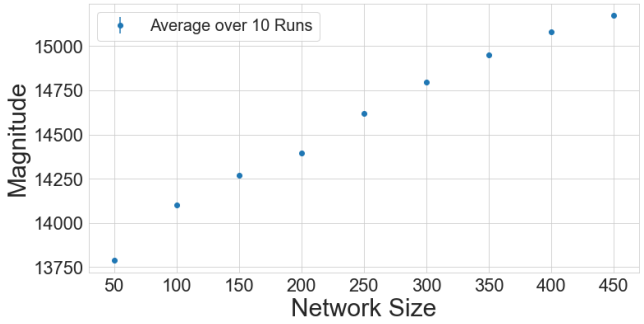

(c) Magnitude with increasing network size.

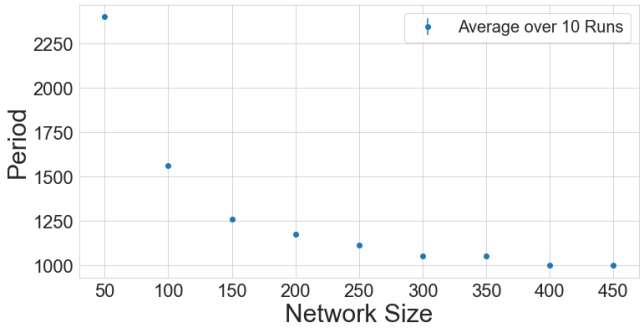

(d) Period with increasing network size.

Figure 5.2.: Every data point represents ten simulations for fixed parameters except one which is varied. For every simulation run the coherence measure is computed and its frequency analysis made which is used to obtain magnitude and period. The last $20,000$ time steps of runs are used to improve accuracy of the frequency analysis. Then, the average of magnitude and period over these ten runs are shown in the plots. (a)-(b) The network size is increases where the network density and scaled coupling is fixed. Therefore, the number of neighbors increases with increasing network size so that the density is constant. This leads to a better synchronization as the network size grows which is reflected in the decreasing magnitude of the oscillation of the coherence measure. At the same time the length of periods increases until $N \approx 250$ before dropping. Further investigations on the underlying dynamics are required to elaborate this phenomenon. The parameters are network density $\rho = 0.0606$, scaled coupling $\frac{\sigma}{N} = \frac{1}{50}$, $p = 0$, $\frac{T}{\delta t} = 1,000 * 10^2$ time steps and varied network sizes $= \{50l : 1 \leq l \leq 10, l \in \mathbb{N}\}$. (c)-(d) The network size is varied with the difference that the number of neighbors $k = 2$ and coupling strength $\sigma = 30$ are fixed. Note that this leads to a decreasing network density and a decreasing scaled coupling (since it is scaling the strength by the network size). Then, the coherence of the network decreased as the network is increased. This is reflected in the rising magnitudes. In comparison, the periods decrease which is due to the decreasing scaled coupling (opposed to strong scaled coupling leading to the increase of the periods). The parameters are number of neighbors $k = 2$, $p = 0$, coupling strength $\sigma = 30$, $\frac{T}{\delta t} = 1,000 * 10^2$ time steps and varied network sizes $= \{50l : 1 \leq l \leq 10, l \in \mathbb{N}\}$.

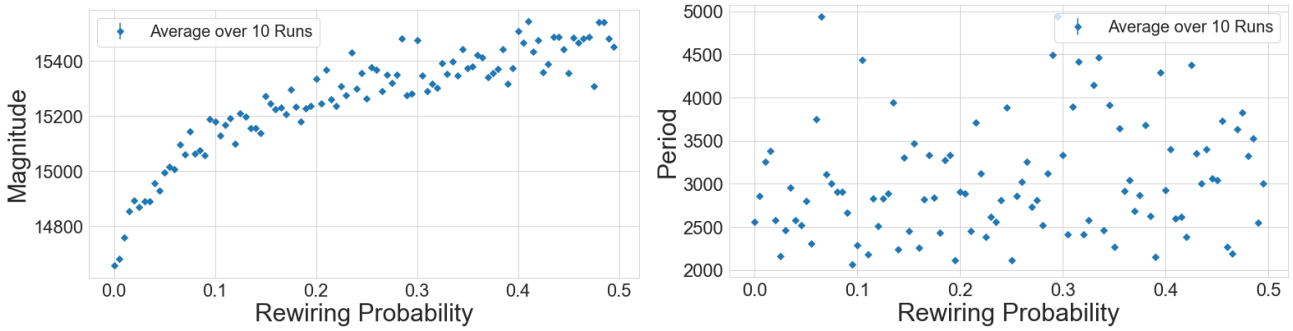

(a) Magnitude with increasing rewiring probability.

(b) Period with increasing rewiring probability.

Figure 5.3.: Every data point represents ten simulations for fixed parameters except the rewiring probability. For every simulation run the coherence measure is computed and its frequency analysis made which is used to obtain magnitude and period. The last $20,000$ time steps of runs are used to improve accuracy of the frequency analysis. Then, the average of magnitude and period over these ten runs are shown in the plots. Note that the magnitudes increase with increasing rewiring probability indicating a decrease of coherence. This is expected since the rising randomness in the network leads to the emergence of regions of incoherence. The parameters are $WS(100, 4, p)$, scaled coupling $\frac{\sigma}{N} = \frac{1}{10}$, $\frac{T}{\delta t} = 1,000 * 10^2$ time steps and varied rewiring probability $p = \{0.005l : 0 \leq l \leq 100\}$.

network structures with low coupling. However, there is a stronger dependence on the initial states, as described in section 4.3. Nevertheless, by comparing these two areas, if a network has a global wave synchronization then it is likely that the network has high density and strong coupling.

Secondly, the parameter region for blinking patterns is shown in Figure 5.4b. Notably, the pattern appears to predominantly manifest in perfect ring network even though initial states have a greater impact on them, as described in section 4.2. This could imply that perfect ring networks have a tendency to wind up in the blinking pattern across coupling strengths as the number of time steps increases. There are other parameter regions where a blinking pattern can manifest which indicates that there are other regions in the parameter space where the initial states have a stronger impact on the emergent synchronization pattern. A finer grain net is needed to identify those which is topic of future research.

Thirdly, the parameter region corresponding to region pairs is revealed in Figure 5.4c. Note that most perfect ring networks arrive here across scaled couplings. This could be an artefact of the threshold parameter η being too small for perfect ring networks. For example, the global wave synchronization in small perfect ring networks in appendix section A.2 would be misclassified. These could potentially arrive in the coherent or the regular regime for longer simulation run times as described above. Additionally, in perfect ring networks with region pairs, travelling waves propagate with high velocity (which can be seen in Figure 3.10c). Therefore, the network appears nearly synchronous but the coherence measure is the irregular regime. This indicates that longer run times are required for perfect ring networks to improve their emergent synchronization pattern. Besides that, region pairs reliably manifest in the low

density and small scaled coupling region. Moreover, this heatmap indicates that region pairs can only manifest in this parameter region. Additionally, it is indicated that in border regions there is a stronger impact of the initial states. It is crucial to note that if rewiring is introduced then this parameter region partitions further which is topic of future research.
Note that there is a narrow parameter region with high density and high coupling term. This region correspond to nearly locked dynamics. The oscillators exhibit activity resulting in irregular oscillations in the coherence measure. However, they do not synchronize (shown in Figure 3.10e).
Above this region the dynamics are locked which is illustrated in Figure 5.4d. Then, the coherence measure is constant and no synchronization pattern emerges.

Lastly, these four heatmaps reveal distinct parameter regions even though there is some overlap. Therefore, it is possible to merge them into one plot with only small loss of information. In Figure 5.5 the parameter regions for blinking pattern, region pairs, global waves, nearly locked and locked dynamics are shown.

Remarks:

1. The most common synchronization patterns are global wave and region pair synchronization.
2. When it is known that $p = 0$ then conjectures about the network structure can be made from the emergent synchronization pattern:
    - If there are global waves then it is likely a high density network with high scaled coupling.
    - If there are region pairs then it is likely a low density network with low scaled coupling.
3. The overlap between regimes for the same parameter configurations suggests that:
    - emerging synchronization pattern have a stronger dependence on the initial states in borders region of the parameter space and
    - there might be regions within regions.

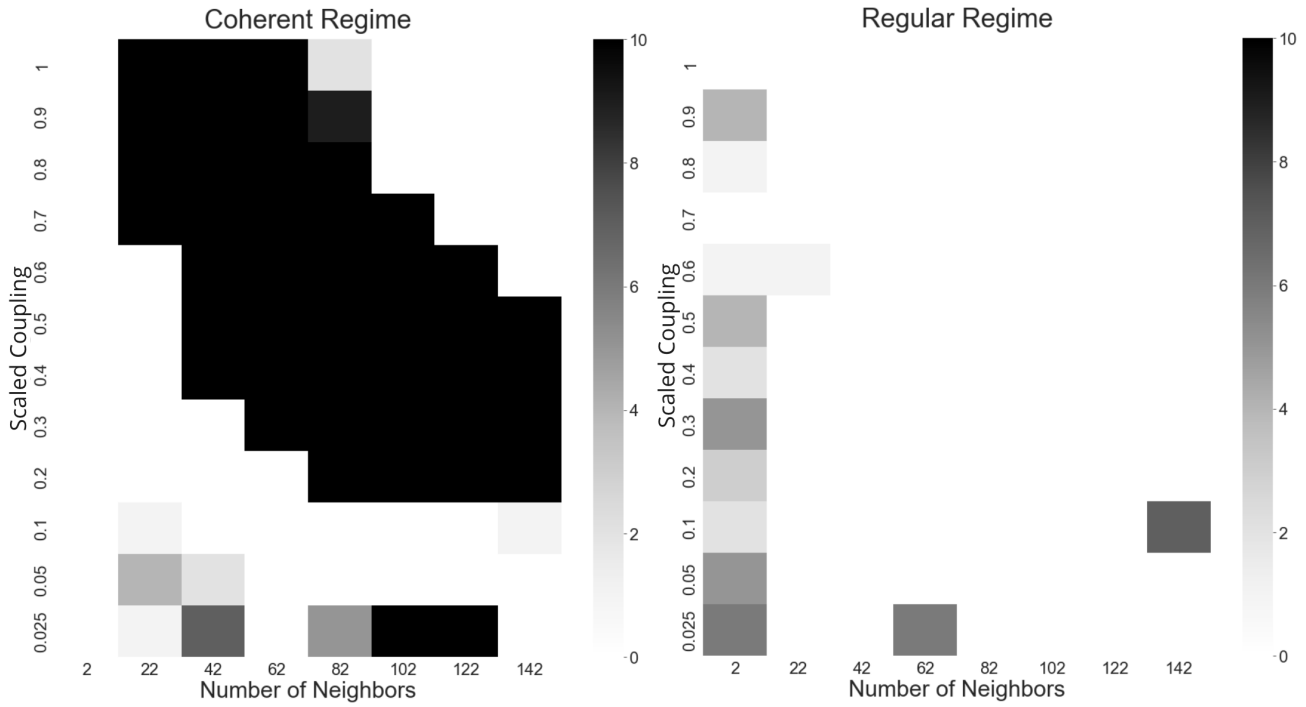

(a) Coherent Regime

(b) Regular Regime

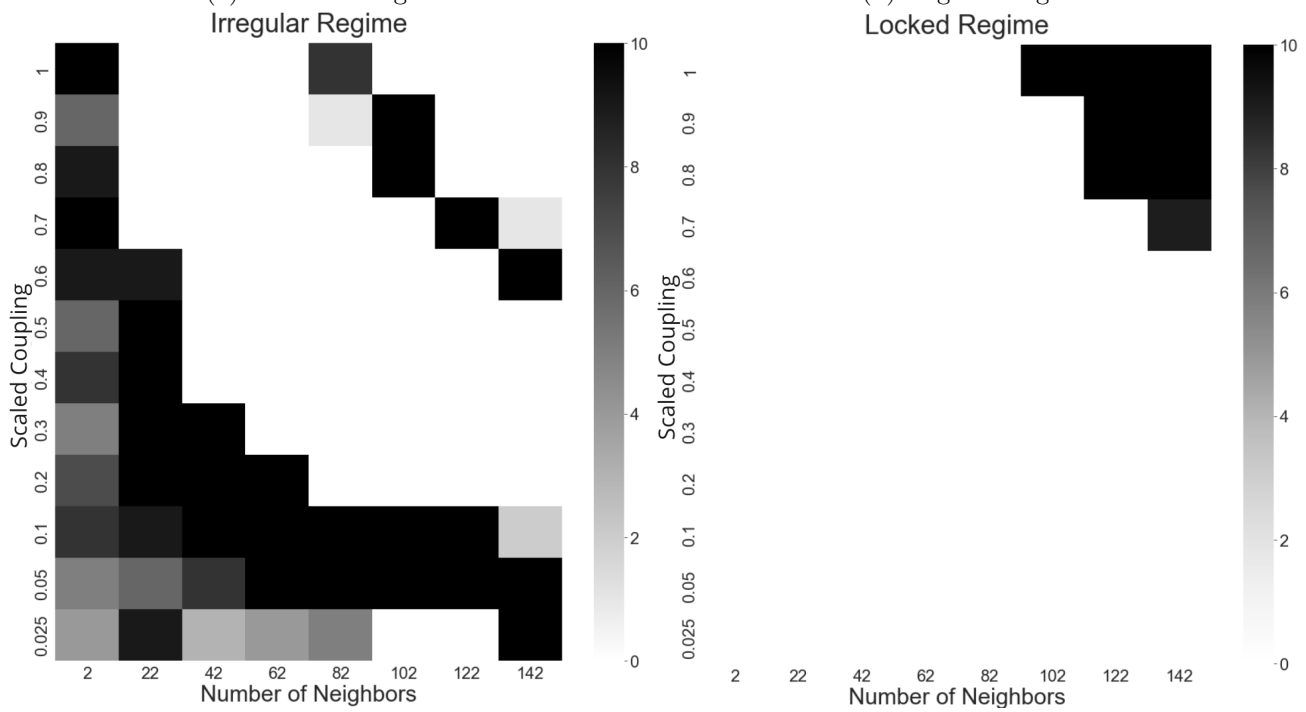

(c) Irregular Regime

(d) Oscillators are locked

Figure 5.4.: The parameter space of number of neighbors and scaled coupling is sparsely sampled. Ten simulations are run for every parameter pair $(k, \frac{\sigma}{N})$. Therefore, this is a 12×8 grid. Then, the regime of the coherence measure was counted in every simulation run where additionally the locked regime is detected. The heatmap colors correspond to the number of runs (out of ten) which arrived in the respective regime. White indicates zero runs arrived in that regime and black indicated that every run wound up there. There are distinct parameter regions leading to the emergence of global waves, region pairs and locked dynamics. However, the blinking pattern overlaps with region pairs and potentially longer run times are necessary. The network size $N = 200$ and rewiring $p = 0$ are fixed and every simulation ran for $\frac{T}{\delta t} = 1,500 * 10^2$ time steps. Then, the number of neighbors $k \in \{2, 22, 42, 62, 82, 102, 122, 142\}$ and the scaled couplings $\frac{\sigma}{N} \in \{0.025, 0.05, 0.1, 0.2, 0.3, 0.4, 0.5, 0.6, 0.7, 0.8, 0.9, 1\}$ are used.

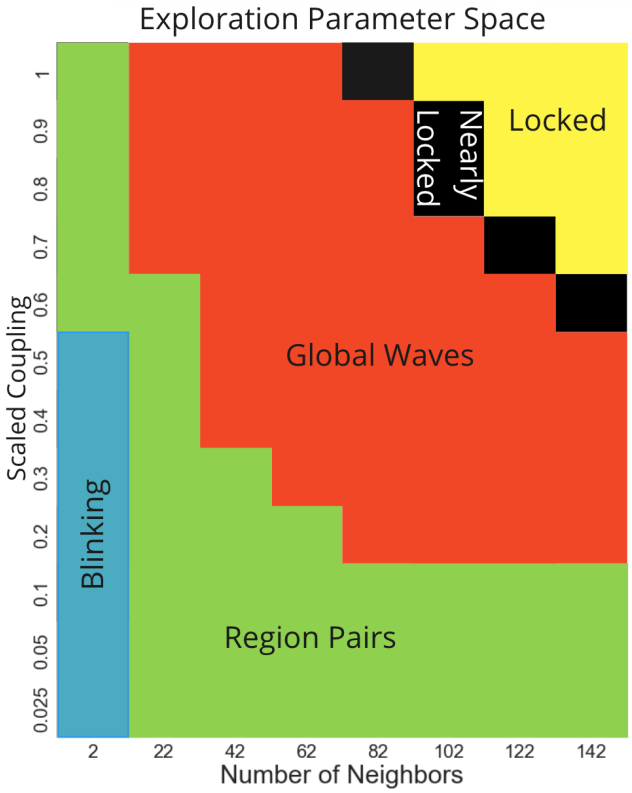

Figure 5.5.: A network size = 200, rewiring $p = 0$ and $\frac{T}{\delta t} = 1,500 * 10^2$ time steps are used. Then, the "number of neighbor vs scaled coupling" parameter space is mapped to the emerging synchronization pattern where ten simulations are taken for every parameter configuration (of the 12×8). Even though this heatmap is coarse grained, it reveals a close relation between network structures and emerging synchronization patterns. Additionally, it shows that the influence of initial states can be controlled with the network configuration and scaled coupling. However, in boundary regions of the synchronization patterns there is an overlap between them and the initial states impact the emerging pattern. The greatest influence is in the blinking pattern case in perfect ring networks, as described in sections 4.2 and 4.3. The corresponding descriptions of the synchronization patterns are: blinking pattern in section 4.2, global waves in section 4.3 and region pairs in section 4.4. The locked and nearly locked dynamics are described in section 3.5.

6. Summary and Discussion

In this thesis, we investigate emergent synchronization patterns of a non-linear dynamical system on ring networks. More precisely, we studied a Watts-Strogatz networks where every node follows FitzHugh-Nagumo dynamics which are in a limit cycle regime. For this purpose a numerical approach was chosen. However, the computational complexity of simulations does not scale linearly with the number of nodes in the network, simulation run time and step size. Therefore, neither long simulation run times nor simulations for large networks are feasible. Another next step is to optimize the program. It was found that there are five possible synchronization patterns which can be achieved, depending on the network structure. In addition, complete synchronization was only observed when the network started in a synchronous state thus independent of network structure. Moreover, the dynamics can be locked when the coupling is too strong and no synchronization pattern emerge. The five synchronization patterns could be obtained (relatively) reliably by manipulating the network structure (N, k, p) and scaled coupling $\frac{\sigma}{N}$ despite the impact of initial states and the high dimensionality of this problem. The influence of initial states was not investigated further and is topic of future research.
In the absence of rewiring, different synchronization patterns are reflected in the behaviour of the coherence measure thus can be categorized. Consequently, this was used to more systematically explore the parameter space of network density and scaled coupling. This revealed the relation between distinct parameter regions and synchronization patterns. However, an in-depth analysis of frequency spectra is required to improve the classification accuracy and to enable to distinguish between region pairs, chimera and chaotic patterns. A natural next step is to improve the resolution of Figure 5.5 by increasing the number of parameter configurations and increasing the number of simulation runs per parameter pair. The findings and results in this thesis are groundwork to build up from. A natural next step is to compare them to synchronization patterns on (larger) real world networks. Additionally, it is of interest to infer network structure from an observed synchronization pattern.

There is a plethora of potential next steps besides the ones described above:

- Theoretical analysis of the numerical results: For example,

  What are the underlying dynamics leading to e.g. the emergence of region pairs and overthrowing

events?

How do initial states influence the emergent pattern?

- Draw initial conditions according to different probability distributions.
- Derive equations of the emergent dynamics from the set of individual equations.
- Use networks of non-identical oscillators.
- Robustness of the network:
  - What happens if an attack on a ring network removes a shortest path from a given node to itself where the paths runs around the network once? Here a perfect ring would be removed from a ring network.
  - What if an attack is the propagation of corrosion of nodes or misinformation? In the sense that perturbations of nodes are spread/propagated driving the system away from a "normal state". For example, if there is some disturbance in the cell cycle such that small errors are induced and propagated. Then, after "enough" cycles the perturbation becomes large enough to have a damaging impact.
- What are synchronization pattern on (ring) network with substructures that are ring network. For example, the metabolism circuit [29].

Bibliography

[1] JR Waldram. The josephson effects in weakly coupled superconductors. *Reports on Progress in Physics*, 39(8):751, 1976.

[2] Steven H Strogatz, Daniel M Abrams, Allan McRobie, Bruno Eckhardt, and Edward Ott. Crowd synchrony on the millennium bridge. *Nature*, 438(7064):43–44, 2005.

[3] Juan A Acebrón, Luis L Bonilla, Conrad J Pérez Vicente, Félix Ritort, and Renato Spigler. The kuramoto model: A simple paradigm for synchronization phenomena. *Reviews of modern physics*, 77(1):137, 2005.

[4] Moritz Gerster, Rico Berner, Jakub Sawicki, Anna Zakharova, Antonín Škoch, Jaroslav Hlinka, Klaus Lehnertz, and Eckehard Schöll. Fitzhugh–nagumo oscillators on complex networks mimic epileptic-seizure-related synchronization phenomena. *Chaos: An Interdisciplinary Journal of Nonlinear Science*, 30(12):123130, 2020.

[5] Markus K. Youssef, Joel Hancock, Felix Müller, Loan Vulliard, Ruth Byrne, Hans P. Kiener, Berend Snijder, Giulio Superti-Furga, Herbert Edelsbrunner, and Jörg Menche. The emergence of ring structures in biological networks. *unpublished*.

[6] Thomas House. Modelling epidemics on networks. *Contemporary Physics*, 53(3):213–225, 2012.

[7] Albert-László Barabási and Réka Albert. Emergence of scaling in random networks. *science*, 286(5439):509–512, 1999.

[8] Malbor Asllani, Paul Expert, and Timoteo Carletti. A minimally invasive neurostimulation method for controlling abnormal synchronisation in the neuronal activity. *PLoS computational biology*, 14(7):e1006296, 2018.

[9] Jörg Menche. Lecture notes: Introduction to complex network analysis, October-January 2021/2022.

[10] Richard FitzHugh. Impulses and physiological states in theoretical models of nerve membrane. *Biophysical journal*, 1(6):445–466, 1961.

[11] SA Plotnikov, J Lehnert, AL Fradkov, and E Schöll. Synchronization in heterogeneous fitzhugh-nagumo networks with hierarchical architecture. *Physical Review E*, 94(1):012203, 2016.

[12] Tanya Kostova, Renuka Ravindran, and Maria Schonbek. Fitzhugh–nagumo revisited: Types of bifurcations, periodical forcing and stability regions by a lyapunov functional. *International journal of bifurcation and chaos*, 14(03):913–925, 2004.

[13] Alex Arenas, Albert Díaz-Guilera, Jurgen Kurths, Yamir Moreno, and Changsong Zhou. Synchronization in complex networks. *Physics reports*, 469(3):93–153, 2008.

[14] Francisco A Rodrigues, Thomas K DM Peron, Peng Ji, and Jürgen Kurths. The kuramoto model in complex networks. *Physics Reports*, 610:1–98, 2016.

[15] Hyunsuk Hong, Moo-Young Choi, and Beom Jun Kim. Synchronization on small-world networks. *Physical Review E*, 65(2):026139, 2002.

[16] Gerald Teschl. *Ordinary differential equations and dynamical systems*, volume 140. American Mathematical Soc., 2012.

[17] Zhan Yong, Zhang Su-Hua, Zhao Tong-Jun, An Hai-Long, Zhang Zhen-Dong, Han Ying-Rong, Liu Hui, and Zhang Yu-Hong. The synchronization of fitzhugh–nagumo neuron network coupled by gap junction. *Chinese Physics B*, 17(6):2297, 2008.

[18] Sebastian Rost and Christine Thomas. Array seismology: Methods and applications. *Reviews of geophysics*, 40(3):2–1, 2002.

[19] Lawrence P Panych. Theoretical comparison of fourier and wavelet encoding in magnetic resonance imaging. *IEEE transactions on medical imaging*, 15(2):141–153, 1996.

[20] Paul Heckbert. Notes 3, computer graphics 2, 15-463: Fourier transform and the fast fourier transform (fft) algorithm, February 1995.

[21] Amin Gasmi. *What is Fast Fourier Transform?* PhD thesis, Société Francophone de Nutrithérapie et de Nutrigénétique Appliquée, 2022.

[22] Karl Bernhard Riepl BSc. Fitzhugh-nagumo-on-networks. https://github.com/KarlR24/FitzHugh-Nagumo-on-Networks, 2023.

[23] Daniel M Abrams and Steven H Strogatz. Chimera states for coupled oscillators. *Physical review letters*, 93(17):174102, 2004.

[24] Eckehard Schöll. Synchronization patterns and chimera states in complex networks: Interplay of topology and dynamics. *The European Physical Journal Special Topics*, 225:891–919, 2016.

[25] Renato E Mirollo and Steven H Strogatz. Synchronization of pulse-coupled biological oscillators. *SIAM Journal on Applied Mathematics*, 50(6):1645–1662, 1990.

[26] Martin Kassabov, Steven H Strogatz, and Alex Townsend. A global synchronization theorem for oscillators on a random graph. *Chaos: An Interdisciplinary Journal of Nonlinear Science*, 32(9), 2022.

[27] Malik Muhammad Ibrahim and Il Hyo Jung. Complex synchronization of a ring-structured network of fitzhugh-nagumo neurons with single-and dual-state gap junctions under ionic gates and external electrical disturbance. *Ieee Access*, 7:57894–57906, 2019.

[28] Tommaso Menara, Giacomo Baggio, Dani Bassett, and Fabio Pasqualetti. Functional control of oscillator networks. *Nature communications*, 13(1):4721, 2022.

[29] Conor M O'Brien, Bhanu Chandra Mulukutla, Douglas G Mashek, and Wei-Shou Hu. Regulation of metabolic homeostasis in cell culture bioprocesses. *Trends in biotechnology*, 38(10):1113–1127, 2020.

A. Appendix

A.1. Blinking Pattern, WS(50, 2, 0) and scaled coupling $= 1$

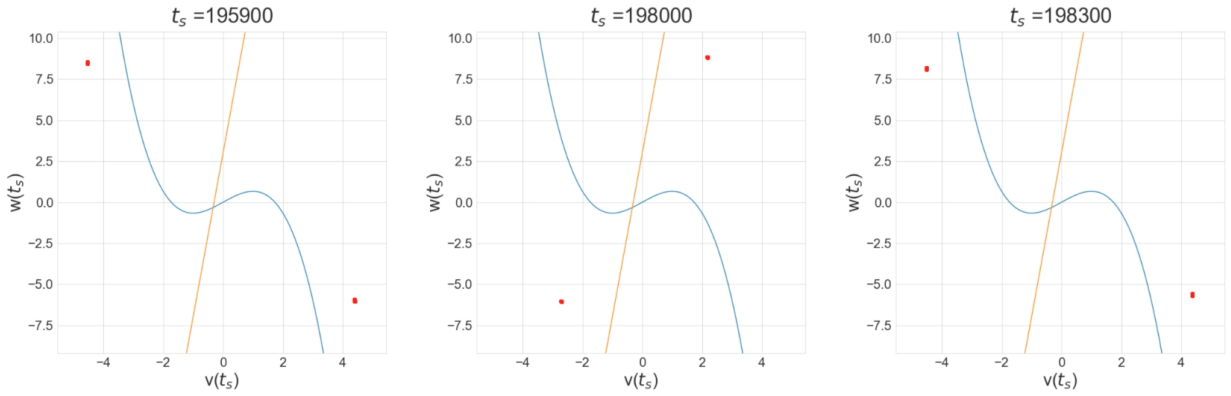

(a) Two clumps of oscillators travel around the limit cycle.

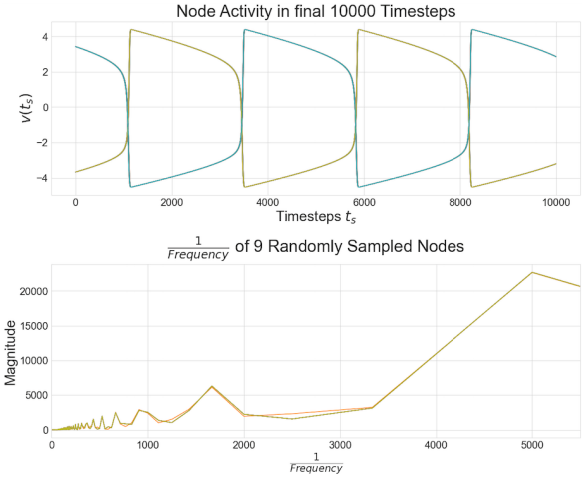

(b) The activity of nodes corresponds to the two clumps in the final $10,000$ time steps and the frequency spectra of 9 randomly sampled nodes are taken.

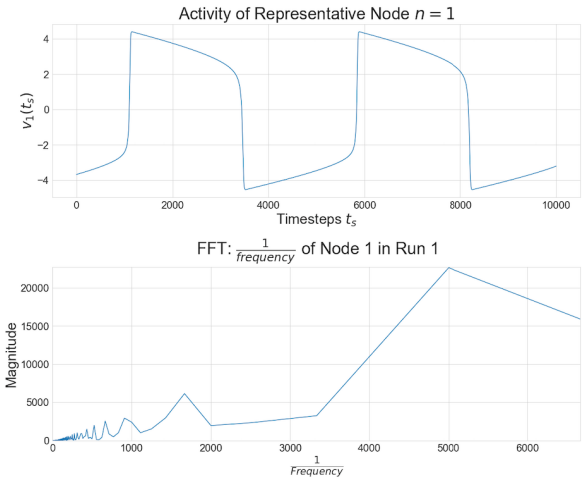

(c) A representative oscillation and its frequency analysis.

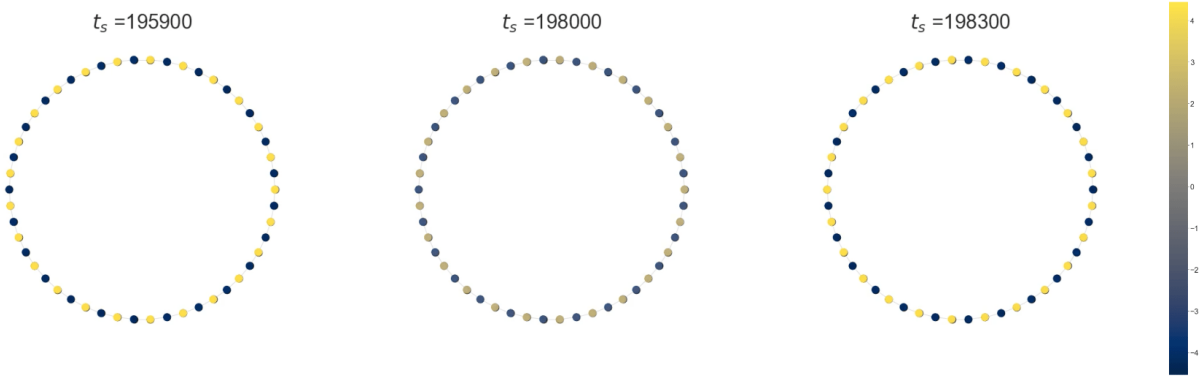

(d) Neighboring nodes alternate in phases.

Figure A.1.: First part of the plot collection corresponding to a blinking pattern on a $WS(50, 2, 0)$ with scaled coupling $= 1$ and $\frac{T}{\delta t} = 2,000 * 10^2$ time steps. The visualizations of the oscillators in (a) the phase plane, (b)-(c) the node analysis and (c) the spatiotemporal propagation are shown, as described in section 4.2. The colorbar continuously assigns colors from blue to yellow to the fast variable v on the limit cycle.

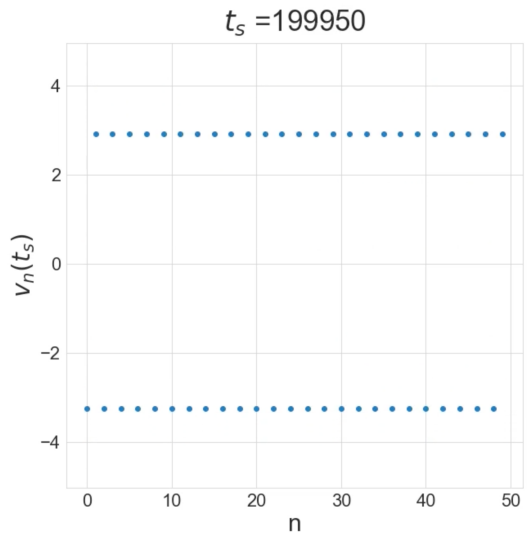

(a) Oscillators are locked in two phases.

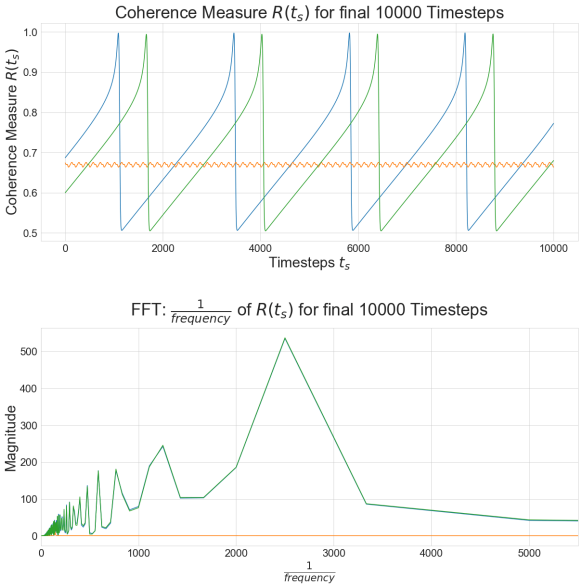

(e) The final 10,000 time steps of three simulations and of their frequency spectra.

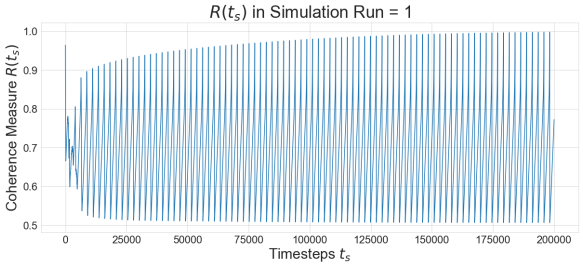

(b) The coherence measure is in the regular regime.

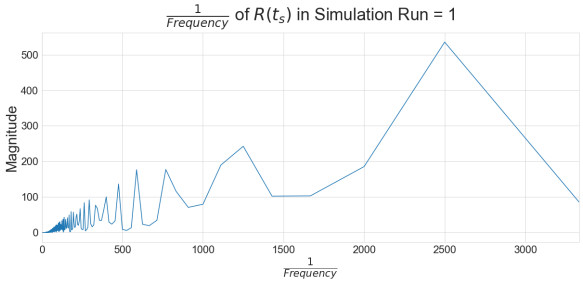

(c) The frequency spectrum corresponds to the coherence measure.

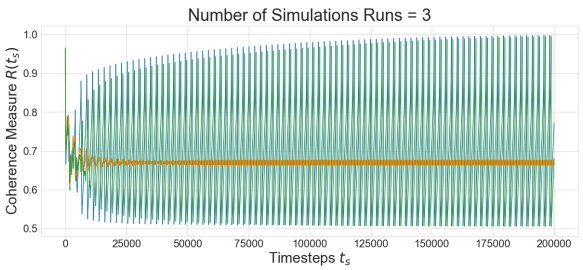

(d) Two out of three coherence measures are in the regular regime.

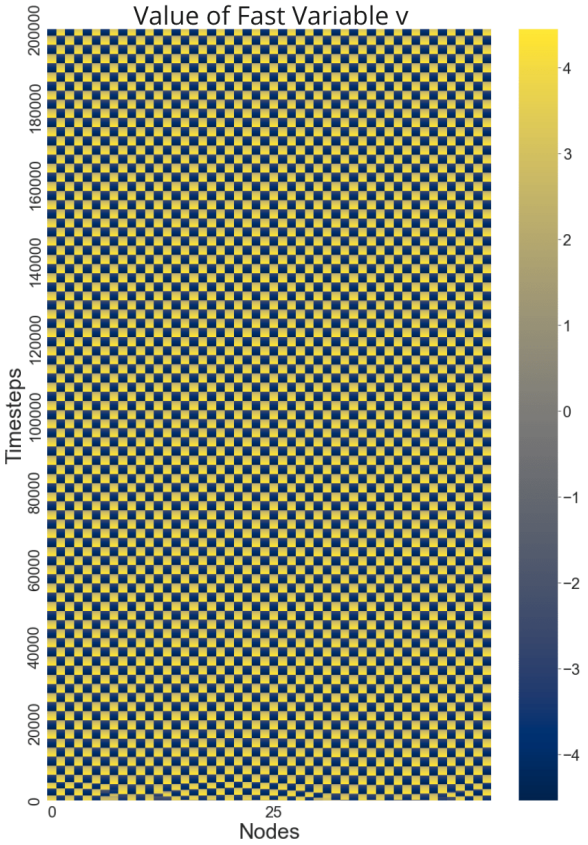

(f) The heatmap appears as a checkered board.

Figure A.2.: Second part of the plot collection corresponding to a blinking pattern on a $WS(50, 2, 0)$ with scaled coupling = 1 and $\frac{T}{\delta t} = 2,000 * 10^2$ time steps. The visualizations of the (a) chimera pattern plot, (b), (c) coherence measure and its frequency spectrum, (d) coherence measure of three simulation runs, (e) the final 10,000 time steps of the three coherence measures and their frequency spectra and (f) the heatmap of the evolution of the network are shown, as described in section 4.2.

A.2. Global Waves, WS(50, 2, 0) and scaled coupling $= \frac{1}{5}$

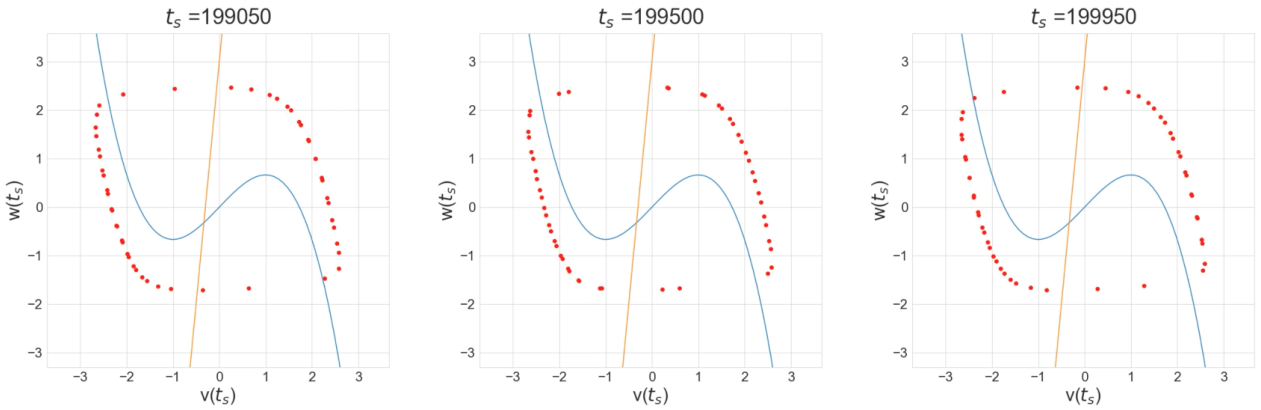

(a) Oscillators distribute on the limit cycle.

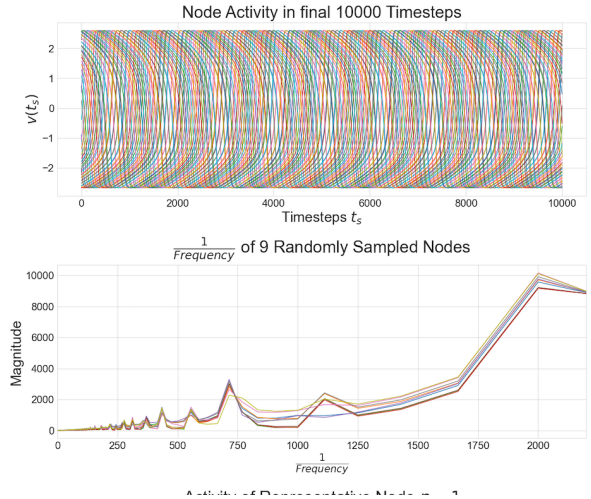

(b) The activity of nodes in the final $10,000$ time steps and the frequency spectra of 9 randomly sampled nodes are taken.

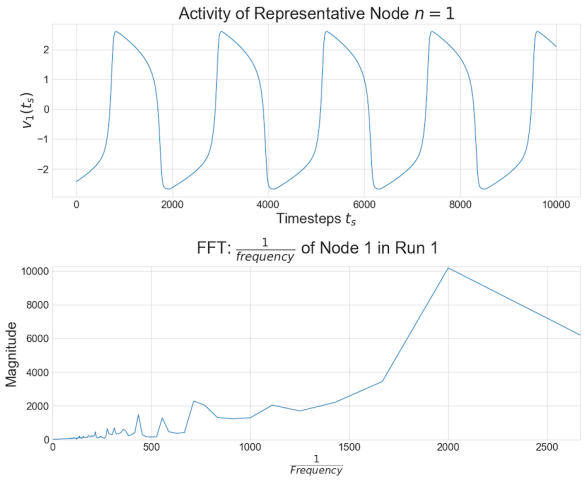

(c) A representative oscillation and its frequency analysis.

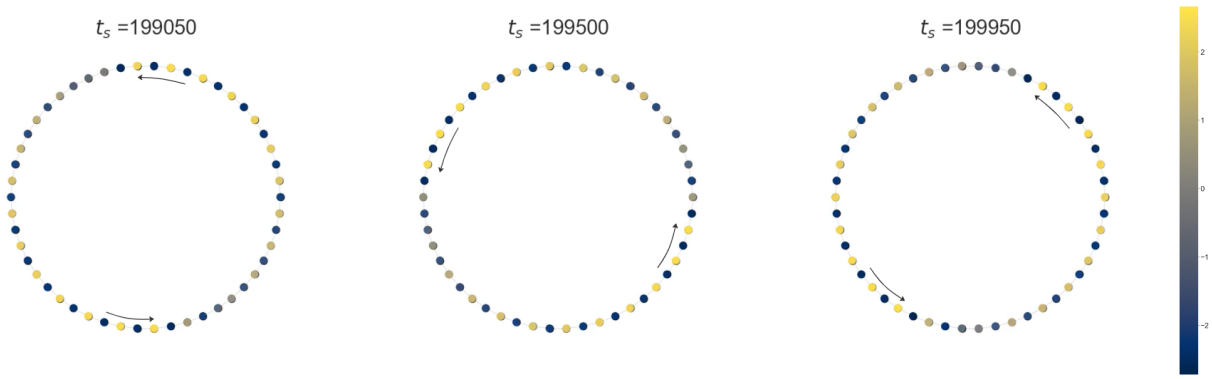

(d) Global waves are interlaced which was only observed in perfect ring networks.

Figure A.3.: First part of the plot collection corresponding to global waves on a perfect ring network $WS(50, 2, 0)$ with scaled coupling $= \frac{1}{5}$ and $\frac{T}{\delta t} = 2,000 * 10^2$ time steps. The visualizations of the oscillators in (a) the phase plane, (b)-(c) the node analysis and (c) the spatiotemporal propagation are shown, as described in section 4.3. The colorbar continuously assigns colors from blue to yellow to the fast variable v on the limit cycle.

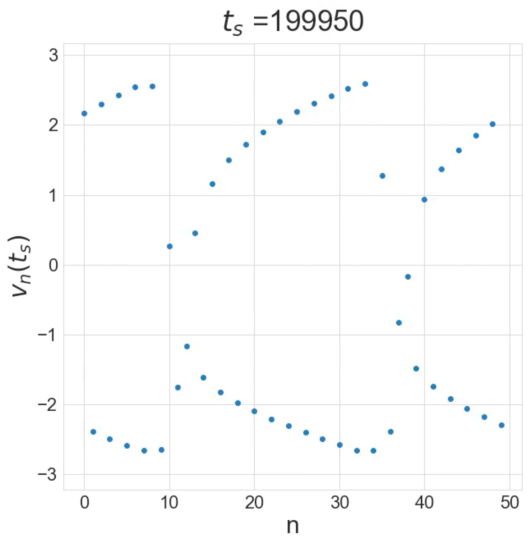

(a) Waves are captured in the plot.

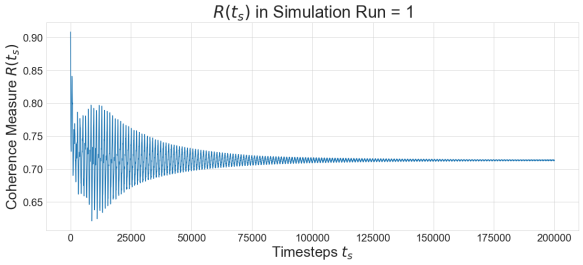

(b) The coherence measure oscillates with small amplitude.

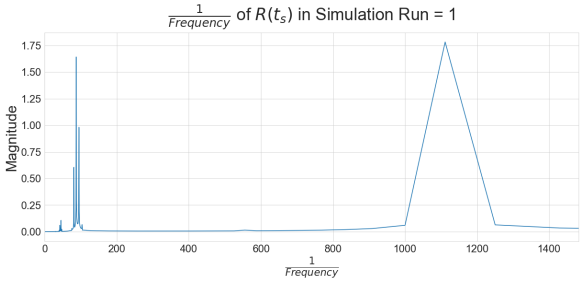

(c) The frequency spectrum corresponds to the coherence measure.

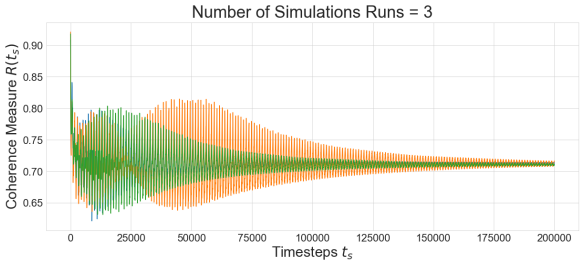

(d) All three coherence measures are in the irregular regime indicating that longer run times or a larger threshold are required to correctly classify them.

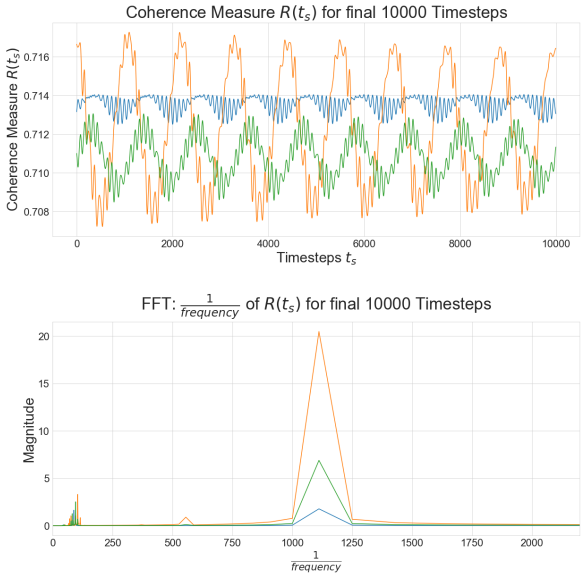

(e) The final 10,000 time steps of three simulations and of their frequency spectra.

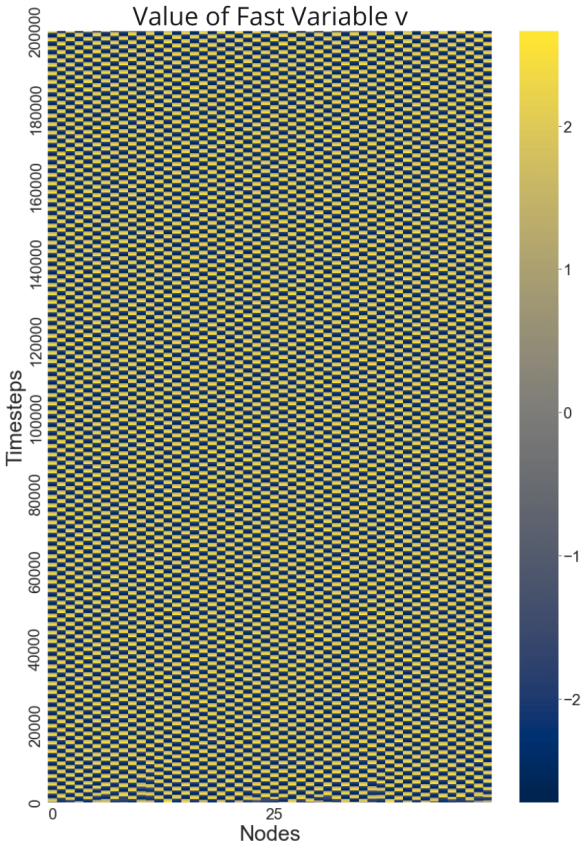

(f) The heatmap appears as a checkered board but lines have a slope $\neq 0$.

Figure A.4.: Second part of the plot collection corresponding to global waves on a perfect ring network $WS(50, 2, 0)$ with scaled coupling $= \frac{1}{5}$ and $\frac{T}{\delta t} = 2,000 * 10^2$ time steps. The visualizations of the (a) chimera pattern plot, (b), (c) coherence measure and its frequency spectrum, (d) coherence measure of three simulation runs, (e) the final 10,000 time steps of the three coherence measures and their frequency spectra and (f) the heatmap of the evolution of the network are shown, as described in section 4.3.

A.3. Global Waves, WS(500, 100, 0) and scaled coupling $= \frac{1}{50}$

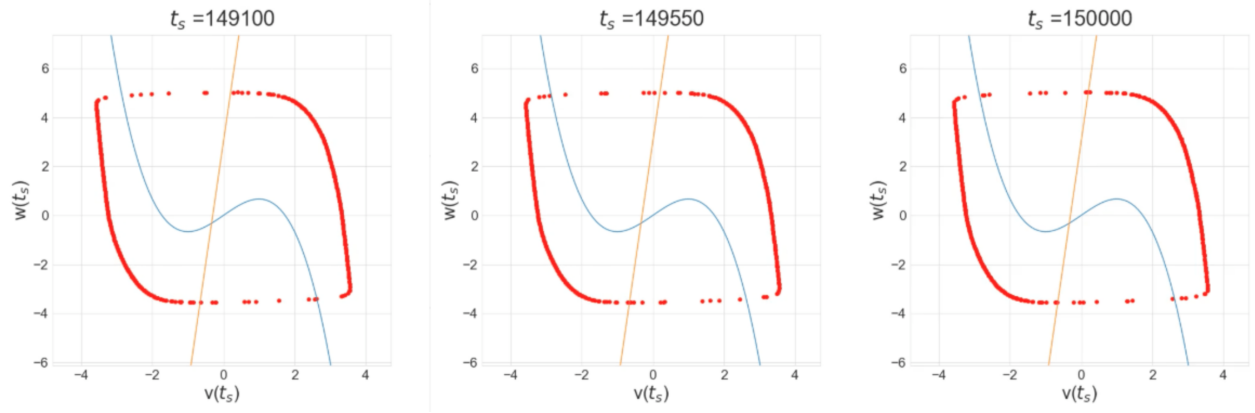

(a) Oscillators distribute on the limit cycle.

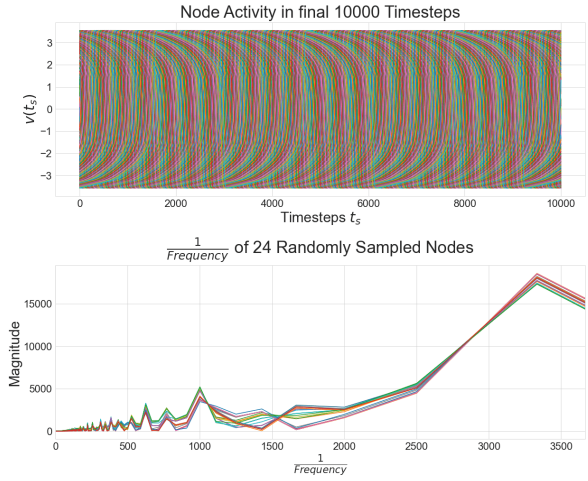

(b) The activity of nodes in the final 10,000 time steps and the frequency spectra of 24 randomly sampled nodes are taken.

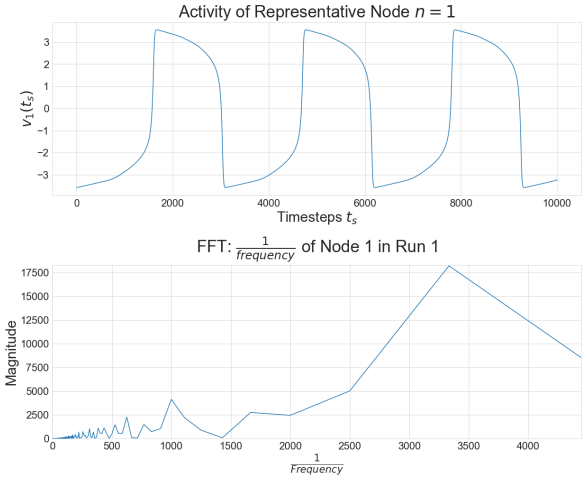

(c) A representative oscillation and its frequency analysis.

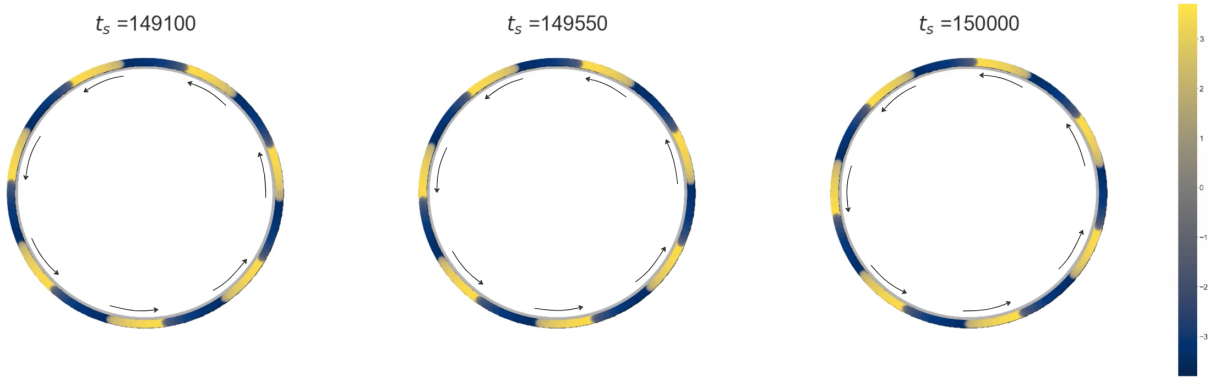

(d) Global waves are not interlaced.

Figure A.5.: First part of the plot collection corresponding to global waves on a high density network $WS(500, 100, 0)$ with scaled coupling $= \frac{1}{50}$ and $\frac{T}{\delta t} = 1,500 * 10^2$ time steps. The visualizations of the oscillators in (a) the phase plane, (b)-(c) the node analysis and (c) the spatiotemporal propagation are shown, as described in section 4.3. The colorbar continuously assigns colors from blue to yellow to the fast variable v on the limit cycle.

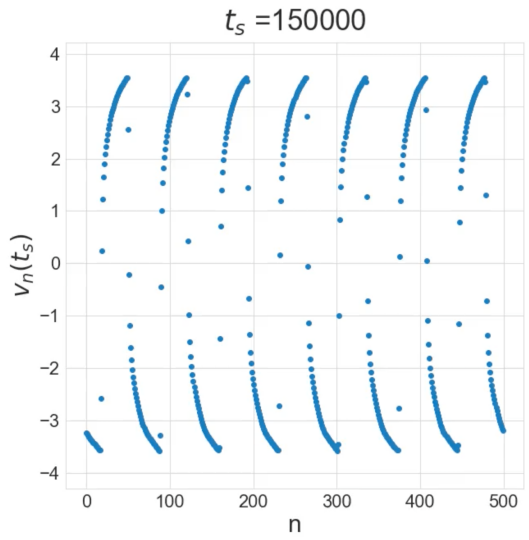

(a) Waves are captured in the plot.

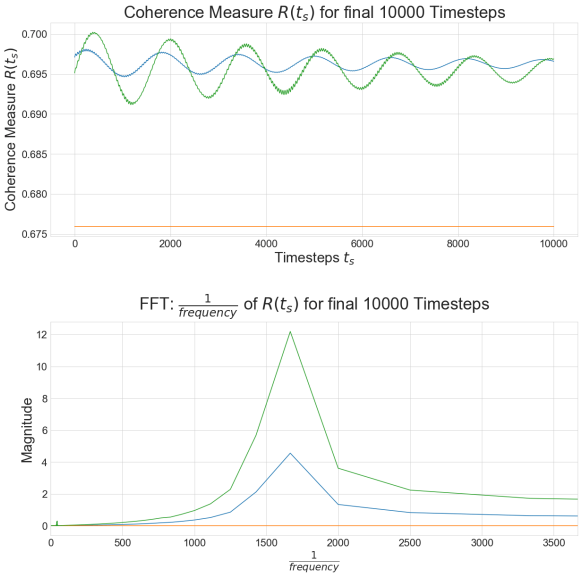

(e) The final 10,000 time steps of three simulations and of their frequency spectra.

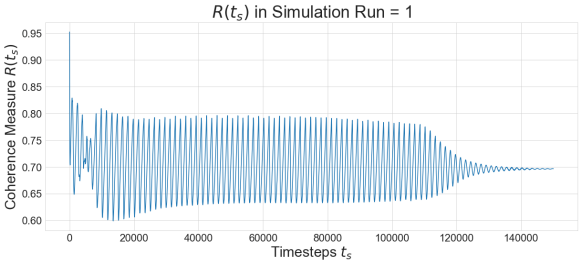

(b) The coherence measure oscillates with small amplitude.

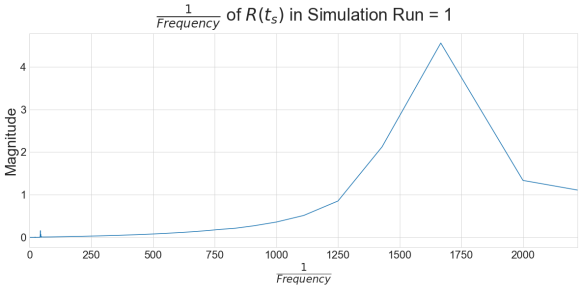

(c) The frequency spectrum corresponds to the coherence measure.

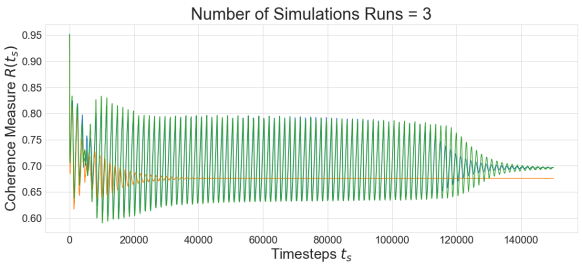

(d) All three coherence measures are in the coherent regime.

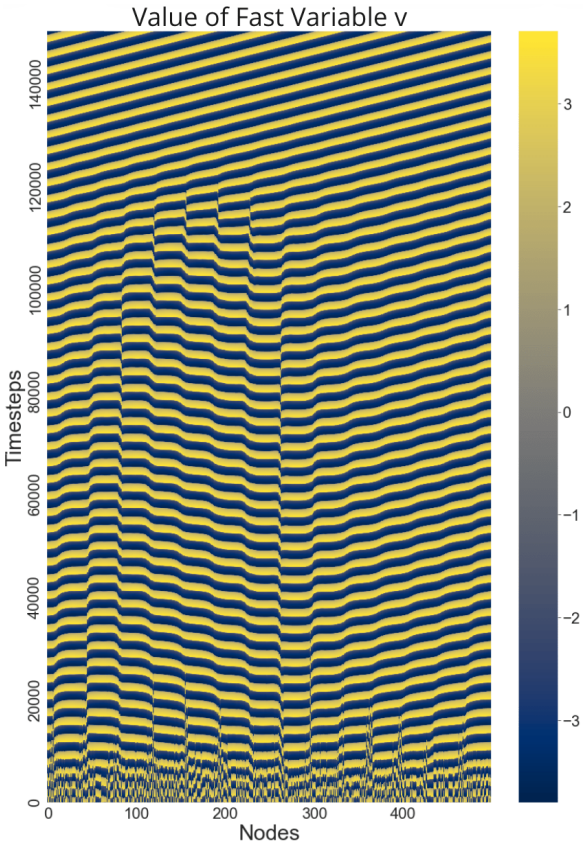

(f) The heatmap clearly shows the global waves.

Figure A.6.: Second part of the plot collection corresponding to global waves on a high density ring network $WS(500, 100, 0)$ with scaled coupling $= \frac{1}{50}$ and $\frac{T}{\delta t} = 1,500 * 10^2$ time steps. The visualizations of the chimera pattern plot, (b), (c) coherence measure and its frequency spectrum, (d) coherence measure of three simulation runs, (e) the final 10,000 time steps of the three coherence measures and their frequency spectra and (f) the heatmap of the evolution of the network are shown, as described in section 4.3.

A.4. Region Pairs, WS(200, 2, 0) and scaled coupling $= \frac{1}{10}$

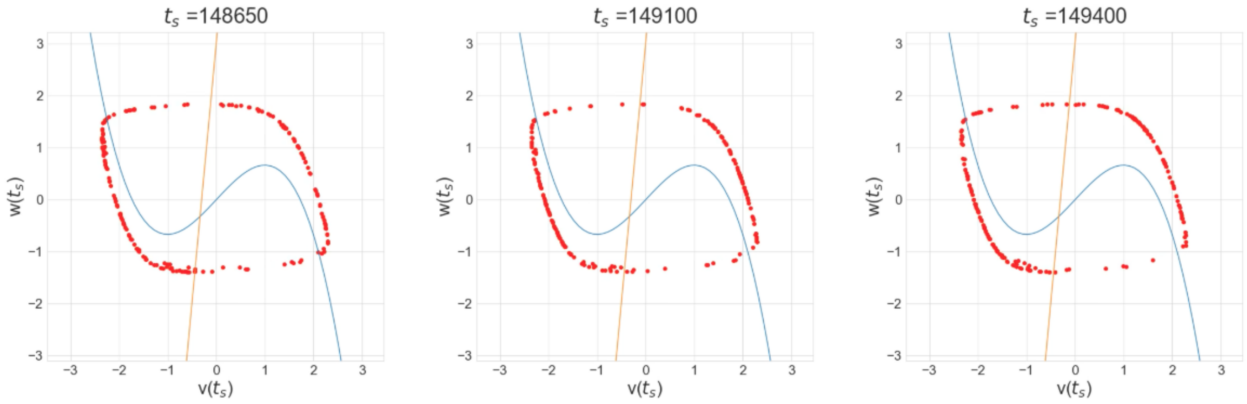

(a) Oscillators scatter around the limit cycle.

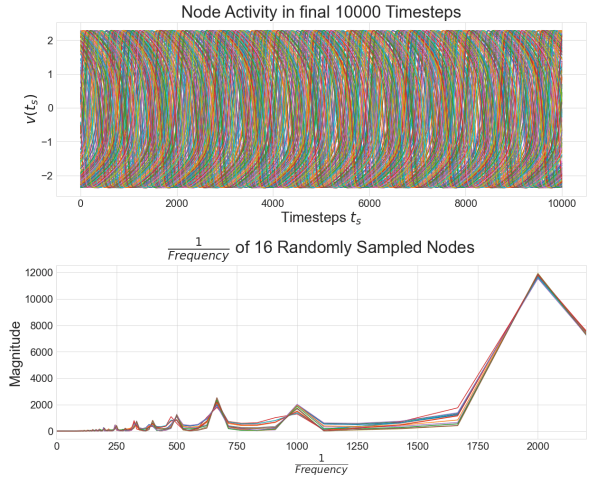

(b) The activity of nodes in the final 10, 000 time steps and the frequency spectra of 16 randomly sampled nodes are taken.

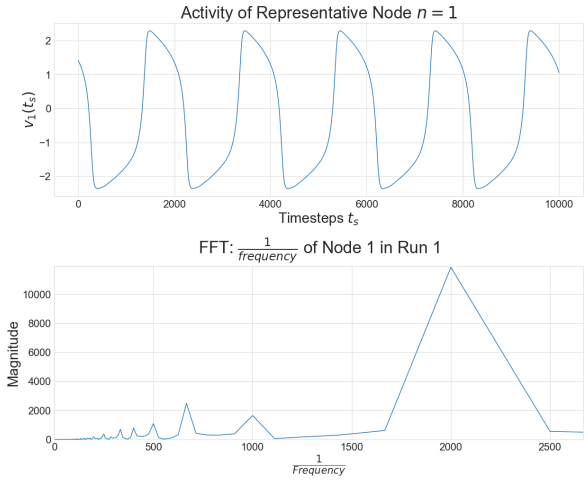

(c) A representative oscillation and its frequency analysis.

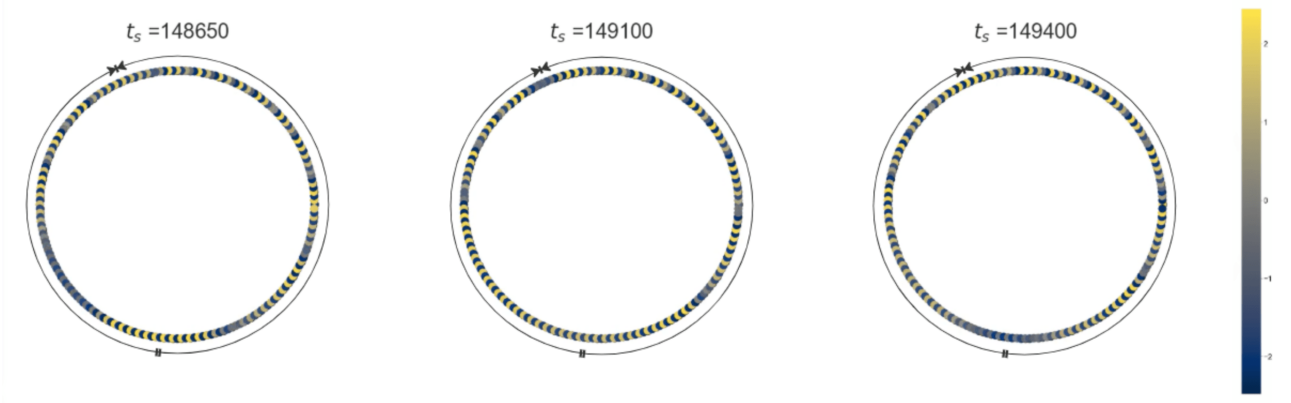

(d) Waves and region pairs are interlaced for perfect ring networks. Generating regions are indicated by two lines on the circle and annihilating regions by two opposing arrows.

Figure A.7.: First part of the plot collection corresponding to region pairs on a perfect ring network $WS(200, 2, 0)$ with scaled coupling $= \frac{1}{10}$ and $\frac{T}{\delta t} = 1,500 * 10^2$ time steps. The visualizations of the oscillators in (a) the phase plane, (b)-(c) the node analysis and (c) the spatiotemporal propagation are shown, as described in section 4.4. The colorbar continuously assigns colors from blue to yellow to the fast variable v on the limit cycle.

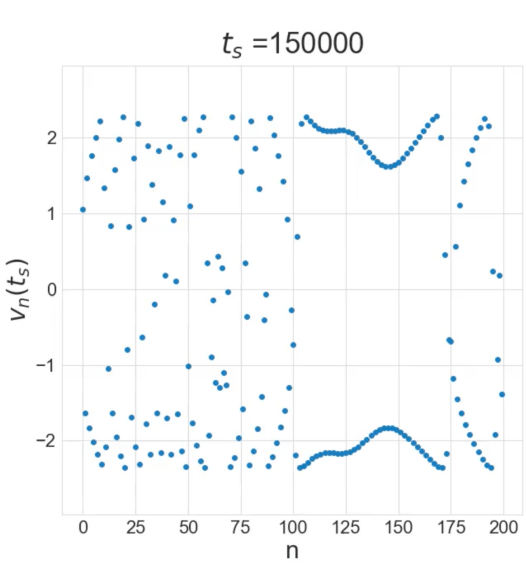

(a) Region pairs are phase locked with travelling waves in between.

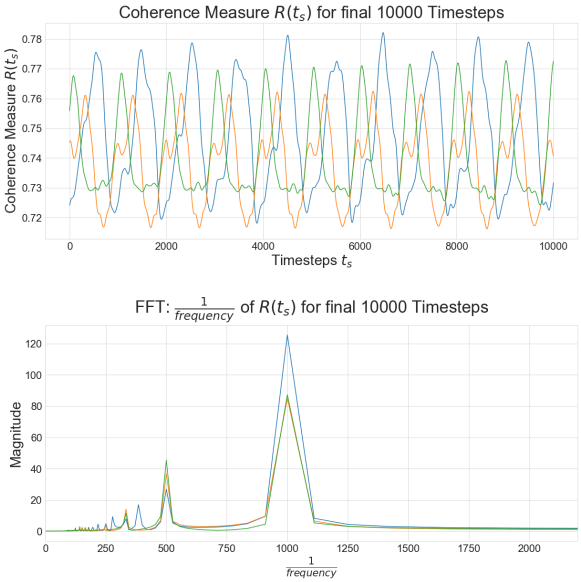

(e) The final 10,000 time steps of three simulations and of their frequency spectra.

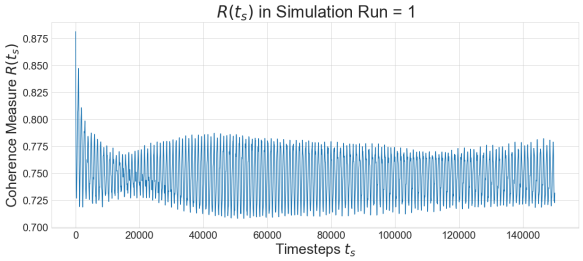

(b) The coherence measure oscillates irregularly.

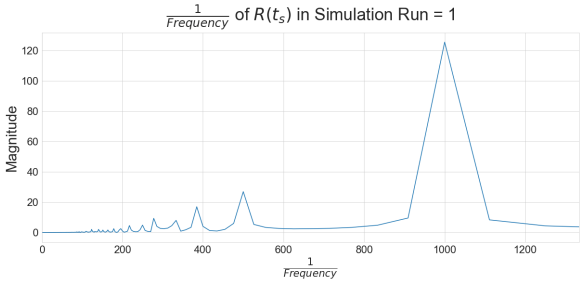

(c) The frequency spectrum corresponds to the coherence measure.

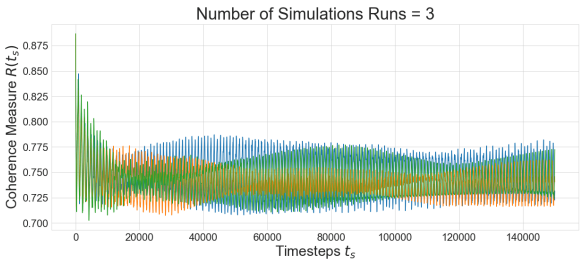

(d) All three coherence measures are in the irregular regime.

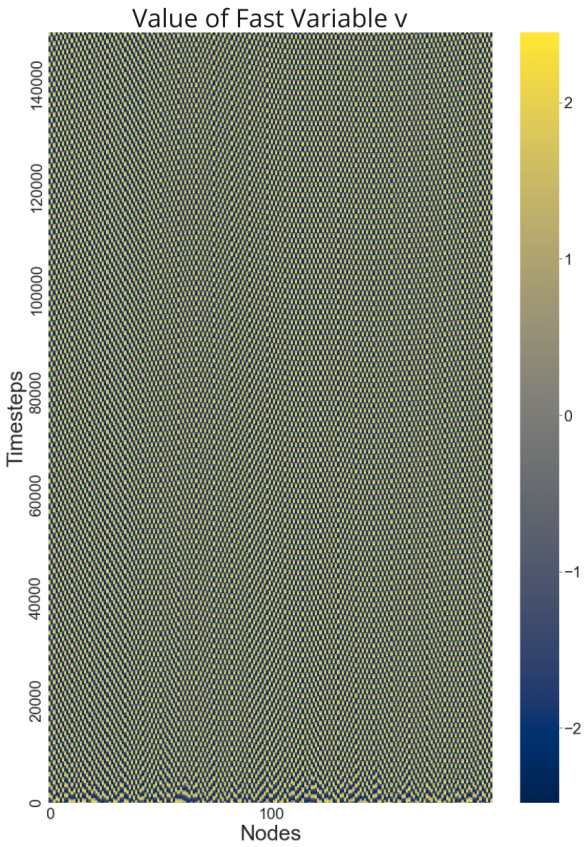

(f) The heatmap illustrates a region pair and high propagation velocity.

Figure A.8.: Second part of the plot collection corresponding to region pairs on a perfect ring network $WS(200, 2, 0)$ with scaled coupling = $\frac{1}{10}$ and $\frac{T}{\delta t} = 1,500 * 10^2$ time steps. The visualizations of the (a) chimera pattern plot, (b), (c) coherence measure and its frequency spectrum, (d) coherence measure of three simulation runs, (e) the final 10,000 time steps of the three coherence measures and their frequency spectra and (f) the heatmap of the evolution of the network are shown, as described in section 4.4.

A.5. Region Pairs, WS(500, 16, 0) and scaled coupling $= \frac{1}{10}$

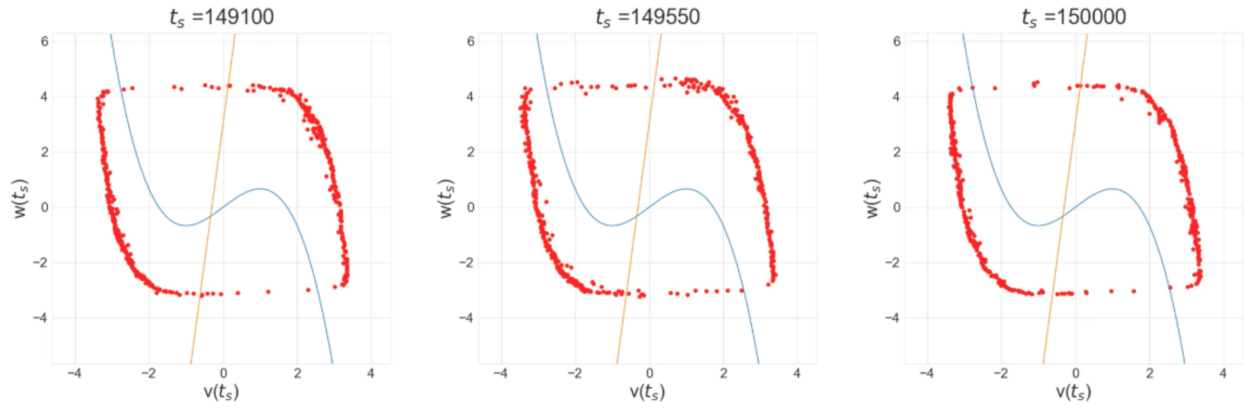

(a) Oscillators scatter around the limit cycle.

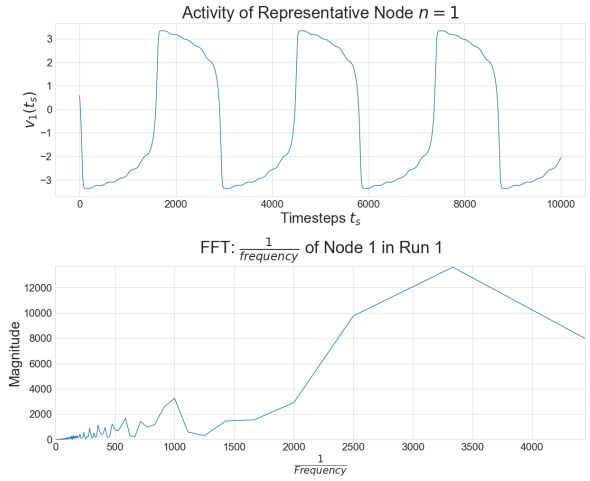

(b) The activity of nodes in the final 10,000 time steps and the frequency spectra of 24 randomly sampled nodes are taken.

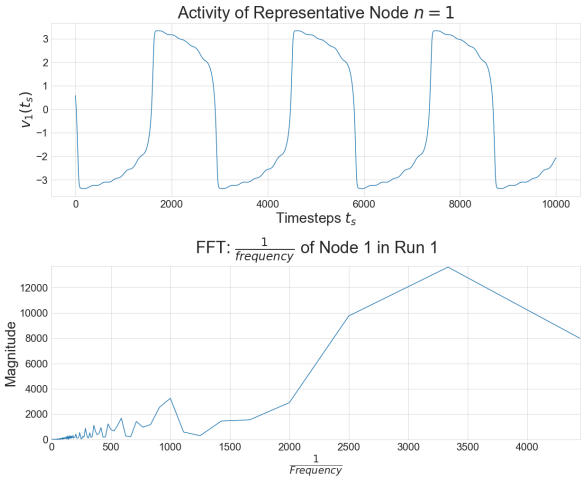

(c) A representative oscillation and its frequency analysis.

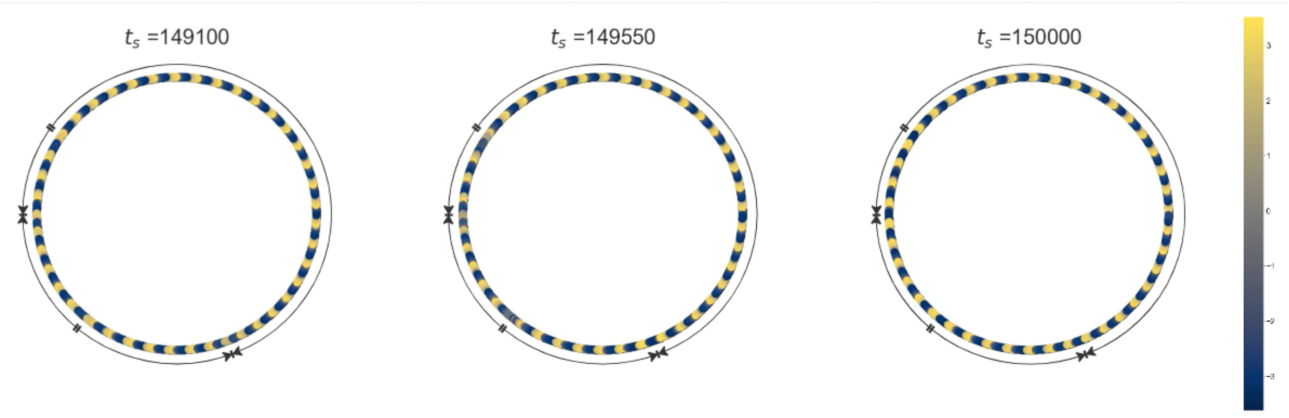

(d) Waves and region pairs are not interlaced in higher density networks. Generating regions are indicated by two lines on the circle and annihilating regions by two opposing arrows.

Figure A.9.: First part of the plot collection corresponding to region pairs on a density ring network $WS(500, 16, 0)$ with scaled coupling $= \frac{1}{10}$ and $\frac{T}{\delta t} = 1,500{*}10^2$ time steps. The visualizations of the oscillators in (a) the phase plane, (b)-(c) the node analysis and (c) the spatiotemporal propagation are shown, as described in section 4.4. The colorbar continuously assigns colors from blue to yellow to the fast variable v on the limit cycle.

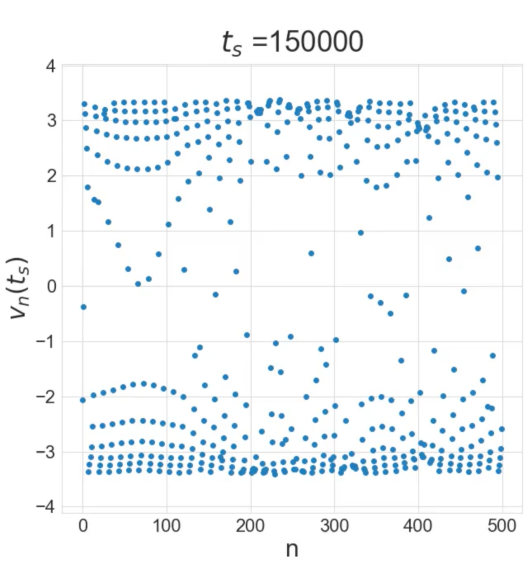

(a) Region pairs (=clumps) are phase locked with travelling waves (=arcs) in between.

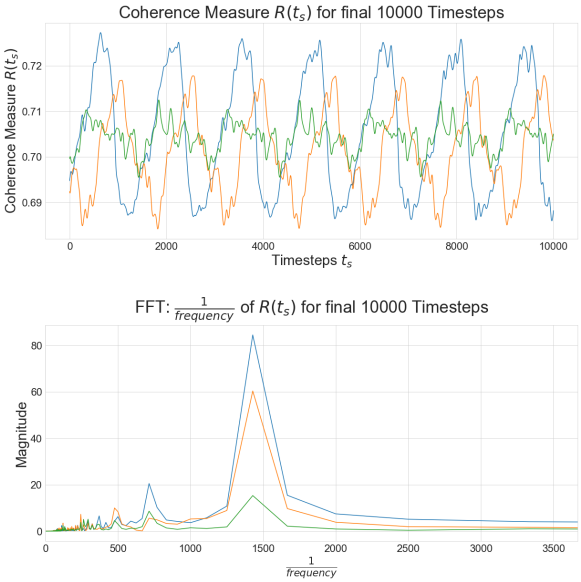

(e) The final 10,000 time steps of three simulations and of their frequency spectra.

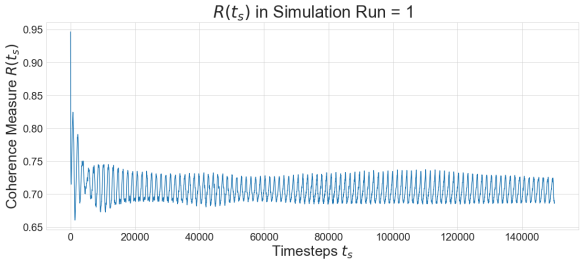

(b) The coherence measure oscillates irregularly.

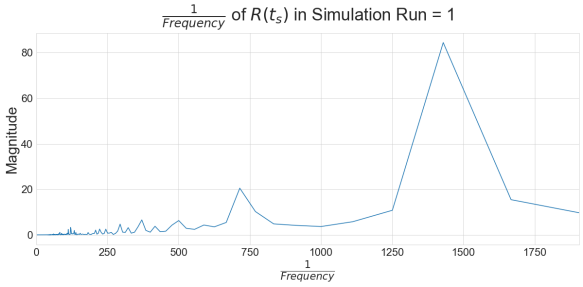

(c) The frequency spectrum corresponds to the coherence measure.

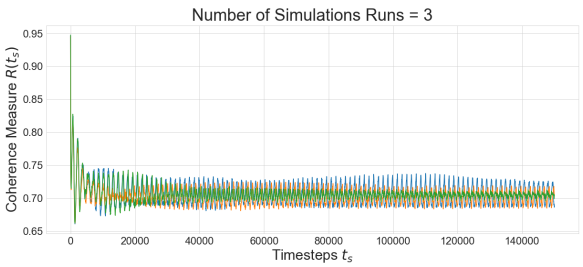

(d) All three coherence measures are in the irregular regime.

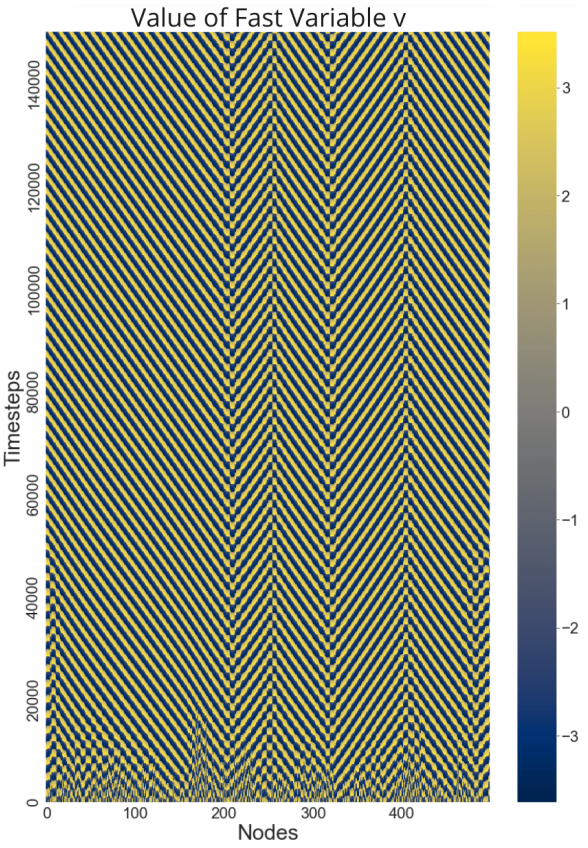

(f) The heatmap makes region pairs clearly visible.

Figure A.10.: Second part of the plot collection corresponding to region pairs on a higher density ring network $WS(500, 16, 0)$ with scaled coupling = $\frac{1}{10}$ and $\frac{T}{\delta t} = 1,500 * 10^2$ time steps. The visualizations of the (a) chimera pattern plot, (b), (c) coherence measure and its frequency spectrum, (d) coherence measure of three simulation runs, (e) the final 10,000 time steps of the three coherence measures and their frequency spectra and (f) the heatmap of the evolution of the network are shown, as described in section 4.4.

A.6. Region Pairs, WS(500, 16, 0,005), scaled coupling $= \frac{1}{10}$

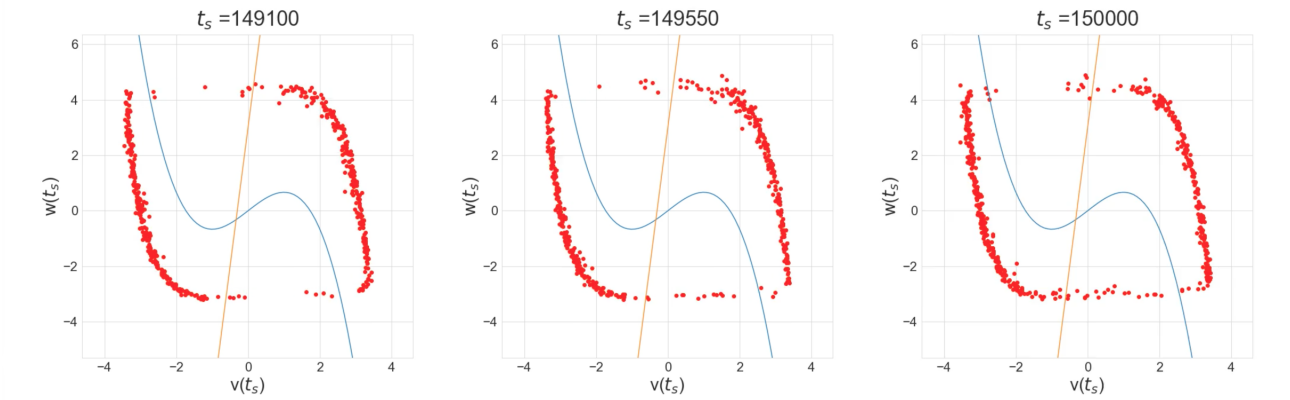

(a) Oscillators scatter around the limit cycle.

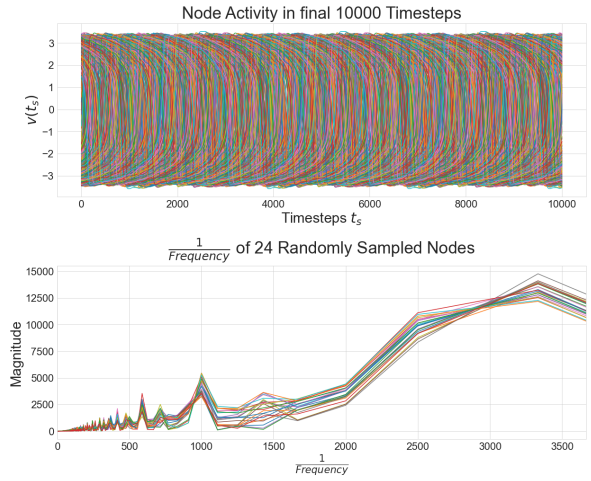

(b) The activity of nodes in the final 10, 000 time steps and the frequency spectra of 24 randomly sampled nodes are taken.

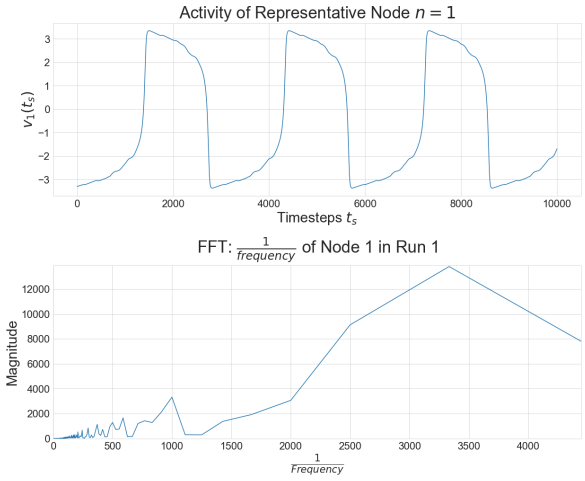

(c) A representative oscillation and its frequency analysis.

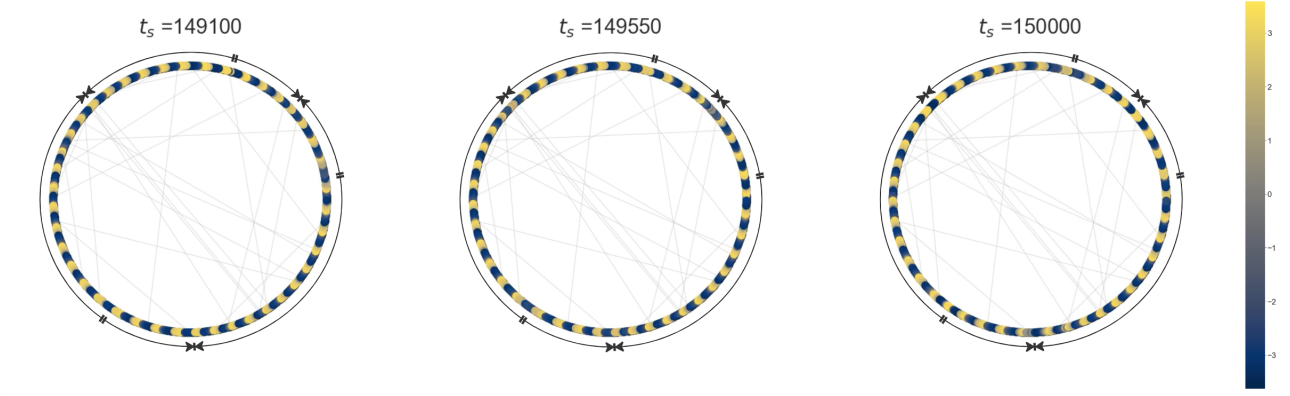

(d) Waves and region pairs are not interlaced. Generating regions are indicated by two lines on the circle and annihilating regions by two opposing arrows.

Figure A.11.: First part of the plot collection corresponding to region pairs on a higher density ring network $WS(500, 16, 0, 005)$ with scaled coupling $= \frac{1}{10}$ and $\frac{T}{\delta t} = 1,500 * 10^2$ time steps. The visualizations of the oscillators in (a) the phase plane, (b)-(c) the node analysis and (c) the spatiotemporal propagation are shown, as described in section 4.4. The colorbar continuously assigns colors from blue to yellow to the fast variable v on the limit cycle.

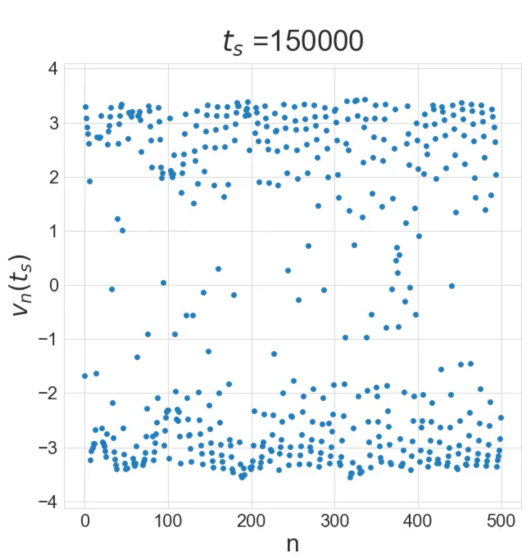

(a) Region pairs (=clumps) are phase locked with travelling waves (=arcs) in between.

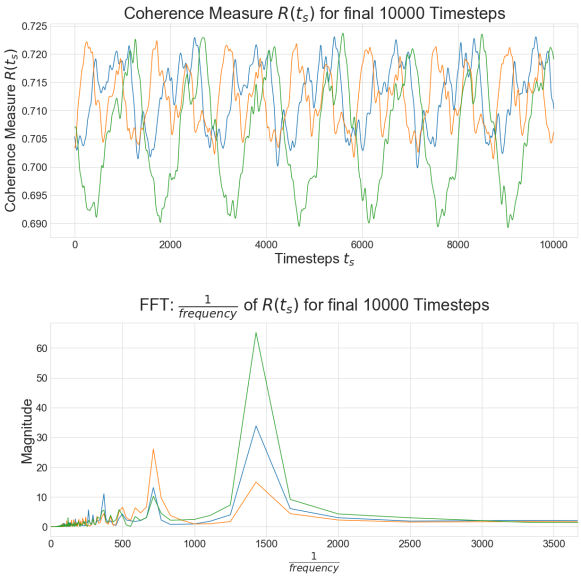

(e) The final 10,000 time steps of three simulations and of their frequency spectra.

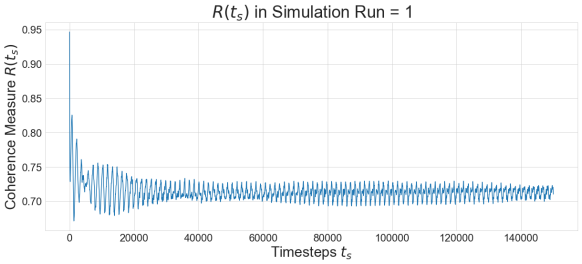

(b) The coherence measure oscillates irregularly.

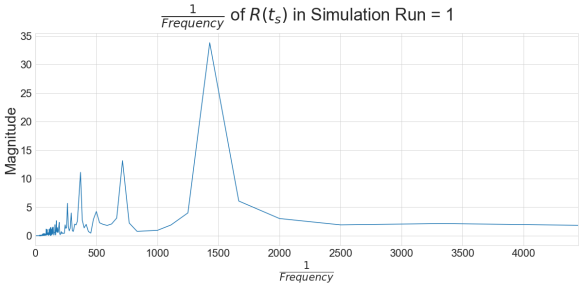

(c) The frequency spectrum corresponds to the coherence measure.

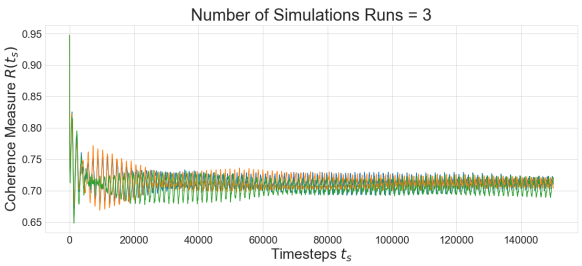

(d) All three coherence measures are in the irregular regime.

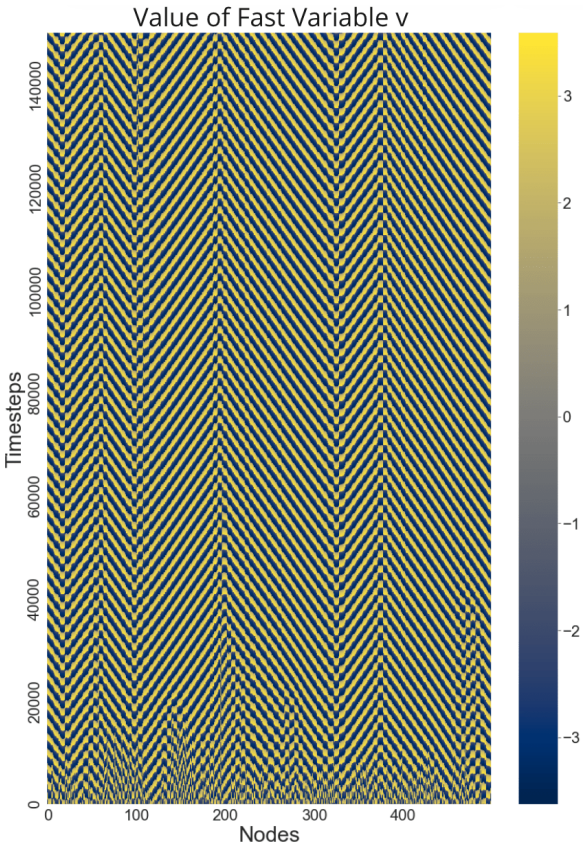

(f) The heatmap makes region pairs clearly visible.

Figure A.12.: Second part of the plot collection corresponding to region pairs on a higher density ring network $WS(500, 16, 0, 005)$ with scaled coupling = $\frac{1}{10}$ and $\frac{T}{\delta t} = 1,500 * 10^2$ time steps. The visualizations of the (a) chimera pattern plot, (b), (c) coherence measure and its frequency spectrum, (d) coherence measure of three simulation runs, (e) the final 10,000 time steps of the three coherence measures and their frequency spectra and (f) the heatmap of the evolution of the network are shown, as described in section 4.4.

A.7. Region Pairs, WS(500, 16, 0,01) and scaled coupling $= \frac{1}{10}$

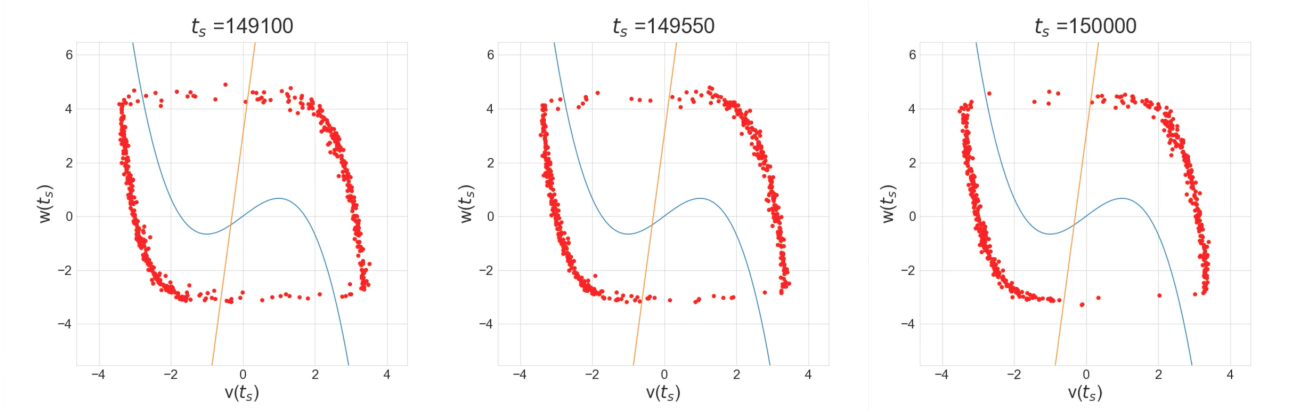

(a) Oscillators scatter around the limit cycle.

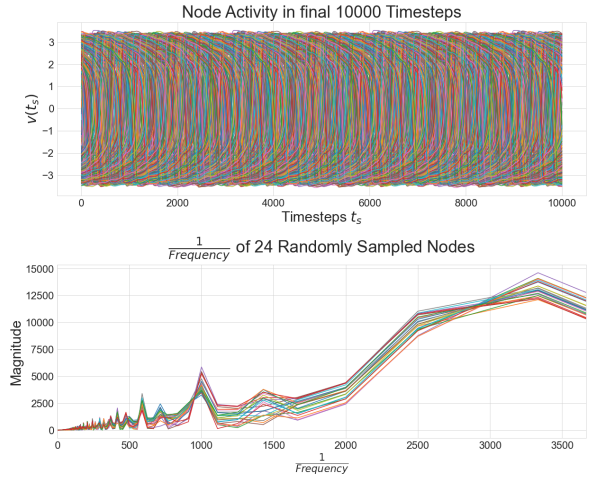

(b) The activity of nodes in the final 10, 000 time steps and the frequency spectra of 24 randomly sampled nodes are taken.

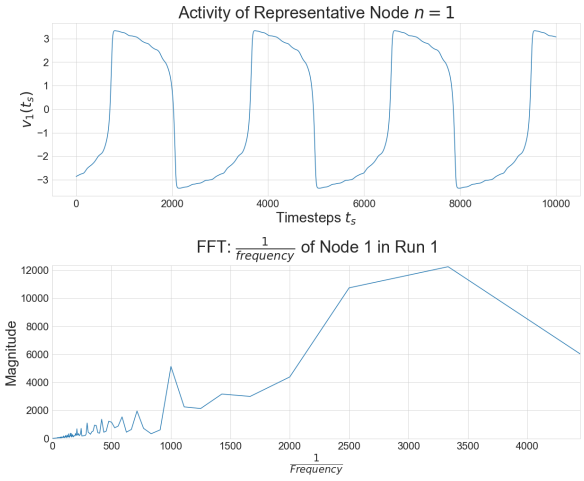

(c) A representative oscillation and its frequency analysis.

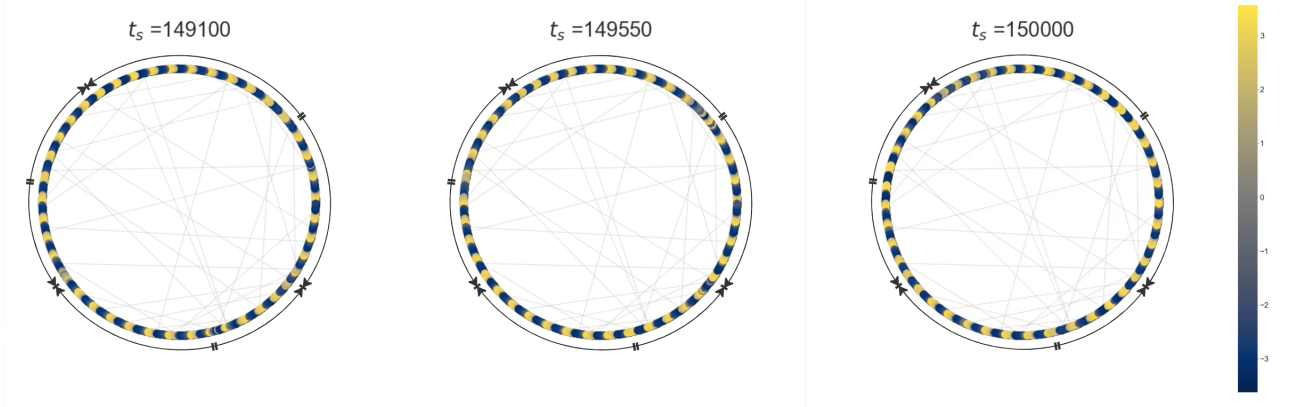

(d) Waves and region pairs are not interlaced. Generating regions are indicated by two lines on the circle and annihilating regions by two opposing arrows.

Figure A.13.: First part of the plot collection corresponding to region pairs on higher density ring network $WS(500, 16, 0, 01)$ with scaled coupling $= \frac{1}{10}$ and $\frac{T}{\delta t} = 1,500 * 10^2$ time steps. The visualizations of the oscillators in (a) the phase plane, (b)-(c) the node analysis and (c) the spatiotemporal propagation are shown, as described in section 4.4. The colorbar continuously assigns colors from blue to yellow to the fast variable v on the limit cycle.

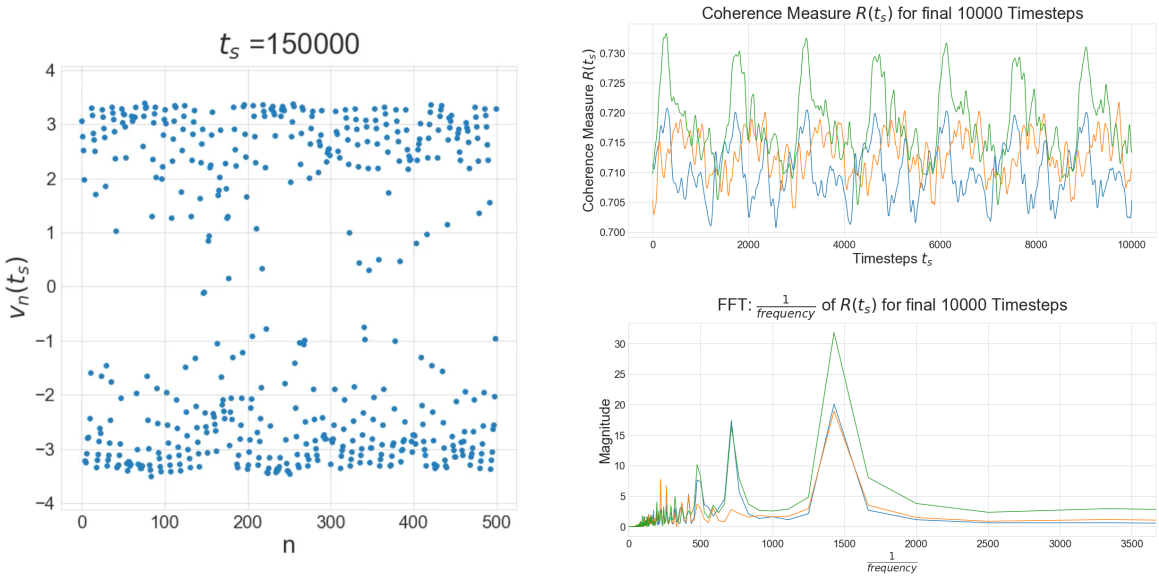

(a) Region pairs (=clumps) are phase locked with travelling waves (=arcs) in between.

(e) The final 10,000 time steps of three simulations and of their frequency spectra.

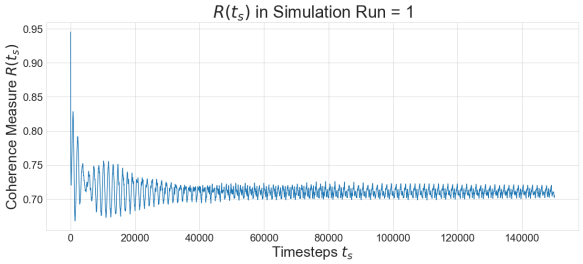

(b) The coherence measure oscillates irregularly.

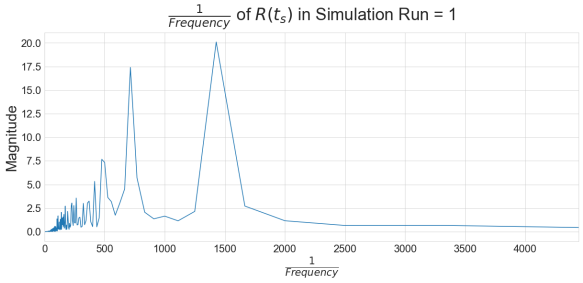

(c) The frequency spectrum corresponds to the coherence measure.

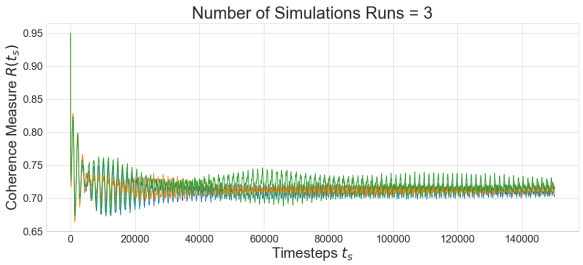

(d) All three coherence measures are in the irregular regime.

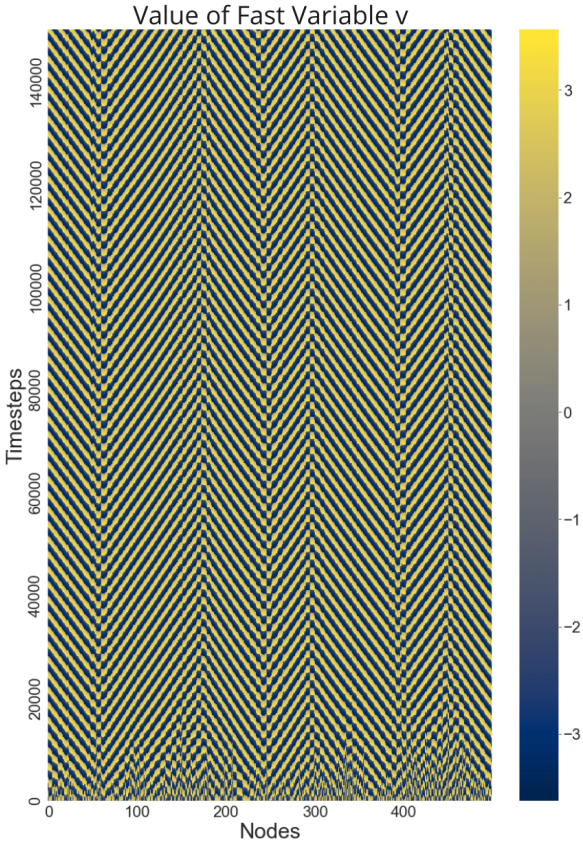

(f) The heatmap makes region pairs clearly visible.

Figure A.14.: Second part of the plot collection corresponding to region pairs on a higher density ring network $WS(500, 16, 0, 01)$ with scaled coupling = $\frac{1}{10}$ and $\frac{T}{\delta t} = 1,500 * 10^2$ time steps. The visualizations of the (a) chimera pattern plot, (b), (c) coherence measure and its frequency spectrum, (d) coherence measure of three simulation runs, (e) the final 10,000 time steps of the three coherence measures and their frequency spectra and (f) the heatmap of the evolution of the network are shown, as described in section 4.4.

A.8. Chimera Pattern, WS(500, 16, p=0.1) and scaled coupling $= \frac{1}{50}$

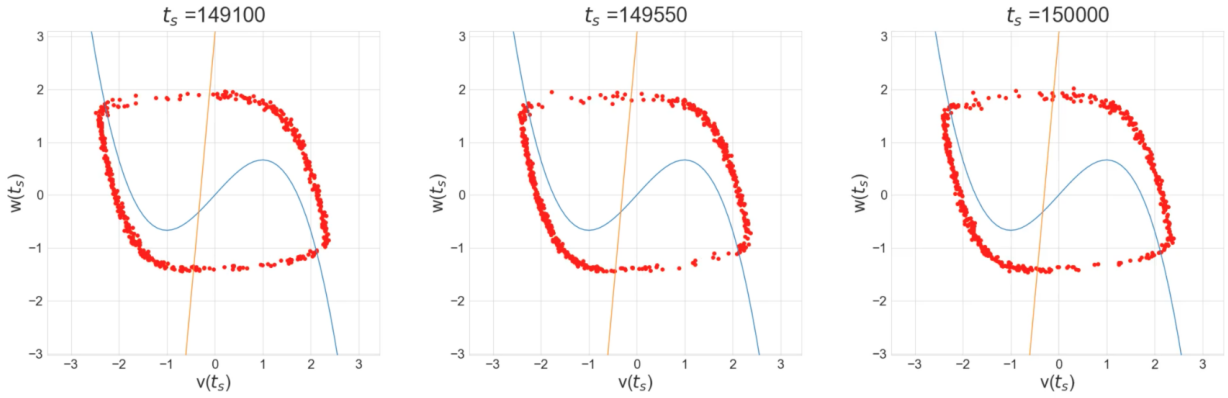

(a) Oscillators distribute on the limit cycle.

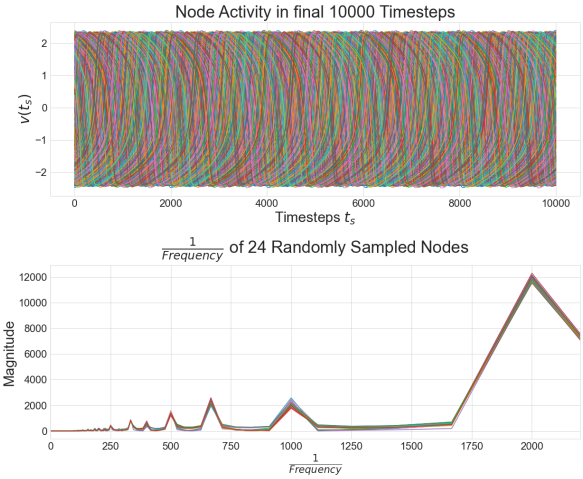

(b) The activity of nodes in the final 10,000 time steps and the frequency spectra of 24 randomly sampled nodes are taken.

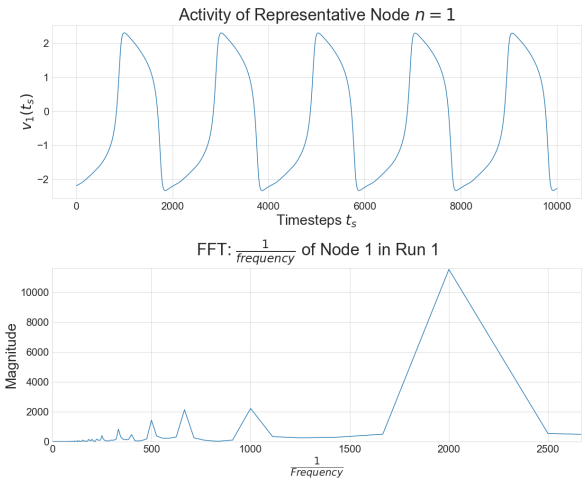

(c) A representative oscillation and its frequency analysis.

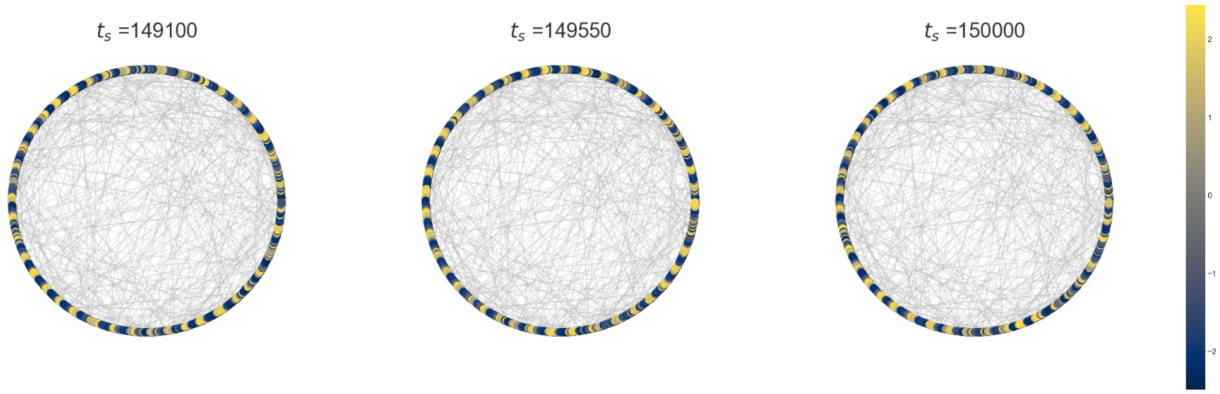

(d) Spatiotemporal activity: Regions of incoherence are manifested.

Figure A.15.: First part of the plot collection corresponding to chimera synchronization patterns on higher density ring network $WS(500, 16, 0, 1)$ with scaled coupling $= \frac{1}{50}$ and $\frac{T}{\delta t} = 1,500 * 10^2$ time steps. The visualizations of the oscillators in (a) the phase plane, (b)-(c) the node analysis and (c) the spatiotemporal propagation are shown, as described in section 4.5. The colorbar continuously assigns colors from blue to yellow to the fast variable v on the limit cycle.

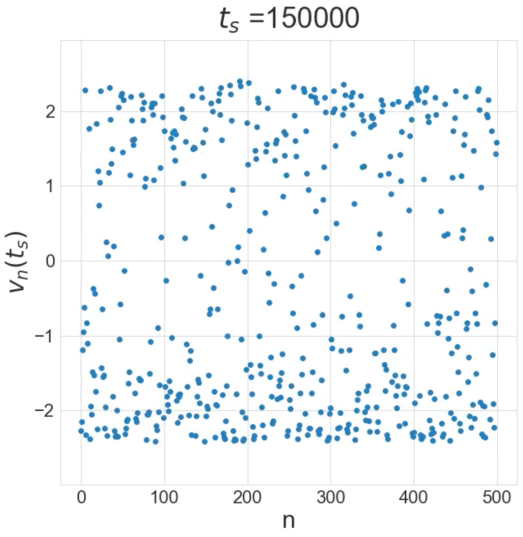

(a) Oscillators tend to agglomerate on top and bottom regions.

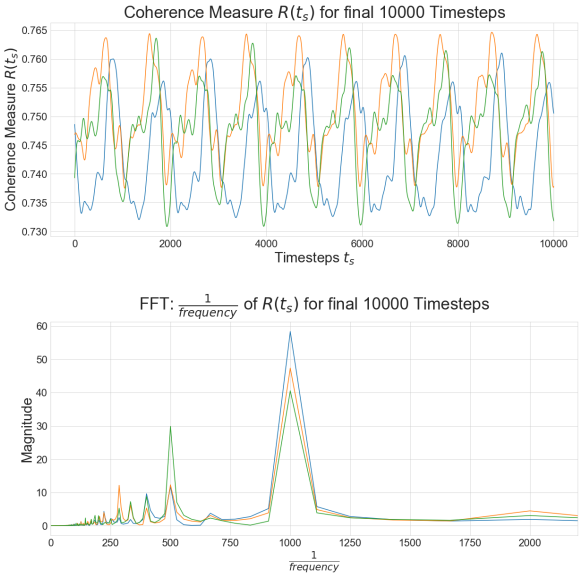

(e) The final 10,000 time steps of three simulations and of their frequency spectra.

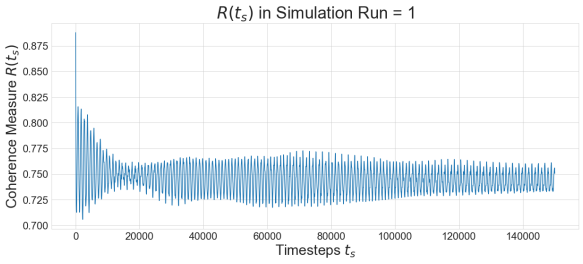

(b) The coherence measure oscillates irregularly.

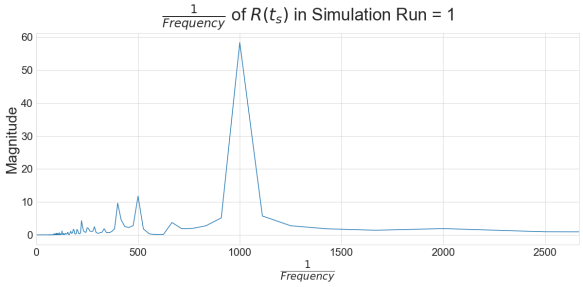

(c) The frequency spectrum corresponds to the coherence measure.

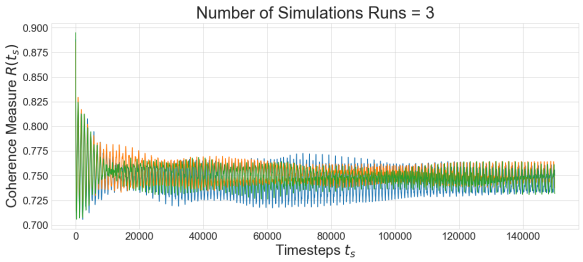

(d) All three coherence measures are in the irregular regime.

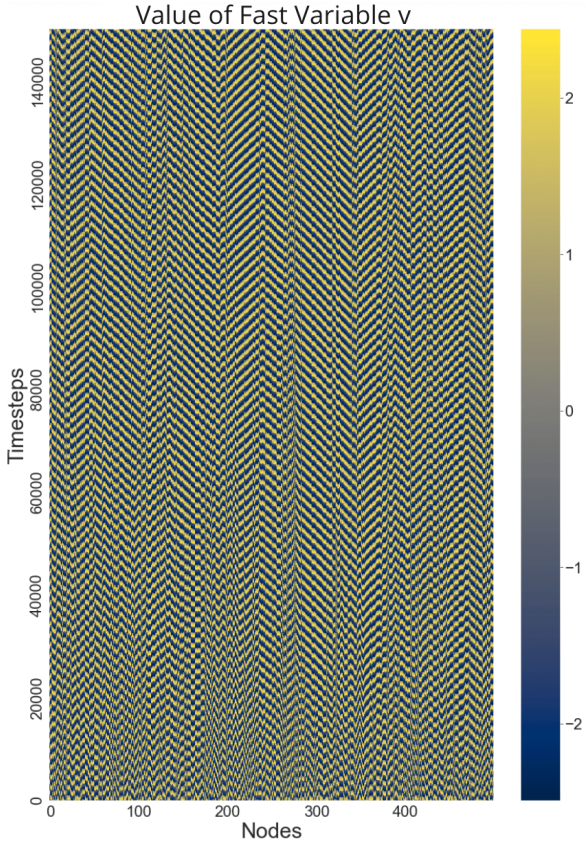

(f) The heatmap makes incoherent regions visible.

Figure A.16.: Second part of the plot collection corresponding to chimera synchronization patterns on a higher density ring network $WS(500, 16, 0, 1)$ with scaled coupling = $\frac{1}{50}$ and $\frac{T}{\delta t} = 1,500 * 10^2$ time steps. The visualizations of the (a) chimera pattern plot, (b), (c) coherence measure and its frequency spectrum, (d) coherence measure of three simulation runs, (e) the final 10,000 time steps of the three coherence measures and their frequency spectra and (f) the heatmap of the evolution of the network are shown, as described in section 4.5.

A.9. Chaotic Pattern, $WS(500, 8, 0.4)$ and scaled coupling $\frac{1}{50}$

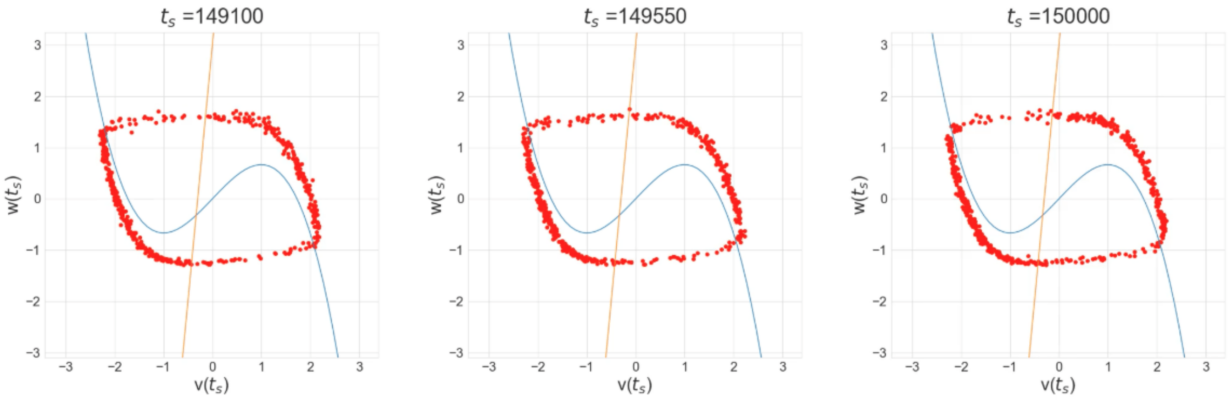

(a) Oscillators travel around a limit cycle with small diameter.

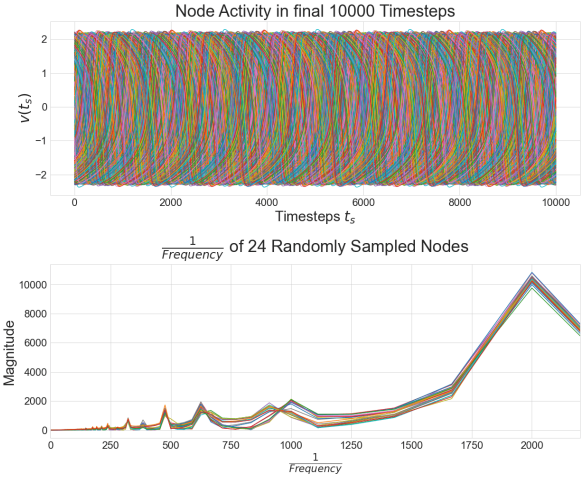

(b) The activity of nodes in the final 10,000 time steps and the frequency spectra of 24 randomly sampled nodes are taken.

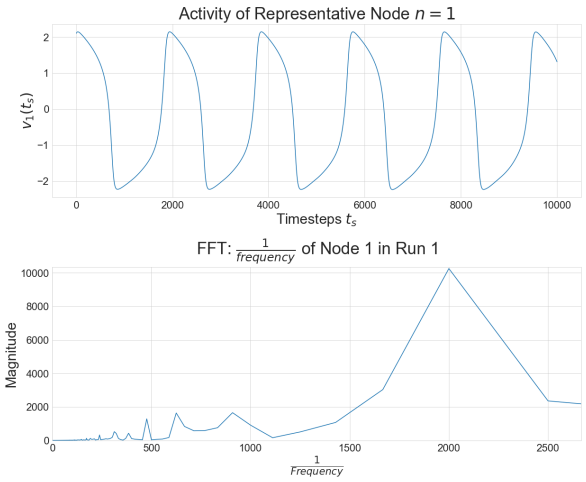

(c) A representative oscillation and its frequency analysis.

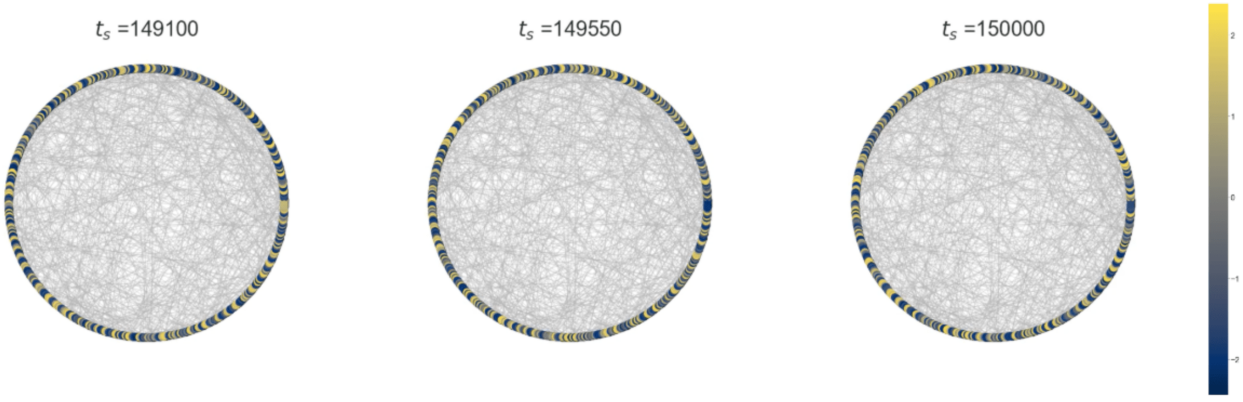

(d) A chaotic pattern is shown where no coherence can be observed close to the end of the simulation.

Figure A.17.: First part of the plot collection corresponding to chaotic patterns on a $WS(500, 8, 0.4)$ with scaled coupling $= \frac{1}{50}$ and $\frac{T}{\delta t} = 1,500 * 10^2$ time steps. The visualizations of the oscillators in (a) the phase plane, (b)-(c) the node analysis and (c) the spatiotemporal propagation are shown, as described in section 4.6. The colorbar continuously assigns colors from blue to yellow to the fast variable v on the limit cycle.

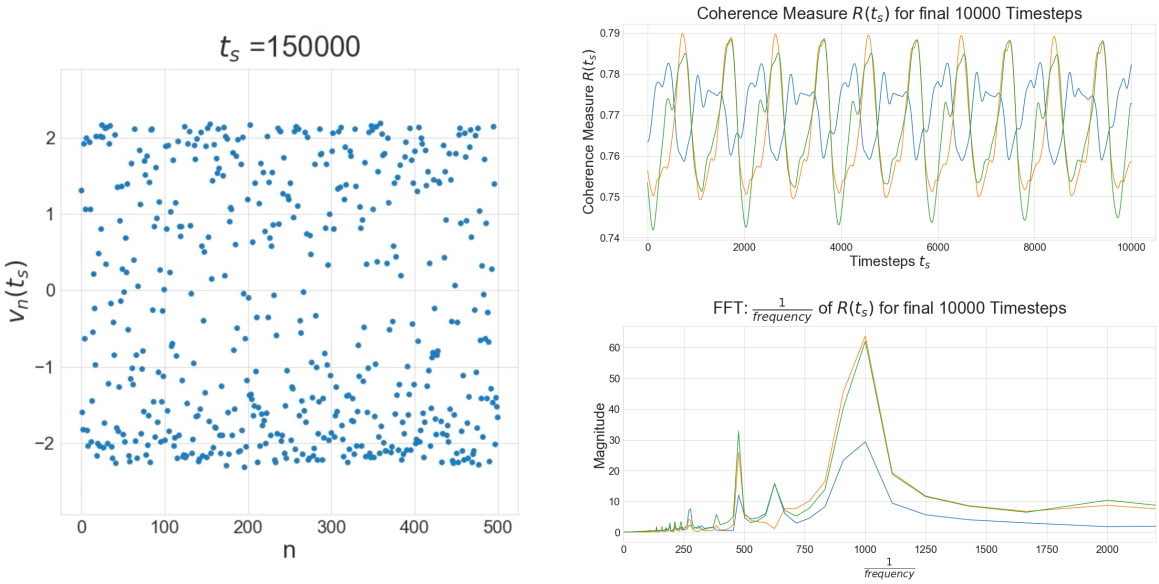

(a) Neither waves nor region pairs can be identified.

(e) The final 10,000 time steps of three simulations and of their frequency spectra.

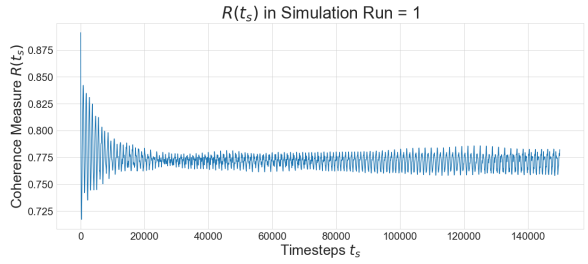

(b) The coherence measure is in the irregular regime.

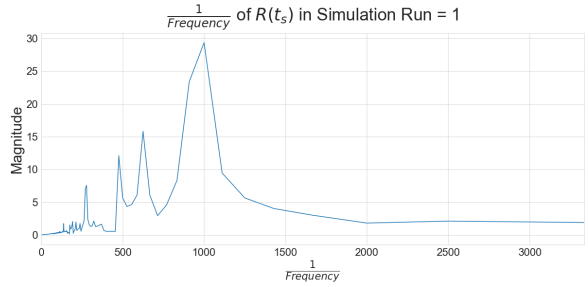

(c) The frequency spectrum corresponds to the coherence measure.

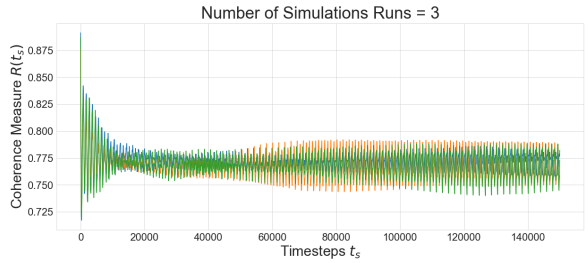

(d) The coherence measures of all three simulation runs exhibit irregular oscillations.

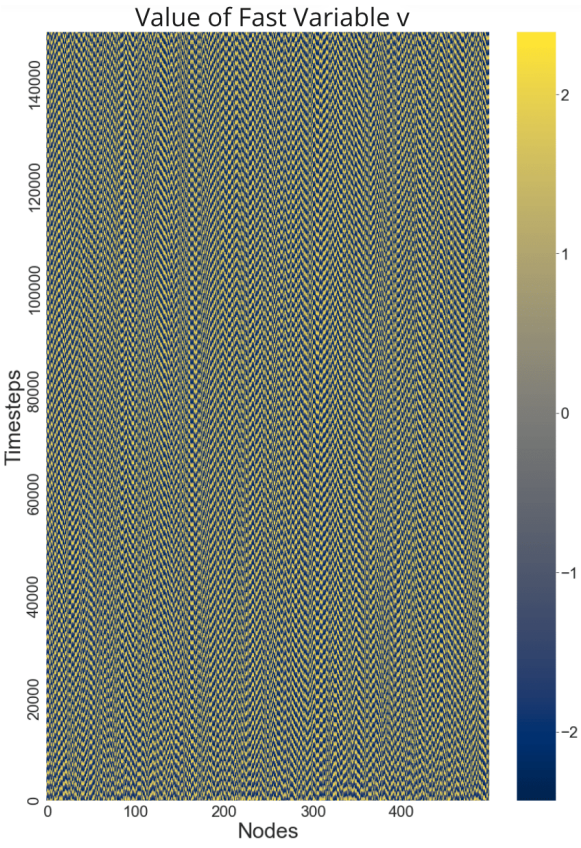

(f) The network does not synchronize and incoherence persists.

Figure A.18.: Second part of the plot collection corresponding to chaotic patterns on a $WS(500, 8, 0.4)$ with scaled coupling $= \frac{1}{50}$ and $\frac{T}{\delta t} = 1,500 * 10^2$ time steps. The visualizations of the (a) chimera pattern plot, (b), (c) coherence measure and its frequency spectrum, (d) coherence measure of three simulation runs, (e) the final 10,000 time steps of the three coherence measures and their frequency spectra and (f) the heatmap of the evolution of the network, as described in section 4.6.